ELECTRICAL AND OPTICAL PROPERTIES OF PLASMA POLYMERIZED 2-FURALDEHYDE THIN FILM

A dissertation submitted to the Department of Physics, Bangladesh University of Engineering and Technology in partial fulfillment of the requirement for the degree of MASTER OF PHILOSOPHY (M.Phil.) in PHYSICS

by

Humayun Kabir

Roll No. 040814027p

Session: April, 2008

BUET

Department of Physics

BANGLADESH UNIVERSITY OF ENGINEERING AND TECHNOLOGY (BUET)
DHAKA-1000

March, 2013

BANGLADESH UNIVERSITY OF ENGINEERING & TECHNOLOGY (BUET), DHAKA
DEPARTMENT OF PHYSICS

CERTIFICATION OF THESIS

The thesis titled "**Electrical and Optical Properties of Plasma Polymerized 2-Furaldehyde Thin Films**" submitted by **Humayun Kabir**, Roll No: **040814027P**, Registration No: **040814027**, Session: **April/2008**, has been accepted as satisfactory in partial fulfillment of the requirement for the degree of **Master of Philosophy (M.Phil.) in Physics** on **16th March, 2013.**

BOARD OF EXAMINERS

1. _____
Dr. Md. Abu Hashan Bhuiyan — **Chairman (Supervisor)**
Professor
Department of Physics, BUET, Dhaka-1000

2. _____
Head — **Member (Ex-Officio)**
Department of Physics,
BUET, Dhaka-1000

3. _____
Dr. A. K. M. Akther Hossain — **Member**
Professor
Department of Physics, BUET, Dhaka-1000

4. _____
Dr. A. B. M. Obaidul Islam — **Member (External)**
Professor
Department of Physics
University of Dhaka, Dhaka-1000

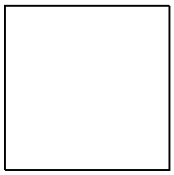

BUET

CANDIDATE'S DECLARATION

It is hereby declared that this thesis or any part of it has not been submitted elsewhere for the award of any degree or diploma.

Signature of the candidate

_____

(**Humayun Kabir**)

Roll No. 040814027P

Session: April/2008

Dedicated to

My beloved Parents

Who inspired and influenced me in this research work

CONTENTS

List of Figures

List of Tables

Abbreviations and symbols

ABS	Absorbance
AC	Alternating Current
Al	Aluminum
Cr-Al	Chromel-Alumel
CBD	Chemical Bath Deposition
CC	Capacitively Coupled
d	Sample Thickness
DC	Direct Current
DTA	Differential Thermal Analysis
E_{qd}	Direct transition energy gap
E_{qi}	Indirect transition energy gap
EDAX	Energy-Dispersive Analysis of X-rays
FDH	2-furaldehyde
FL	Fermi Level
FTIR	Fourier Transform Infrared
I	Current
I	Intensity of Radiation
IC	Inductively Coupled
IR	Infrared
k	Boltzmann Constant
K	Extinction Co-efficient
MHz	Mega Hertz
PECVD	Plasma Enhanced Chemical Vapor Deposition
PPDEA	Plasma Polymerized 2, 6 Diethylaniline
PPDP	Plasma Polymerized Dipheny1
PPFDH	Plasma Polymerized 2-furaldehyde
PPm-X	Plasma Polymerized m-Xylene
PPPA	Plasma Polymerized Polyaniline
PVD	Physical Vapour Deposition
RF	Radio Frequency
SCLC	Space Charge Limited Conduction

SEM	Scanning Electron Microscopy
T_g	Glass Transition Temperature
T_m	Melting Point
TGA	Thermogravimetric Analysis
TSDC	Thermally Stimulated Depolarization Current
UV-vis	Utraviolet-Visible
V	Voltage
XPS	X-ray Photoelectron Spectroscopy
•	Absorption Coefficient
β_{exp}	Experimental β Coefficient
β_S	Schottky Coefficient
β_{PF}	Poole-Frenkel Coefficient
ϕ	Columbic barrier height of the electrode polymer interface
ϕ_c	Ionization potential of the PF centers
λ	Wavelength
ΔE	Activation Energy
σ	Electrical Conductivity
ε'	Dielectric Constant
ε_0	Permittivity of Free Space
μ	Mobility of Charge Carrier
θ	Trapping Factor

Acknowledgements

To complete any work requires the support of many people. At first, I express my satisfaction to praise the almighty Allah who has given me strength and opportunity to complete my research work.

Regarding the outcomes and completion of this research work, I express my deepest sense of gratitude and profound respect to my supervisor Prof. Dr. Md. Abu Hashan Bhuiyan, Department of Physics, BUET, for his invaluable time dedication, close supervision, inspiration and helpful attitude provided during the work as well as for acquainting me with the arena of advanced research.

I am grateful to my respected teacher Prof. Dr. Md. Mostak Hossain, Head and Prof. Department of Physics, BUET for providing necessary facilities to carry out this research work. I am obliged to Prof. Dr. Mominul Huq, Prof. Dr. Jiban Podder, Prof. Dr. Md. Feroz Alam Khan, Prof. Dr. A. K. M. Akther Hossain and Dr. Md. Forhad Mina, Associate Professor, Department of Physics, BUET for their inspiration, affection and constructive suggestions for advanced research during the theoretical classes. I am thankful to my respectable teacher Prof. Dr. Md. Abdul Mannan Chowdhury, Prof. Dr. Robindra Chandra Sinha, Prof. Dr. Md. Abul Hossain and Prof. Dr. Farid Ahmed, Department of Physics, Jahangirnagar University for their valuable suggestions regarding my research work.

I am thankful to Mrs Rummana Matin, Mrs Tammana Afroza, Dr. Suniarmal Majumder and Dr. Rama Bijoy Sarker for their cooperation and inspiration throughout the work.

I am thankful to the authority of BUET for giving me necessary permission and providing with the financial support for this research work.

I am thankful to the authority of Jahangirnagar University for providing support to perform this work and also thankful to Mr. Nikhil Chandro Voumic, officer, Wazed Miah Science Research Center, JU, for helping me to take FTIR spectra.

I would like to thank the authority of Pilot Plant & Process Development Center (PP & PDC) of Bangladesh Council for Scientific & Industrial Research (BCSIR), Dhaka, for their excellent cooperation by allowing me to use the available facilities in that laboratory.

I am grateful to the Authority, Atomic Energy Centre, Dhaka for permitting me to use the scanning electron microscope (SEM) for surface morphological measurements. I

would like to thank Mr. Md. Al-Mamun and Mr. Hari Narayan Das, Engineer Materials Science Division, AECD, for helping me to take the SEM micrographs.

I am also thankful to all the staff members Mr. Md. Idris Munshi, Mr. Md. Liaquat Ali, Mr. Md. Nurul Haque, Mr. Md. Lutfur Rahman Sarker, Mr. Swapan Kumar Das, Mr. Md. Mozammel Haque, Mr. Md. Abu Taher and Lutfur Rahman, Department of Physics, BUET for their sincere help.

Finally, I would like to express my gratitude to my beloved parents and all other family members for their excellent support through all these years during my work.

Humayun Kabir
March, 2013

Abstract

Monomer 2-furaldehyde (FDH) was used to obtain plasma polymerized 2-furaldehyde (PPFDH) thin films of different thicknesses on to glass substrates in optimum condition through glow discharge using a capacitively coupled parallel plate reactor. The thickness of the plasma polymerized films deposited on glass substrates was measured by using multiple-beam interferometric method.

The surface morphology of the PPFDH thin films was found to be smooth, flawless and homogeneous. The PPFDH thin films showed highest percentage of Carbon (C) with small percentage of Oxygen (O) in the energy dispersive analysis of X-Ray spectrum. The structural analysis of PPFDH by Fourier transform infrared spectroscopy indicate that structural rearrangements occur may be due to the removal of bonds and it contains certain amount of conjugation.

The thermogravimetric analysis (TGA) of PPFDH shows that the PPFDH is stable up to 520 K. The differential thermal analysis shows an exothermic broad band which has a maximum centered around 600 K indicating a gradual change of its original properties. The corresponding TGA trace shows a uniform weight loss up to 760 K.

Ultraviolet visible (UV-vis) spectral of PPFDH thin films showed that the absorbance increases with the increase. From the UV-vis absorption spectra, absorption coefficient (•), allowed direct (E_{qd}) energy gap, allowed indirect (E_{qi})energy gaps, Urbach energy (E_U) and steepness parameter (•) were determined and found to be between 3.23-3.31 eV, 2.09-2.30 eV, 0.51-0.61 eV and 0.042-0.050 respectively for PPFDH thin films of different thicknesses.

The current density (J)-voltage (V) characteristics at different temperature (T) follow a power law of the form $J \bullet V^n$. In the low voltage region the values of n are $0.80 \bullet n \bullet 1.12$ and that in the high voltage region lies between $1.91 \bullet n \bullet 2.58$, indicating Ohmic conduction in the low voltage region and non-Ohmic conduction in the high voltage region. Theoretically calculated and experimental results of Schottky (β_s) and Poole-Frenkel (β_{PF}) coefficients show that the most probable conduction mechanism in PPFDH thin films is Schottky type. From the Arrhenius plots of J vs. 1/T for the applied voltages 5 and 35 V, the activation energies (• E) were calculated. For 5V, it is about 0.13 ± 0.02 and 0.50 ± 0.05 eV in the low and high temperature region respectively. For 35V, it is found to be around 0.11 ± 0.01 eV and 0.55 ± 0.02 eV, respectively in low and high temperature region.

CHAPTER 1

GENERAL INTRODUCTION

1.1 Introduction

Plasma polymerization is achieving an important position for last few decades as a tool to polymerize organic vapors at low temperatures using plasma enhancement. The formation of materials in plasma has been recognized as a means of synthesizing polymers, and the process when used to make a special coating on metals, has been referred to as plasma polymerization or glow discharge polymerization. Since plasma contains ions, electrons, photons, radicals and excited molecules, it becomes important to identify their reactive species controlling the propagating processes of the polymerization. It is the one of the modern techniques that can be used to deposit thin polymer films from a variety of organic compounds [1-3].

The polymer thin films obtained by plasma polymerization technique are different from those obtained by other conventional techniques. Plasma polymerized films are generally highly cross-linked and therefore insoluble in organic solvents. The structures and properties of plasma polymer thin films depend on plasma polymerization parameters; especially discharge power, monomer flow rate, substrate temperature, steady–state pressure in the reactor chamber and time of polymerization [4, 5].

Interests on organic thin films have been increasing for the last several years because of their attractive properties in the field of microelectronics and photovoltaic [6]. Thin films of organic compounds have applications in the fields of mechanics, electronics and optics; applications include chemical, physical and biological sensors, microelectronic and optoelectronic devices, nonlinear optical device, molecular devices, coatings for chemical fibers and films, passivation of metals, surface hardening of tool, spaceship components, etc.[7-8]. Therefore, it is of great interest to develop polymer thin films of high quality for a variety of industrial applications. As a consequence, the study of the structural, electronic, electrical and optical, etc. properties of organic polymers thin films as potential advance materials received special attention of the solid state and materials scientists.

The films obtained by plasma polymerization are generally of high quality, homogeneous, adherent, thermally stable and pinhole free [9-11]. Plasma polymers are used as dielectric and optical coatings to inhibit corrosion. The investigation of the optical properties of polymer films is of particular interest because of their use in optical devices [12].

Study on different plasma polymerized organic polymer is being led out in the Solid State Laboratory of Bangladesh University of Engineering and Technology over the past few years [13-23]. It is seen that the plasma polymerization emerges as a very important technique for thin film deposition and surface modification. So in the present research work, plasma polymerization technique has been used for the preparation of thin films. The major objective of this research work is to prepare polymer thin films of 2-furaldehyde (FDH) by glow discharge technique and to study their structural, optical and electrical properties. The present thesis reports structural, optical, direct current (DC) electrical and thermal properties of plasma polymerized 2-furaldehyde (PPFDH) thin films. The results of the present investigation are discussed in the thesis.

Correlation of the different properties namely structural, optical, thermal and electrical, with the composition of the polymer is highly essential for tailoring these materials for various applications.

1.2 Review of Earlier Research Work

The plasma polymers have been widely recognized during last few decades and several successful applications have come into view. Goodman's [24] work in this field has inspired several investigators to characterize the polymerization process and polymers produced from organic monomers. The development of scientific interest in application of materials of organic compound produced through plasma polymerization technique has drawn much attention of the scientists to investigate the various properties of the polymers such as structural, physical, chemical, optical, thermal and electrical properties. The attention in plasma-polymerized thin films as a possible dielectric material has triggered academic interest in the polymerization process [25].

The structural behavior of plasma polymerized thin films is different than that of the conventionally prepared polymer thin films. Fourier transformed infrared (FTIR) spectroscopic analysis, scanning electron microscopy (SEM) etc. provide information about the chemical structure of the plasma polymers. Ultraviolet-Visible (UV-Vis) spectroscopic analyses of organic or inorganic materials can give the information about electronic structure and find out the existence of optical transition mechanisms: allowed direct, indirect transitions and forbidden transitions.

Rummana and Bhuiyan [26] investigated the electrical transport mechanism in plasma polymerized 2, 6, diethylaniline (PPDEA) thin film. They reported that the low voltage region, conduction current obeys Ohm's law. The thickness dependence of current

density (J) in the higher voltage (V) region has indicated a Schottky type conduction mechanism. They also investigated the temperature dependence of the current density for different bias voltages and confirmed the possibility of Schottky emission in PPDEA thin films.

Tamanna and Bhuiyan [27] studied plasma polymerized 1, 1, 3, 3 tetramethoxypropane (PPTMP) by infrared and UV-Vis spectroscopy and reported that as deposited PPTMP thin films contain C =C bond and C =O bonds and these bonds form due to heat treatment. The red shift in the maximum absorption wavelength for PPTMP thin films substantiates the formation of conjugation in PPTMP thin films. The absorption coefficient (•), allowed direct transition (E_{qd}) allowed indirect transition (E_{qi}) and energy gap were determined. The E_{qd} and E_{qi} were found to be about 2.92 to 3.16 eV and 0.80 to 1.53 eV respectively for as deposited PPTMP samples of different thicknesses. The E_{qi} of two samples of different thickness heat treated at 673 K for 1 hour is 0.55 and 0.65 eV.

Investigation on conducting Plasma Polymerized Polypyrrole (PPPy) Thin Films as Carbon Dioxide Gas Sensors by plasma enhanced chemical vapor deposition (PECVD) method [28] revealed that the plasma polymerized PPy films can act as a gas sensor for carbon dioxide monitoring.

Blaszczyk-Lezak et al. [29] reported the preparation and optical properties of plasma polymerized perylene thin films. They obtained these films as highly absorbent and fluorescent with a root mean square (rms) roughness in the range 0.3 -0.4 nm. They described that the films are formed by a matrix formed by cross-linked fragments of perylene and intact molecules that confer the observed optical properties to this material. The optical and microstructural characteristics of this type of thin films make them suitable for their integration into photonic components for various applications.

Current density–voltage (J-V) characteristics of plasma polymerized 1-Benzyl-2-methylimidazole (PPBMI) thin films were studied by Sarker and Bhuiyan [30] over the temperature range from 300 to 423 K and reported that the dominant conduction mechanism in PPBMI thin films is space charge limited conduction.

Rummana and Bhuiyan [31] investigated the heat treatment and aging effect on the structural and optical properties of plasma polymerized 2,6 -diethylaniline (PPDEA) thin films.

They reported that the optical parameters of as-deposited PPDEA thin films changes due to heat treatment and do not change appreciably due to aging.

Cho et al. [32] investigated electrical and physical properties of plasma-polymerized as-grown and the annealed pure ethylcyclohexane thin films at various deposition radio frequency (RF) powers and annealing temperatures by using PECVD. The IR spectra showed that the plasma-polymer thin films had totally different chemical functionalities from those of the ethylcyclohexane precursor and that the chemical functionalities of the thin films changed with the RF power and annealing temperature. They observed a shrinkage (%) in the thicknesses of the thin films before and after the annealing the films which was measured by using SEM cross-sectional images.

Zhao et al. [33] prepared poly (4-biphenylcarbonitrile) (PBPCN) thin films using plasma polymerization technique. They studied the effect of discharge power on the chemical structure and surface compositions of PBPCN thin films using FTIR, UV-Vis absorption and XPS. UV-Vis spectra showed that a larger •-conjugated system formed in the PBPCN thin films at low plasma discharge of 30 W. The FTIR results suggest that the plasma polymerization of PBPCN has proceeded mainly via the opening of •-bonds of the C≡N functional groups under low discharge power of 30 W. A high discharge power of 50 W brings about more severe molecular (aromatic ring) fragmentation and thus the conjugation length of PBPCN films decreases due to the formation of a non-conjugated polymer.

Majumder and Bhuiyan [34] employed electrical glow discharge technique for the preparation of plasma polymerized vinylene carbonate (PPVC) thin films of aluminum/thin film/aluminum sandwich structure at room temperature by a parallel plate capacitively coupled reactor. The structural investigation of the monomer VC and PPVC was performed by Fourier transform infrared spectroscopy. They found Ohmic current conduction in the low voltage region and non Ohmic conduction in the high voltage region and the most probable conduction mechanism in the PPVC thin films is of Schottky type.

Plasma polymerized tetraethylorthosilicate (PPTEOS) thin films were deposited by Zaman and Bhuiyan [35] on to glass substrates at room temperature by a parallel plate capacitively coupled glow discharge reactor. The conduction in PPTEOS is dominated by hopping of carriers between the localized states at the low temperature and thermally excited carriers from energy levels within the band gap in the vicinity of high temperature.

Nespurek et al. [36] reported that shapes of I-V characteristics of thin films strongly depend on temperature, presence of charge carrier traps, and their distribution in energy, spatial inhomogeneity of the sample and electrode configuration in case of space charge limited conduction (SCLC). The presence of traps influences generation-recombination noise which can be used for the determination of density-of-states function. Thus for a new material to be used in electronic technology, it is necessary to study the charge transport mechanism.

Chowdhury and Bhuiyan [37, 38] investigated the optical and electrical properties of plasma polymerized diphenyl (PPDP) thin films. They have concluded that the band gap is not affected appreciably by heat treatment whereas it is modified on aging. The AC conductivity is more dependent on temperature in the low frequency region than in the high frequency region. Dielectric constant is dependent on frequency above 303 and 343 K in the as deposited and heat treated PPDP, respectively. The dielectric data analysis showed the existence of distribution of relaxation time in these materials.

Guermat et al. [39] studied plasma-polymerized films of hexamethyldisiloxane as sensing layer for humidity sensor development by using a capacitively coupled parallel plate reactor. The change in electrical impedance of the sensing film was monitored as the device was exposed to humidity. They reported that thickness and discharge power were two main parameters that govern sensor characteristics for moisture detection. Films with lower thickness and low discharge power provide the optimum deposition condition for fabricating high performance humidity sensors.

The structural analyses of plasma polymerized N, N, 3, 5 Tetramethylaniline (PPTMA) thin films have revealed that PPTMA thin films are formed with certain amount of conjugation, which modified on heat treatment [40, 41]. From the UV-Vis absorption spectra, they found that the allowed direct and indirect transition energy gaps were modified when the samples were heat treated and Tauc parameter (B) for all the samples indicated an increase in structural order/conjugation in PPTMA thin films improved by heat treatment. From UV-Vis spectroscopy they found that indirect energy gap varies from 1.49 to 1.86 eV with film thickness. J-V characteristics indicated that the conduction mechanism in PPTMA thin films is SCLC. From the electrical and optical measurements they suggested that the top of valence band and the bottom of the conduction band may have gap states and the middle of the energy gap may be equal to the high temperature activation energy.

Sakthi Kumar and Yoshida [42] reported that PPPy produced by RF plasma polymerization has large increase in the capacitance towards the low frequency region which indicated the possibility of an interfacial polarization mechanism prevailing in that region. They have concluded that to consider a material to be a good dielectric material it should have high dielectric constant with small variations against frequency and temperature, low dielectric losses, chemical inertness and also stability against environment.

Vikram Kumar et al. [43] examined the temperature dependence of the exponential trap model of the SCLC in organic semiconductors and determine trap parameters from the temperature dependent of J characteristics at two or more temperatures. It is observed that the technique is applicable if the J characteristics follow a power law of the form $J\text{-}V^{m}$.

Sajeev and Anantharaman [44] studied with the carrier transport mechanism of polyaniline (PA) thin films prepared by RF plasma polymerization. The mechanism of electrical conduction and carrier mobility of PA thin films for different temperatures were examined using the aluminium–PA–aluminium structure. It is found that the mechanism of carrier transport in these thin films is SCLC.

Akhmedov et al. [45] observed SCLC in films prepared in glow discharge plasma. The electrical current in thin films obtained by the polymerization of acetonitrile in glow discharge on a heated substrate was investigated in order to determine the mechanism of electrical conduction. The results of the field dependence, sample thickness dependence of the dark conductivity, supported by the results of photocurrent measurements, suggest an exponential energy distribution of traps inside the band gap of the polymer.

Olayo et al. [46] studied the electric conductivity, activation energy and morphology of polythiophene synthesized by RF resistive plasmas. The continuous collisions of particles in the plasma induce the polymerization of thiophene but also break some of the monomer molecules producing complex polymers with thiophene rings and aliphatic hydrocarbon segments. These multidirectional chemical reactions were more marked at longer reaction times. The intrinsic conductivity of plasma polymers of thiophene was found to be sensitive to the water content in the polymers and the activation energy increased with the reaction time.

Cherpak et al. [47] formed poly(*o*-methoxyaniline) (POMA) thin films by thermovacuum deposition in the temperature range of 350–450 °C and at a pressure of 5×10^{-5} Torr and found that the structure properties of vacuum deposited POMA are similar to those observed for the emeraldine form of polyaniline. On the basis of the dependence of conductivity on frequency they showed that hopping mechanism dominates in a polymer film and such mechanism was typical of non-ordered systems.

Fischer et al. [48] yields ultrathin insoluble, low-molecular-weight polymer films by the electropolymerization of *o*-methoxyaniline under self-limiting deposition conditions. Fundamental understanding of the structure/property relationships derived from the investigations can be applied to three-dimensional electrode nanoarchitectures that incorporate such electroactive coatings for enhanced charge-storage functionality.

Electrochemical polymerization of aniline was carried out by Raj et al. [49] in micellar solutions of camphor sulphonic acid. The surface morphology observed from different surfactant molecules was found to be distinctly different and showed uniform nanosized globular structures.

Therefore it is observed that a lot of research work has been performed in this field and potential applications was found. These encourage me to prepare thin films of plasma polymerized organic materials.

1.3 Objectives of the Present Study

From review of earlier research, it is found that few works have been done with monomer 2-furaldehyde. This monomer is in liquid form and not sticky so that no heating system is needed to inject the monomer into the chamber. This monomer is also available in local market. This type of materials is used as coatings, insulators, dielectrics, etc. That is why this material was chosen as a potential organic monomer for thin film preparation.

In the present investigation, plasma polymerized 2-furaldehyde (PPFDH) thin films were prepared at optimized conditions by a capacitively coupled glow discharge plasma polymerization method. The surface structure, chemical structure, absorption co-efficient, optical energy gaps and direct current (DC) electrical conduction mechanism were investigated.

The morphology was studied to know its surface properties and Fourier transform infrared spectroscopy of the monomer and as deposited PPFDH were investigated to know the structural change due to plasma polymerization.

Differential thermal analysis and thermogravimetric analysis of PPFDH were performed to understand the thermal properties. Ultraviolet-Visible spectroscopy was done to calculate the absorption coefficient and from which the direct and indirect band gaps of PPFDH were calculated. Aluminium-thin film-aluminium sandwiched structure samples were used for J-V and J-T measurements. DC electrical measurements were performed at different applied voltage and different temperatures on samples of different thicknesses to understand the DC conduction mechanism in PPFDH thin films.

1.4 Thesis Summary

To make this research work reader friendly this dissertation has been configured into five chapters.

Chapter 1: This chapter basically focuses on the reviews of earlier research works of different plasma polymerized thin films and discusses the aim of the present study.

Chapter 2: This chapter describes the details about polymers, plasma polymers, different polymerization processes, advantages and disadvantages of plasma polymers. Application of plasma polymerized organic thin films and theories of different measurements are presented at the end of this chapter.

Chapter 3: The experimental techniques are briefly explained in this chapter along with the description of the plasma polymerization set up, generation of glow discharge, film thickness measurements, sample formation, etc. The monomer, substrate materials and its cleaning process are also included here. A brief description of the instrumentation of the different characterization techniques are also presented here.

Chapter 4: The morphological, structural, thermal and optical properties are presented in this chapter. This chapter ends with analyses of J-V and J-T characteristics.

Chapter 5 : Finally, the conclusions of the work done and suggestions for future research on this material are included in this chapter.

CHAPTER 2

THEORETICAL BACKGROUND

2.1 Introduction

Polymeric materials have vast potential exciting new applications in the foreseeable future. Polymer uses are being developed in such diverse areas namely: conduction and storage of electricity, molecular based information storage and processing, molecular composites, unique separation membranes, new forms of food processing and packaging, health, housing, and transportation. Indeed, polymers will play an increasingly important role in all aspects of everyday life. The large number of current and future applications of polymeric materials has created a great interest for scientists to carry out research and development in polymer science and engineering.

This chapter presents a literature survey on polymers, general properties polymers and different-polymerization processes. The details of plasma, an overview of gas discharge plasma, plasma polymerization, different types of glow discharge reactors, plasma polymerization mechanism, advantages and disadvantages of plasma polymerized thin films, application of plasma polymerized organic thin films are illustrated in this chapter [50]. The theory of Fourier Transform Infrared (FTIR) Spectroscopy, Ultraviolet-Visible (UV-Vis) spectroscopy and direct current (DC) conduction mechanism are also focused at the end of this chapter.

2.2 Polymers

The term ‘polymer’is derived from the Greek words: *polys* meaning *many*, and *meros* meaning *parts*. Polymers are the substances, which are made of large number of molecules or macromolecules. These molecules or giant molecules are composed of covalently bounded repetition of small repeating units, which are called ‘monomer’. The length of polymer chain is specified by the nummber of repeat units in the chain, which is known as the degree of polymerization. Polymers are thought to be colloidal substance i.e. glue-like materials. From chemical point of view, the colloidal substances are in fact large molecules and their behavior could be explained in terms of the size of the individual molecules.

In some cases the repetition is linear to form linear chain, in others the chains are branched or inter connected to form three-dimensional networks. The repeat unit is usually equivalent to the monomer, or starting material from which it is formed. Polymers have anomalous properties because they were so different from the properties of low molecular weight compounds. When more than one kind of repeat unit is present in the polymer, it is

known as a copolymer. Polymers having molecular weight roughly in the range of 1000-20,000 are called low polymers and those having molecular weight higher than 20,000 as high polymers [51].

2.2.1 Classification of Polymers

Linear Polymers: Linear polymers are most common. They can occur whenever two reacting chains join to make a chain. If the long-chains pack regularly, side-by-side, they tend to form crystalline polymers. If the long chain molecules are irregularly tangled, the polymer is amorphous since there is no long range order. Sometimes this type of polymer is called glassy. Cross-Linking: In addition to the bonds which hold monomers together in a polymer chain, many polymers form bonds between neighboring chains. These bonds are called cross links. These bonds can be formed directly between the neighboring chains, or two chains may bond to a third common molecule. Though not as strong or rigid as the bonds within the chain, these cross-links have an important effect on the polymer. Polymers with a high enough degree of cross-linking have "memory". When the polymer is stretched, the cross-links prevent the individual chains from sliding past each other. The chains may straighten out, but once the stress is removed they return to their original position and the object returns to its original shape.

Homo-polymers: They consist of chains with identical bonding linkages to each monomer unit. This usually implies that the polymer is made from all identical monomer molecules. These may be represented as: -[A-A-A-A-A-A]-

Copolymers: They consist of chains with two or more linkages usually implying two or more different types of monomer units. These may be represented as: -[A-B-A-B-A-B]-

Addition Polymers: Here, the monomer molecules bond to each other without the loss of any other atoms. Alkene's monomers are the biggest groups of polymers in this class.

Condensation Polymers: In this case, usually two different monomers combine with the loss of a small molecule, usually water. Polyesters and polyamides (nylon) are in this class of polymers.

Thermoplastics: Thermoplastic polymers can be repeatedly softened by heating and then solidified by cooling. Most linear and slightly branched polymers are thermoplastic. All the major thermoplastics are produced by chain polymerization. Thermoplastics have a wide range of applications because they can be formed and reformed in so many shapes. Some examples are food packaging, insulation, automobile bumpers and credit cards.

Thermosets: Thermosets usually are three-dimensional networked polymers in which there is a high degree of cross-linking between polymer chains. The cross-linking restricts the motion of the chains and leads to a rigid material. Thermosets are strong and durable. They primarily are used in automobiles and construction. They also are used to make toys, varnishes, boat hulls, and glues.

Elastomers: They are rubbery polymers that can be stretched easily to several times their unstretched length and which rapidly return to their original dimensions when the applied stress is released. Elastomers are cross-linked, but have a low cross-link density. The polymer chains still have some freedom to move, but are prevented from permanently moving relative to each other by the cross-links. To stretch, the polymer chains must not be part of a rigid solid - either a glass or a crystal. Rubber bands and other elastics are made of elastomers.

2.2.2 States of polymers

Polymers can exist in three different states: a) Viscofluid state b) Rubbery state c) Glassy state.

a) **Viscofluid state:** This state of polymer is characterized by the intensive thermal motion of individual units, large fragments of the polymeric chain and the movement of the macromolecule as a whole. This state is typical of most liquids. The most important specific feature of polymers existing in this state is the ability to flow under the influence of the applied stress (fluidity).

b) **Rubbery state:** The rubbery (high elastic) state is the characteristics of polymer only. In the rubbery state individual units, atomic groups and segments undergo intensive thermal motion. Polymers in this state possess remarkable mechanical properties. The folded flexible long chains straighten out under the influence of the applied stress and return to their original shape after the stress is removed as a result of thermal motion.

c) **Glassy state:** When the temperature is lowered, a liquid can crystalline or pass to the glassy state. The transition to the glassy state is possible for both low molecular mass substances and polymers. In this state polymers are no longer capable of undergoing segmental motion. The glassy state is characterized by the vibrational motion, small units in the main chain and also atomic groups. The morphology of

most polymers is semi-crystalline. That is, they form mixtures of small crystals and amorphous material and melt over a range of temperature instead of at a single melting point. There are some polymers that are completely amorphous, but most are a combination with the tangled and disordered regions surrounding the crystalline areas. Such a combination is shown in fig. 2.1.

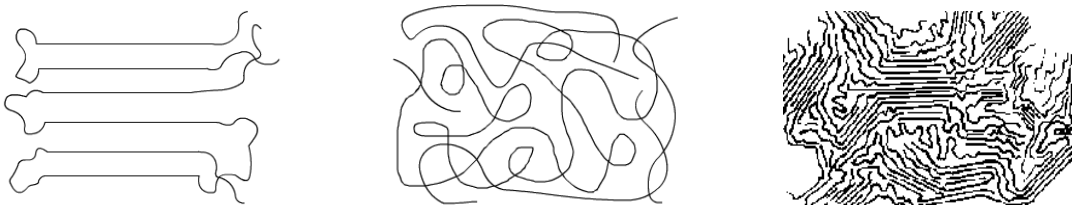

Crystalline Amorphous Semi crystalline

Fig. 2.1 Different states of Polymers

An amorphous solid is formed when the chains have little orientation throughout the bulk polymer. The glass transition temperature is the point at which the polymer hardens into an amorphous solid. This term is used because the amorphous solid has properties similar to glass.

2.2.3 General properties of polymers

The properties of polymers of same kind or groups may vary depending on how they are prepared and treated thermo-mechanically before being tested. The structural, chemical as well as physical properties of polymers are largely based on the factors namely: molecular weight, polarity, crystallinity, molar cohesion, linearity and non-linearity of polymeric chains, thermo-chemical history of the polymers and temperature of observation etc. [52].

2.3 Plasma and Plasma Polymerization

2.3.1 Plasma

Plasma is typically an ionized gas. Plasma is considered to be a distinct state of matter because of its unique properties. As a result the plasma state is often referred to as the fourth state of matter. Ionized refers to presence of one or more free electrons, which are not bound to an atom or molecule. The free electric charges make the plasma electrically conductive so that it responds strongly to electromagnetic fields. Plasma typically takes the form of neutral gas-like clouds (e.g. stars) or charged ion beams, but may also include dust and grains called dusty plasmas. Stars, as well as visible interstellar matter, are in the plasma state. Besides the astroplasmas, which are omnipresent in the universe, there are

two main groups of laboratory plasma, i.e., the high-temperature or fusion plasmas, and the low-temperature plasma or gas discharges [53, 54]. In general, a subdivision can be made between plasmas which are in the thermal equilibrium and those which are not in the thermal equilibrium. Thermal equilibrium implies that the temperature of all species (electrons, ions, and neutral species) is the same. High temperature is required to form these equilibrium plasmas, typically ranging from 4000 K to 20000 K. This is true for stars, as well as for fusion plasmas. On the other hand, interstellar plasma matter is typically not in thermal equilibrium [55].

In recent years, the field of gas discharge plasma applications has rapidly expanded [56]. The wide variety of chemical non-equilibrium conditions is possible since parameters can easily be modified such as, chemical input, pressure, electromagnetic field structure, discharge configuration and temporal behavior, etc. Because of these multi- dimensional parameter space of the plasma conditions, there exists a large variety of gas discharge plasmas employed in a large range of applications. Four types of plasma i.e., the glow discharge (GD), capacitively coupled plasma (CCP), inductively coupled plasma (ICP), and the microwave-inductively plasma (MIP), are commonly used in plasma spectrochemistry and are therefore familiar to most spectrochemists. However these plasmas, as well as related gas discharges, are more widely used in technological fields.

To generate the plasma, it is necessary to ionize atoms or molecules in the gas phase. When an atom or molecules gains enough energy from an external excitation source or through collisions with another molecule, ionization occurs [57]. This happens usually when the molecules are under specific conditions, like extreme heat which generates the so-called *hot plasmas*, or under electrical glow discharge which generates the *cold plasmas* [58]. The plasmas loose energy to their surroundings through collision and radiation processes; as a result, energy must be supplied continuously to the system to maintain the plasma state. The easiest way to supply energy to a system in a continuous manner is with an electrical source. Therefore, electrical glow discharges are the most common plasmas [59].

2.3.2 Gas discharge plasma

Plasma polymerization takes place in low temperature plasma which is provided by a glow discharge operated in an organic gas or vapor (monomer) at low pressure between two electrodes. When a sufficient high potential difference is applied between the two electrodes, the gas will break into positive ions and electrons, giving rise to a gas

discharge. When a potential difference is applied the electrons are accelerated by the electric field in front of the cathode and collide with the gas atoms. The most important collisions are the inelastic collisions leading to excitation and ionization. The excitation collisions create new electrons and ions. The ions are accelerated by the electric field toward the cathode, where they release new electrons by ion-induced secondary electron emission. The electrons give rise to new ionization collisions, creating new ions and electrons. These processes of electron emission at the cathode and ionization in the plasma make the glow discharge self-sustaining plasma.

Another important process in the glow discharge is the phenomenon of sputtering, which occurs at sufficiently high voltage. When the ions and fast atoms from the plasma bombard the cathode, they not only release secondary electrons, but also atoms of the cathode materials, which are called sputtering. This is the basis of the use of glow discharges for analytical spectrochemistry. The ions can be detected with a mass spectrometer and the excited atoms or ions emit characteristic photons, which can be measured with optical emission spectrometry. Alternatively, the sputtered atoms can also diffuse through the plasma and they can be deposited on a substrate, this technique used in materials technology e.g. for the deposition of thin films. Fig. 2.2 shows a schematic overview of the basic processes in a glow discharge.

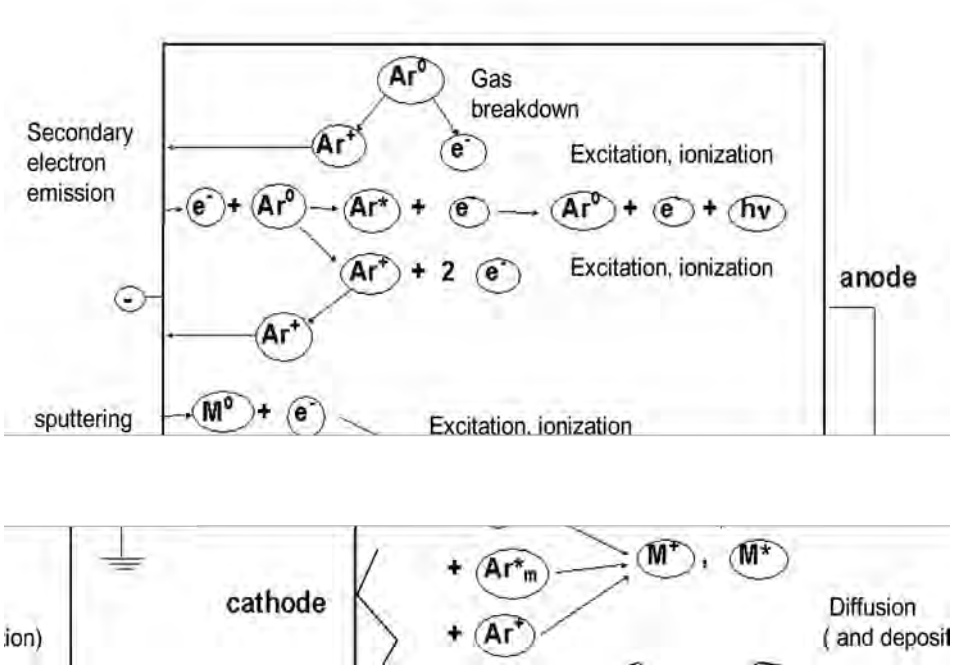

Fig. 2.2 Schematic overview of the basic processes in a glow discharge.

2.3.3 Direct current (DC) glow discharge

Plasma polymerization process takes place usually in a low temperature generated by glow discharge. The space between the electrodes becomes visible when a glow discharge is established; the actual distribution of light in the glow discharge is significant and is dependent on the current-voltage characteristics of the discharge [60].

When a constant potential difference is applied between the cathode and anode, a continuous current will flow through the discharge; giving rise to a direct current (DC) glow discharge. In a DC glow discharge the electrodes play an essential role for sustaining the plasma by secondary electron emission. The potential difference applied between the two electrodes is generally not equally distributed between cathode and anode, but it drops almost completely in the first millimeters in front of the cathode. However, for most of the other applications of DC glow discharges (sputtering, deposition, chemical etching, analytical chemistry etc.), the distance between cathode and anode is generally short. So, normally a short anode zone is present beside cathode dark space and negative glow, where the slightly positive plasma potential returns back to zero at the anode [61].

DC glow voltage can operate over a wide range of discharge conditions. The pressure can vary from below 1 Pa to atmospheric pressure. The product of pressure and distance between the electrodes is a better parameter to characterize the discharge. For instance, at lower pressure, the distance between cathode and anode should be longer to create a discharge with properties comparable to these of high pressure with small distance. The discharge can operate in a rare gas (most often argon or helium) or in a reactive gas (N_2, O_2, H_2, CH_4, SiH_4, SiF_4, etc.), as well as in a mixture of these gases.

2.3.4 Alternating current (AC) glow discharge

The mechanism of AC glow discharge basically depends on the frequency of the excitation. At low frequencies (60 Hz), the system can be looked upon as a DC glow discharge with alternating polarity. By increasing the frequency of the applied voltage, positive ions become immobile, because they can no longer follow the periodic changes in field polarity. At frequencies above 500 KHz, the half - cycle is so short that all electrons and ions stay within the inter-electrode volume. This reduces the loss of charged particles from the system significantly, and regeneration of electrons and ions occurs within the body of the plasma through collisions of electrons with gas molecules. In radiofrequency (RF) plasma (13.56 MHz) therefore, no contact between the electrodes and the plasma is

required. The plasma can be initiated and sustained by external electrodes, at a much lower voltage than is required for maintaining a DC glow discharge [62, 63].

2.4 Deposition of Thin Films by Plasma polymerization

Plasma polymerization is essentially a plasma enhanced chemical vapor deposition process. It refers to the deposition of polymer films due to the excitation of an organic monomer gas and subsequent deposition and polymerization of the excited species on the surface of a substrate. Polymers formed by plasma polymerization are, in most cases, highly branched and highly cross-linking.

In the plasma polymerization process, a monomer gas is pumped into a vacuum chamber where it is polymerized by plasma to from a thin, clear coating. The monomer starts out as a liquid. It is converted to a gas in an evaporator and is pumped into the vacuum chamber. A glow discharge initiates polymerization. The excited electrons created in the glow discharge ionize the monomer molecules. The monomer molecules break a part (fractionate) create free electrons, ions, exited molecules and radicals. The radicals absorb, condense and polymerize on the substrate.

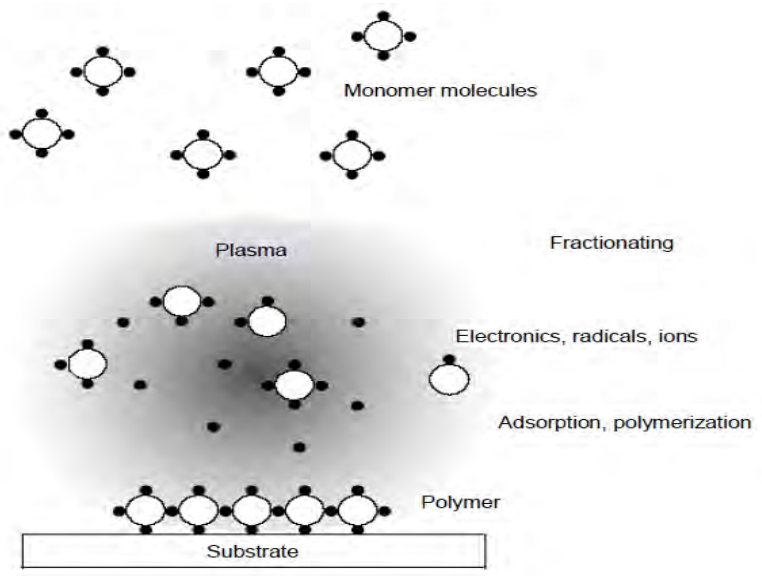

Fig. 2.3 A schematic plasma polymerization configuration.

The electrons and ions crosslink, or create a chemical bond, with the already deposited molecules, creating a harder, denser coating. A schematic plasma polymerization configuration is shown in Fig. 2.3.

The materials obtained by plasma polymerization are significantly different from conventional polymers and also different from most inorganic materials [64]. Hence

plasma polymerization should be considered as a method of forming new types of materials rather than a method of preparing conventional polymers. Comparison of the structures of plasma polymers and conventional polymers is shown in the Fig. 2.4. This polymerization process covers a wide interdisciplinary area of physics, chemistry, science of interfaces and materials science and so on [65]. Thus plasma polymerization is a versatile technique for the deposition of films with functional properties suitable for a wide range of modern applications

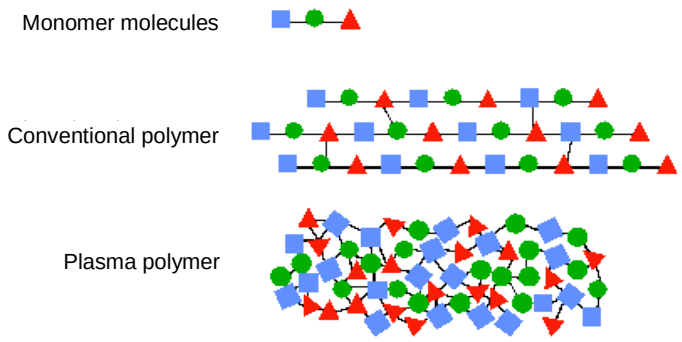

Fig. 2.4 Comparison of the structures of plasma polymers and conventional polymers.

Though, same monomer is used for polymerization, polymers formed by plasma polymerization show distinguished chemical composition and chemical and physical properties from those formed by conventional polymerization. To appreciate the uniqueness of plasma polymerization, it is useful to compare the steps necessary to obtain a good coating by a conventional coating process and by plasma polymerization. Coating a certain substrate with a conventional polymer, at least several steps are required (1) synthesis of a monomer, (2) polymerization of the monomer to form a polymer, (3) preparation of coating solution, (4) cleaning, (5) application of the coating, (6) drying of the coating and (7) curing of the coating. Polymers formed by plasma polymerization aimed at such a coating are in most cases branched and cross-linked [66-68]. Such polymers also depend on (1) synthesis of a monomer, (2) creation of plasma medium, (3) polymerization of the monomer to form a polymer, (4) cleaning, (5) application of the polymer film, and (6) curing of the film.

Among the many types of electric discharge, glow discharge is by far the most frequently used in plasma polymerization. Some other models were proposed based on ion or electron bombardment. The role of ion bombardment is pointed to a competition between etching and deposition processes in plasma polymerization was given by Yasuda.

2.5 Different Types of Glow Discharge Reactors

The plasma polymers are strictly system dependent. The most widely used reactor configurations for plasma polymerization can be broadly divided into three classes, namely, reactors with internal electrodes, reactors with external electrodes and reactors without electrodes [69].

(i) Reactors with internal electrodes

Reactors with internal electrodes have different names, e.g., flat bed, parallel plates, planar, diode etc. Their main features are power supply, coupling system, vacuum chamber, electrode, and eventually one or more substrate holders. Among the internal electrode arrangement, a bell-jar type reactor with parallel plate metal electrodes is most frequently used, by using AC (1-50 kHz) and RF fields for plasma excitation. The vacuum chamber can be made either of glass or of conducting materials, such as metal, to better shield from external sources. Pump-out is usually is at the base of the bell-jar. Monomer injection may be at the base or at some other convenient position over the electrodes or through the centre of upper electrode. The electrodes may be oriented horizontally or vertically as shown in Fig. 2.5. For a DC or low frequency discharges, internal electrodes are required. A common set up is to place circular or square electrodes in a bell jar. If the electrodes diameter is relatively large and they are placed relatively close together a large zone of uniform electric field is created. For this reason this geometry is favored for industrial application.

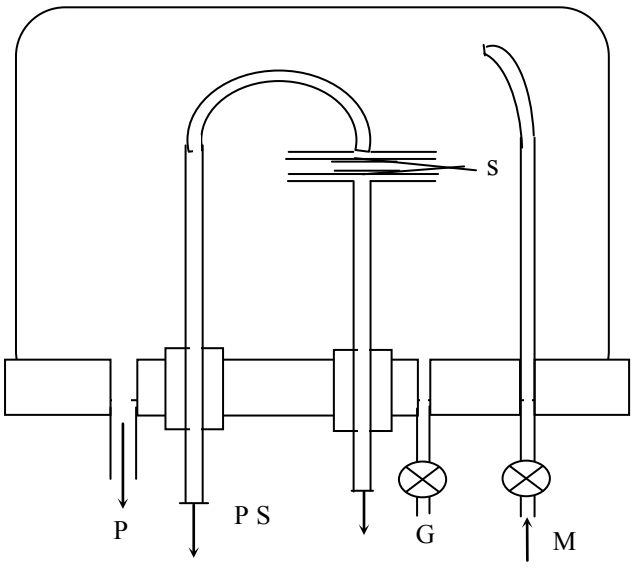

P, Pumps
PS, Power Supply
S, Substrate
M, Feed gas inlet
G, Vacuum gauge
A, Resonant Cavity
C, Tubular reactor

Symbols for fig: (2.5, 2.6, 2.7)

Fig. 2.5 Bell-jar reactor with parallel plate metal electrodes (internal reactor).

(ii) Reactors with external electrodes

External electrode reactors can be either capacitive or inductively coupled. In this case, power is transmitted from the power supply to the gas by a capacitor and coil respectively. Insulating tubular reactors are usually utilized (glass, quartz or alumina for reactor materials). Inductively coupled tubular reactors, when operating at low pressure ($p<<1$ Torr), are not uniformly coupled to the power supply; however, coupling uniformly increases with increasing working pressure. Fig. 2.6 shows a block diagram of an external electrodes reactor.

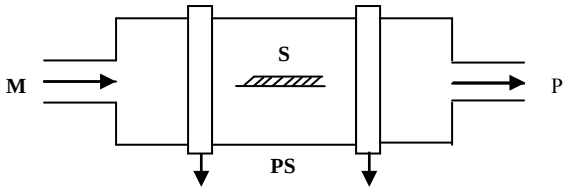

Fig. 2.6 External electrodes reactor

Glow discharge reactor is the important part of plasma polymerization system. Because reactor geometry influences the extent of charge particle bombardment on the growing films which affects the potential distribution in the system.

(iii) Electrodeless microwave (MW) or high frequency(HF) reactors

The name electrode-less reactor implies that no impurities can be sputtered off and incorporated into the growing films in these reactors, microwave power systems characterized by tubular or Pyrex reactors and by a resonant cavity coupled with power supply in the GHz region (typically 2.45GHz). The plasma is generated in the resonant cavity and the polymer is generally collected outside the glow region. Fig. 2.7 represents an electrode less microwave reactor.

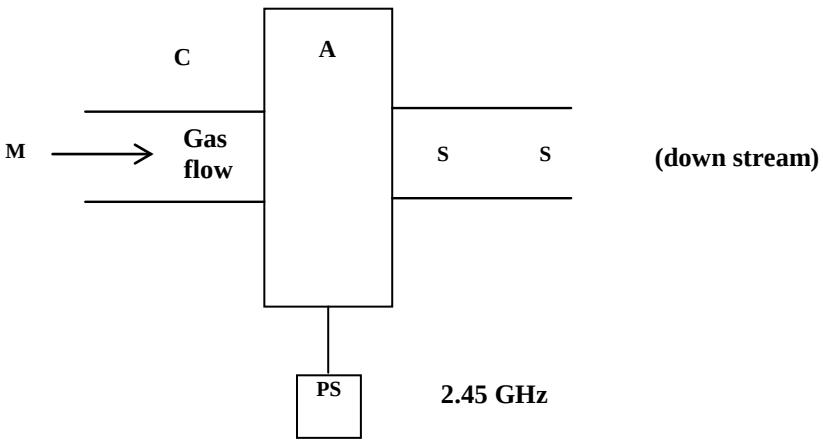

Fig. 2.7 Electrode less microwave reactor.

2.5.1 Capacitively coupled glow discharge

If an AC voltage (up to kHz) is used, the discharge is still basically of a DC type and each electrode really acts as a cathode and anode alternatively. The frequencies generally used for the alternating voltages are typically in the RF range. Capacitively coupled (CC) discharge can also be generated by alternating voltages in another frequency range. Therefore, the term AC discharges as opposite to DC discharges might be more appropriate. The term ‘ capacitively coupled’ refers to the way of coupling the input power into the discharges i.e. by means of two electrodes and their sheaths forming a kind of capacitor. The CC RF discharges which also results from the differences in mass between electrons and ions, is the phenomenon of self bias. The self bias or DC bias is formed when (i) both electrodes differ in size and (ii) a coupling capacitor is present between the RF power supply and the electrode or when the electrode is non conductive. When a certain voltage is applied over the capacitor formed by the electrodes, the voltage over the plasma will initially have the same value as the applied voltage.

When the applied voltage is initially positive the electrons will be accelerated toward the electrode. Hence the capacitor will be rapidly charged up by the electron current and voltage over the plasma will drop. When the applied potential changes the polarity after one half cycle, the voltage over the plasma changes with the same amount. The capacitor will now be charged up the ion current and the voltage over the plasma will, therefore drop as well, this second drop is pronounced, because of much lower mobility of the ions and hence the lower ion flux. At the next half cycle, the applied potential, and hence also the voltage over the plasma, again changes polarity. The voltage over the plasma drops again more rapidly, because the capacitor is again charged up by the electron flux. This process repeats itself, until the capacitor is finally sufficiently negatively charged so that the ion and electron fluxes integrated over one RF -cycle, are equal to each other. This results in a time-averaged negative DC bias at the RF powered electrode.

Because of negative DC bias, the ions continue to be accelerated toward the RF-powered electrode, and they can, therefore cause sputtering of the RF-electrode material. In fact, the CC RF discharge often resembles a DC glow discharge with a similar subdivision in different regions, similar operating conditions and with similar processes occurring in the plasma.

In the current research, capacitively coupled reactor (glow discharge plasma) system was used for the formation of thin films. Fig. 2.8 represents a scheme of a capacitively coupled parallel plate plasma reactor, similar to the bell jar reactor. The possible species present when the plasma is generated are also drawn. Usually plasma reactor can use internal or external electrodes. This model uses internal electrodes.

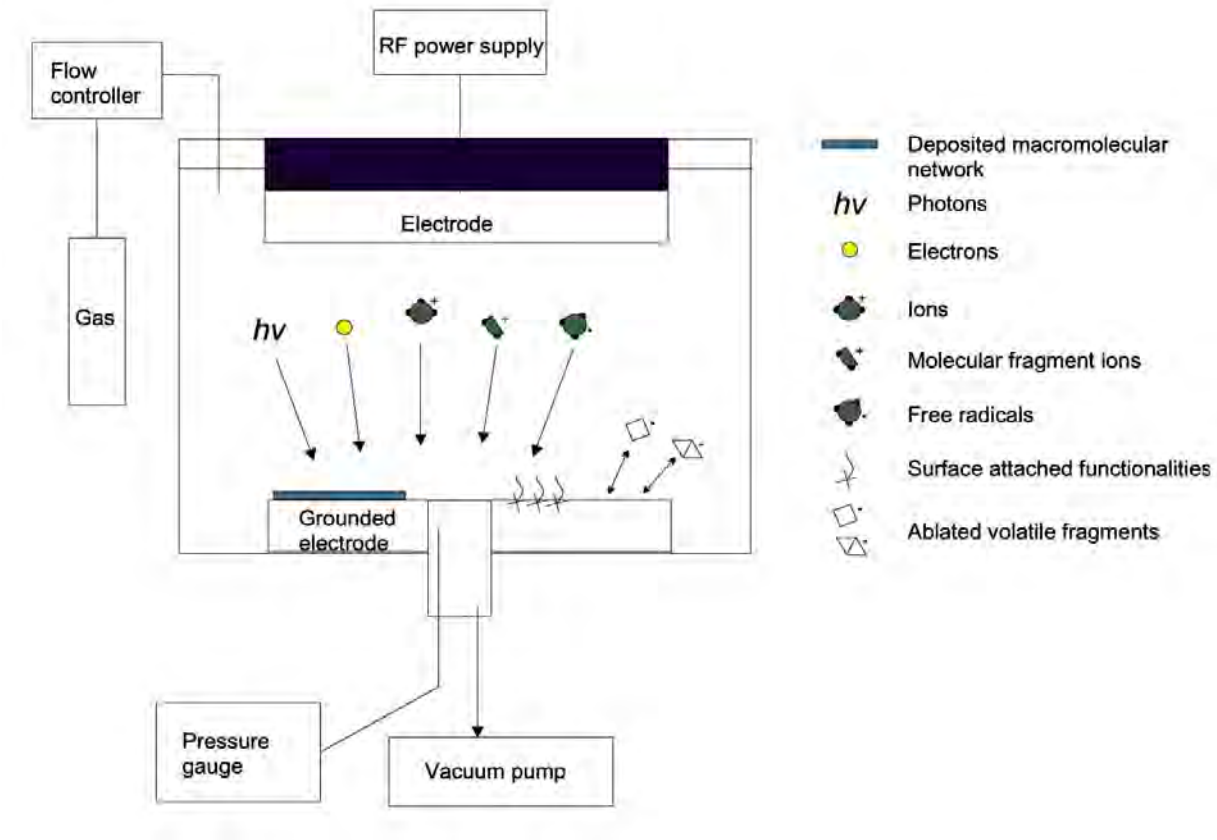

Fig. 2.8 A schematic diagram of the capacitively coupled parallel plate plasma reactor.

The vacuum chambers can be made either of glass or of conductive materials, such as metal. In the case of bell-jar reactors, no particular care is taken for the grounded electrode apart from its area. On the contrary, the design and arrangement of the cathode require special attention: a metallic shield surrounding the electrode highly improves the glow confinement inside interelectrodic space; electrode material and area greatly affect the extension of sputtering on the target.

2.5.2 Inductively coupled glow discharge

In the inductively coupled (IC) source, the plasma chamber is mostly also surrounded by a coil. Simply speaking, the RF currents in the coil generate an RF magnetic flux, which penetrates the plasma region.

Following Faraday's law:

$$\nabla XE = -\partial B / \partial t$$

The time varying magnetic flux density induces a solenoidal RF electric field, which accelerates the free electrons and sustains the discharge [70].

Basically, two different coil configurations can be distinguished in inductive discharges for processing applications, i.e. cylindrical and planar. In the first configuration, a coil is wound around the discharge chamber, as a helix. In the second configuration, which is more commonly used for materials processing, a flat helix or spiral is wound from near the axis to near the outer radius of the discharge chamber, separated from the discharge region by a dielectric. Advantages of the latter are reduced plasma loss and better ion generation efficiency; disadvantage is the higher sputter contamination, UV-damage and heating of neutrals at the substrate. Multipole permanent magnets can be used around the process chamber circumference to increase radial plasma uniformity. The planar coil can also be moved close to the wafer surface, resulting in near-planar source geometry, having good uniformity properties, even in the absence of multipole confinement.

It should be mentioned that the coupling in IC plasma is generally not purely inductive, but has a capacitive component as well, through the wall of the reactor. Indeed, when an inductive coupling is used, deposition on the wall is often observed to follow a pattern matching the shape of the coil. This is an induction of localized stronger electric fields on the walls, showing that the coupling is at least partly capacitive through the walls of the reactor.

It is mentioned that inductive coupled plasma are not only used as materials processing discharges, but they are also applied in other fields. So, IC plasmas are the most popular plasma sources in plasma spectrochemistry.

2.6 Growth Mechanism in Plasma Polymerization

The term "plasma polymerization" is widely used to denote the process of forming high molecular weight products in electrical discharges. Over the past 40 years plasma polymerization has become a very useful method for surface modification and deposition of various materials. Plasma polymerization was first observed in 1874 developed at the end of the 1950,s and beginning of the 1960s in connection with the development of electronics, where plasma polymer films were investigated systematically. In those years plasma polymerization obtained the rapid advancement in

Japan, Germany and U.K.

The mechanism of reaction by which plasma polymerization occurs is quite complex and cannot be specifically described for the general case. Operational parameters such as monomer flow rate, pressure frequency, and power affect the deposition rate and structure of the plasma film. The electrons or atoms generated by partial ionization of the molecules are the principle sources for transferring energy from the electric field to the gas in all glow discharges [71].

In plasma polymerization, free electrons gain energy from an imposed electrical field and then transfer the energy to neutral gas molecules, which lead to the formation of many chemically reactive species. By applying greater power to the RF source, the energy per unit mass of the monomer is increased and may bring about changes in the fragmentation process. As a result, free radicals may become entrapped in the plasma-polymerized film and increase in concentration with increasing RF power. The deposition of polymer films in low-pressure plasma is a complex phenomenon involving reactions, which occur both in the plasma phase and at the surfaces bounding the plasma.

The study of plasma polymerization kinetics is commonly employed to elucidate polymerization mechanisms. With this background a comparison of the polymer formation rates of various monomers by plasma polymerization would provide an overview of the kind of reaction mechanism responsible for plasma polymerization.

The probable chain growth polymerization is represented by

$$M_n^* + M \rightarrow M^*_{n+1}$$

Where M_n^* is the reactive chain carrying species and M is the monomer molecules. But Yasuda and Lamaze [72], on the basis of their observation on plasma polymerization ruled out the chain growth polymerization. The rapid step-growth mechanism is very likely to be the reaction in plasma polymerization and this reaction is expressed as:

$$[M_m^* + M_n^* \rightarrow M_{m+n}^*] \times N$$

Where, N represents the number of repetitions of similar reactions. In this case, the reaction occurs between molecules.

In case of difunctional reactive species, $*M*$ the overall polymerization can be represented by $n*M* \rightarrow *(M_n)*$

If the reactive species are monofunctional *(M*)*, such as free radical *R**, the reaction is given by $M_m^* + M_n^* \rightarrow M_{m+n}$

This is essentially a termination process that occurs in free radical polymerization and does not contribute without additional elementary steps. Yasuda and Lamaze pointed out that the reactivation of the product of an elementary reaction was bound to occur in plasma.

The overall polymerization mechanism based on the rapid step-growth principle is shown in Fig. 2.9. The figure shows the overall reaction, which contains two major routes of rapid step-growth. Cycle-1 is via the repeated activation of the reaction products from mono-functional activated species, Cycle-2 is via di-functional or multifunctional activated species.

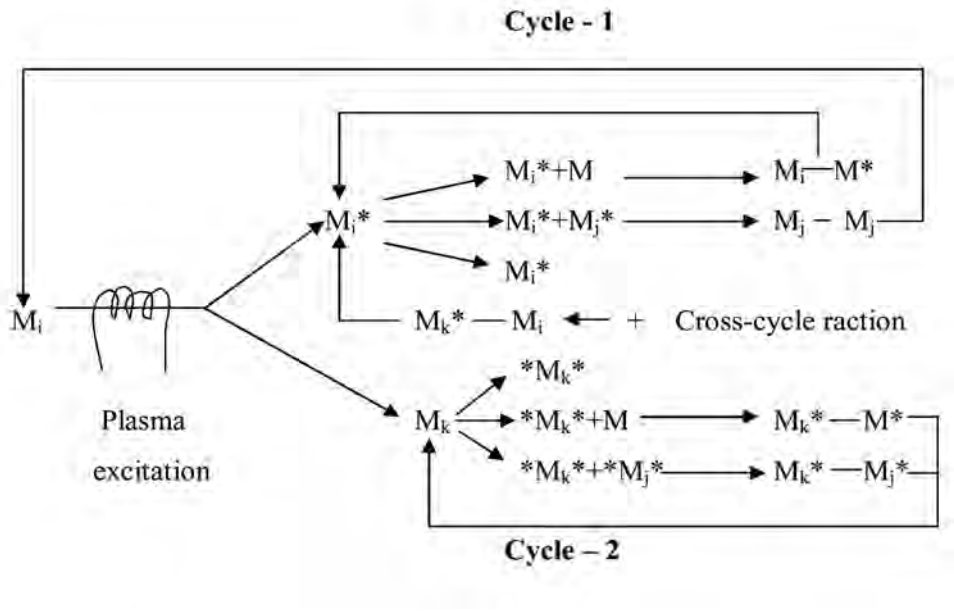

Fig. 2.9 Schematic representation of bicycle step growth mechanism of plasma polymerization.

Here, M_x refers to neutral species that can be original monomer molecule or any of the dissociation products including some atoms, such as hydrogen, chlorine, fluorine and others; M* activated species; **M** difunctional activated species and the subscripts i, j, k indicate the difference in the size of the species involved (i=j is possible, thus i=j=1 for initial monomer.)

One of the most important features of plasma polymers is that a large quantity of free radicals is often trapped in the polymer. Although, the amount varies with the type of monomer and the conditions of the plasma polymerization, it is safe to consider that

plasma polymers contain a certain amount of trapped free radicals. Therefore, the free radicals play important role in plasma polymers.

2.7 Advantages and Disadvantages of Plasma Polymerization

The plasma polymerization process offers several advantages over conventional polymer synthesis. Several advantages of plasma polymerized films are given below:

- The main advantage of plasma polymerization is that it can occur at moderate temperature compared to conventional chemical reaction.
- Time saved in the coating and curing processes and in loading, unloading and transferring parts.
- The ability to surface modify almost any substrates (glass, polymers, metals, etc.) without affecting bulk properties.
- Plasma-polymerized films are generally chemically inert, insoluble, mechanically tough, and thermally stable.
- Plasma polymer films can be easily produced with thickness of 500 A° to 1 μm.
- Good surface uniformity and relatively easy procedure.
- Ultra thin 'Pinhole' free films may be prepared.
- Smooth, clear coating is obtained.
- Polymerization may be achieved without the use of solvent.
- Plasma polymerization is usually reliable, reproducible, relatively inexpensive, and applicable to different sample geometries as well as different materials such as metals, polymers, ceramics, and composite [73].
- Plasma treatment can result in changes of a variety of surface characteristics, for example, chemical, tribological, electrical, optical, biological, and mechanical. Proper applications yield dense and pinhole free coatings with excellent interfacial bonds due to the graded nature of the interface [74].
- Plasma processing can provide sterile surfaces and can be scaled up to industrial production relatively easily. On the contrary, the flexibility of non-plasma techniques for different substrate materials is smaller [75].

- Plasma techniques are compatible with masking techniques to enable surface patterning, a process that is commonly used in the microelectronics industry [76].

The main disadvantages of the plasma polymerization are as follows:

- Low deposition rates. Only very thin films can be deposited economically on high production items.
- The process doesn't discriminate against what is coated. Everything in the coating range of the polymerization process is coated, or can become part of the coating.
- The process, used in mass production, is still in its infancy. More capabilities will likely be available as improvements to the process occur.
- The chemistry produced on a surface is often not well defined, sometime a complex branched hydrocarbon polymer will be produced,
- Contamination can be a problem and care must be exercised to prevent extraneous gases, grease films, and pump oils from entering the reaction zone.
- Costly to retrofit equipment.
- Polymerized coatings have low abrasion resistance.

In spite of the drawbacks, plasma polymerization is far well developed process for many types of modification that simply cannot be done by any other technique.

2.8 Advantages of Plasma Polymers

The specific advantages of plasma-deposited films are summarized below:

i) **Conformal:** Because of the penetrating nature of low-pressure gaseous environment in which mass transport is governed in part by both molecular (line of sight) diffusion and convective diffusion, complex geometry shapes can be treated.

ii) **Pinhole-free:** Under common reaction conditions, the plasma film appears to coalesce during formation into a uniform over layer free of voids. Transport property and electrical property studies suggest this continuous barrier structure.

iii) **Barrier film:** The pinhole-free and dense, cross-linked nature of these films suggests they have potential as barrier and protective films.

iv) **Unique substrates:** Plasma-deposited polymeric films can be placed upon almost any solid substrate including metals, ceramics, and semiconductors. Other surface

grafting or surface modification technologies are highly dependent upon the chemical nature of the substrate.

v) **Good adhesion to the substrate:** The energetic nature of the gas phase species in the plasma reaction environment can induce some mixing and implantation between the film and the substrate.

vi) **Unique film chemistry:** The chemical structure of the polymeric over layer films produced by RF plasma deposition cannot be synthesized by conventional organic chemical methods. Complex gas phase molecular rearrangements account for these unique surface chemical compositions.

vii) **Easy preparation:** Once the apparatus is set up and optimized for a specific deposition, treatment of additional substrates is rapid and simple. Through careful control of the polymerization parameters, it is possible to tailor the films with respect to specific chemical functionality, thickness, and other chemical and physical properties [77, 78].

2.9 Applications of Plasma-polymerized Organic Thin Films

Plasmas are used in a large number of application fields. The most important application is probably in the microelectronics industry and in materials technology, for surface treatment, etching of surfaces (e.g., for the fabrication of integrated circuits), deposition of thin protective coatings. Applications of plasma-polymerized (PP) films are associated with biomedical uses, the textile industry, electronics, optical applications, chemical processing and surface modification [79-80]. Typical uses of PP films are listed below:

- The PP films are used in producing integrated circuits, amorphous semiconductors, amorphous fine ceramic etching.
- These are used in fabricating insulator, thin film dielectrics, separation membrane for batteries in electrical devices.
- PP thin films are used as coating component of protective layers, hydrophobic layers, insulating layers etc.
- In chemical processing the PP films can be applied in reverse osmosis membrane, perm selective membrane, gas-separation membrane, lubrication, insolubilization.

- In electronic industry (quartz manufacturers), and in environmental simulation (UV-radiation, ozone) PP films are used as artificial aging components.
- PP films can be used for surface modification such as in adhesive improvement, protective coating, and abrasion resistant coating, anti-crazing and scratching.
- The PP films are useful in anti-reflection coating, anti-dimming coating, improvement of transparency, optical fiber, optical wave-guide laser and optical window, contact lens.
- In textile industries, it has frequent use in anti-flammability, anti-electrostatic treatment, dying affinity, hydrophilic improvement, water repellence, shrink-proofing.
- In biological science the films are useful in immobilized enzymes, organelles and cells, sustained release of drugs and pesticides, sterilization and pasteurization, artificial kidney, blood vessel [81].

2.10 Scanning Electron Microscopy

The Scanning Electron Microscopy **(**SEM) is one of the techniques used to obtain information of surface structure of PP thin films. The surface of PP thin films is smooth, pinhole free and highly cross-linked. This technique has also been used to determine the granular size of powder particles, to evidence the presence of powder particles in thin films, to see the uniformity and defects of the films produced in plasma and to determine the location of fracture in adhesion studied by means of the lap-shear test [82, 83]. In this work, the surface structure of PPFDH thin film has been investigated by SEM.

2.11 Energy-Dispersive Analysis of X-ray

Energy-Dispersive Analysis of X-ray (EDAX) is an emerging, analytical technique employed for the elemental analysis or chemical characterization of a sample. It is one of the variants of X-ray fluorescence spectroscopy which relies on the investigation of a sample through interactions between electromagnetic radiation and matter. Its characterization capabilities are due to the fundamental principle that each element has a unique atomic structure allowing X-rays that are characteristic of an element's atomic structure to be identified uniquely from one another.

To stimulate the emission of characteristic X-rays from a specimen, a high-energy beam of charged particles such as electrons or protons, or a beam of X-rays is focused into the

sample are to be studied. At rest, an atom within the sample contains ground state (or unexcited) electrons in discrete energy levels or electron shells bound to the nucleus. When the beam is incident on the atom may excite an electron in an inner shell, and ejecting it from the shell while creating an electron hole conceptual particle. An electron from an outer, higher-energy shell then fills the hole, and the difference in energy between the higher-energy shell and the lower energy shell may be released in the form of an X-ray. The number and energy of the X-rays emitted from a specimen can be measured by an energy-dispersive spectrometer. As energy of the X-rays are the characteristic of the difference in energy between the two shells, and of the atomic structure of the element, from which they were emitted, allows the elemental composition of the specimen. Basically the EDAX is an additional equipment to scanning electron microscopy which have four primary components, namely: the beam source, the X-ray detector, the pulse processor and the analyzer. Scanning electron microscopes are equipped with a cathode and magnetic lenses to create and focus a beam of electrons, and since the 1960s they have been equipped with elemental analysis capabilities. A detector is used to convert X-ray energy into voltage signals; this information is sent to a pulse processor, which measures the signals and passes them onto an analyzer for data display and analysis.

2.12 Fourier Transform Infrared Spectroscopy

Spectroscopy is the study of the interaction of electromagnetic (EM) radiation with matter. There are many forms of spectroscopy, each contributing useful information to identify substances and to determine various characteristics of their structure. Atoms and molecules can absorb electromagnetic radiation, but only at certain energies (wavelengths). The diagram in Fig. 2.10 illustrates the relationships between different energy levels within a molecule. The three groups of lines correspond to different electronic configurations. The lowest energy, most stable electron configuration is the ground state electron configuration. Certain energies in the visible (Vis) and ultraviolet (UV) regions of the spectrum can cause electrons to be excited into higher energy orbitals; some of the possible absorption transitions are indicated by the vertical arrows. Very energetic photons (UV to X-ray region of the spectrum) may cause an electron to be ejected from the molecule (ionization). Photons in the infra-red (IR) region of the spectrum have much less energy than photons in the visible or UV regions of the electromagnetic spectrum. They can excite vibrations in molecules. There are many

possible vibrational levels within each electronic state. Transitions between the vibrational levels are indicated by the vertical arrows on the left side of the diagram [84-86].

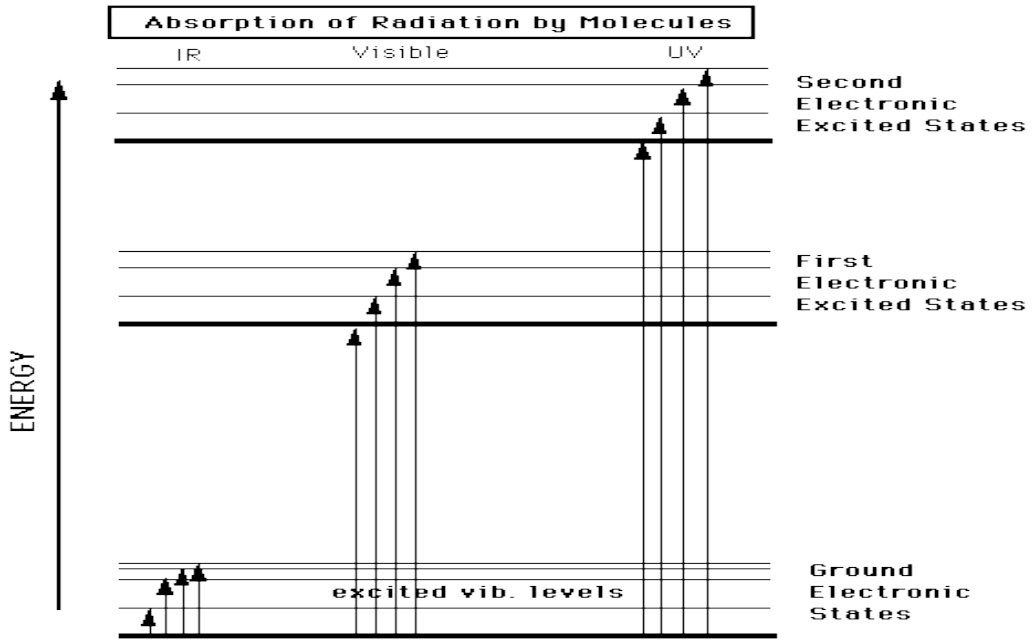

Fig. 2.10 Energy Levels in Molecules.

IR radiation does not have enough energy to induce electronic transitions as seen with UV. Absorption of IR is restricted to compounds with small energy differences in the possible vibrational and rotational states. For a molecule to absorb IR, the vibrations or rotations within a molecule must cause a net change in the dipole moment of the molecule. The alternating electrical field of the radiation (since electromagnetic radiation consists of an oscillating electrical field and an oscillating magnetic field, perpendicular to each other) interacts with fluctuations in the dipole moment of the molecule. If the frequency of the radiation matches the vibrational frequency of the molecule then radiation will be absorbed, causing a change in the amplitude of molecular vibration [87].

Molecular vibrations

The positions of atoms in a molecule are not fixed; they are subject to a number of different vibrations. Vibrations fall into the two main categories of stretching and bending.

Stretching: Change in inter-atomic distance along bond axis

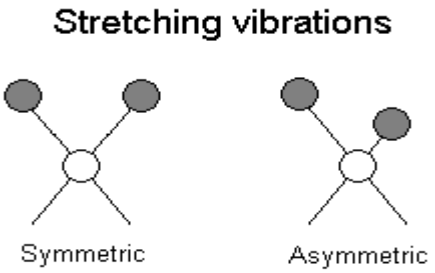

Bending: Change in angle between two bonds. There are four types of bend:

- Rocking
- Scissoring
- Wagging
- Twisting

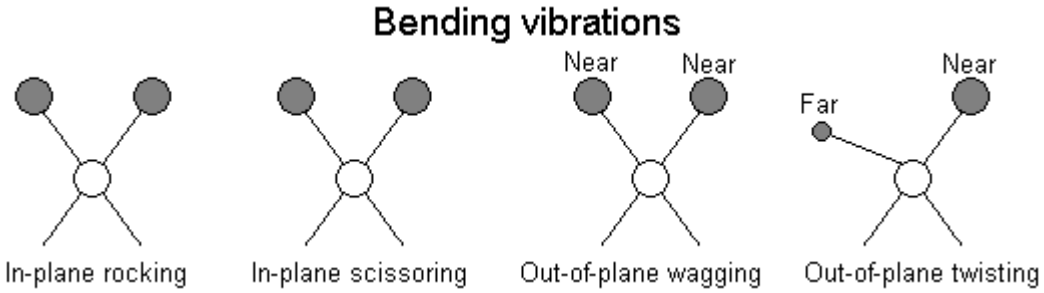

Fig. 2.11 Different kinds of molecular vibrations.

The Effects of Mass on Frequency

Assignments for stretching frequencies can be approximated by the application of Hooke's law. In the application of the law two atoms and there connecting bonds are treated as a simple harmonic oscillator joined by a spring. Following equation derived from Hooke's law states the relationship between frequency of oscillation, atomic masses, and the force constant of the bond.

$$\bullet = \frac{1}{2\pi c}\left[\frac{f}{\frac{MxMy}{Mx+My}}\right]^{1/2}$$

Where • = the vibrational frequency (cm^{-1}),

c = velocity of light (cm/sec)

f = force constant of bond (dynes/cm)

M_x and M_y = mass of atom x and atom y, respectively.

The value of 'f' is approximately 5×10^5 dynes per cm for single bonds and approximately 2 and 3 times of this value for double bonds and triple bonds, respectively.
There are no rigid rules for interpreting an IR spectrum. Certain requirements, however, must be met before an attempt is made to interpret a spectrum.

i) The spectrum must be adequately resolved and of adequate intensity.
ii) The spectrum should be that of a reasonable pure compound.
iii) The spectrometer should be calibrated so that the bands are observed at their proper frequencies or wavelengths. Proper calibration can be made with reliable standards.
iv) The methods of sample handling must be specified. If a solvent is employed, the solvent's concentration and cell thickness should be indicated.

2.13 Ultraviolet-Visible Spectroscopy

Molecular absorption in the UV-vis region of the electromagnetic spectrum depends on the electronic structure of the molecule. Absorption of energy is quantized, resulting in the elevation of electrons from orbital in the ground to higher energy orbital in an excited state. For many electronic structures, the absorption does not occur in the readily accessible portion of the ultraviolet region. The most important application of UV-vis spectroscopy is to determine the presence, nature and extend of conjugation present in the material. Increasing conjugation length generally moves the absorption spectrum to longer wavelength and finally into the visible region.

During promotion, the electron moves from a given vibrational and rotational levels within one electronic mode to some other vibrational and rotational levels within the next electronic mode. Thus there will be a large number of possible transitions responsible for change in electronic, rotational and vibrational levels. Hence a large number of close bands are formed. The total energy of the molecule is the sum of its electronic energy, vibrational energy and rotational energy. The magnitude of these energies decreases in the following order: $E_{elec} > E_{vib} > E_{rot}$. Fig. 2.12 shows the vibrational and rotational energy levels of absorbing materials.

The relationship between the energy absorbed in an electronic transition and the frequency (•) of radiation producing the transition is • E=h•, where h is the Planck's constant, • E is the energy absorbed in an electronic transition by a molecule from a low energy state (ground state) to a higher energy state (excited state). The energy absorbed depends on the

energy difference between the ground state and excited state. The smaller the energy difference, the longer the wavelength of absorption. In most cases, several transitions occur resulting in the formation of several bands.

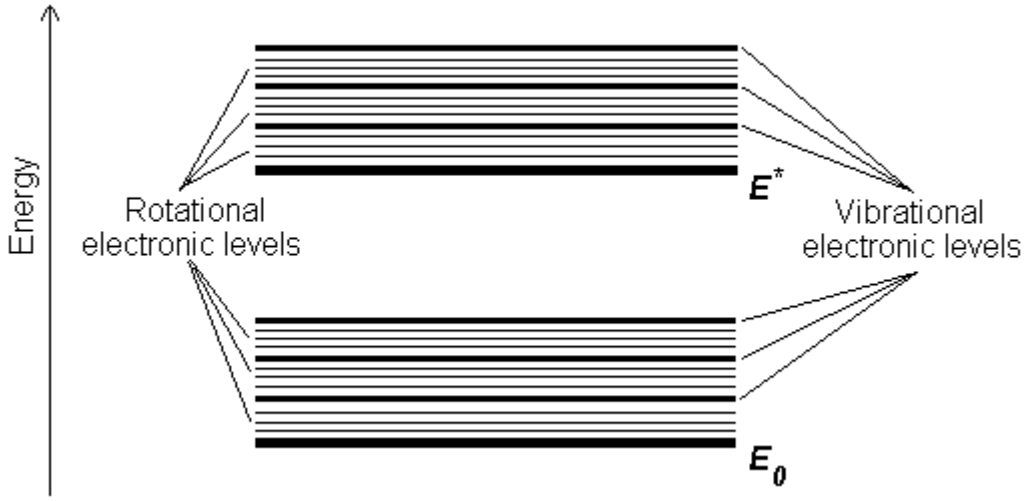

Fig. 2.12 Vibrational and rotational energy levels of absorbing materials.

2.13.1 Different types of transitions

There are several kinds of transitions when a molecule absorbs UV-Vis light; its electrons are promoted from a bonding to an anti-bonding orbital. Fig. 2.13 shows the various orbital and probable transitions. The absorption of UV or Vis radiation corresponds to the excitation of outer electrons.

There are three types of electronic transition which can be considered;

i. Transitions involving π, • and *n* electrons,
ii. Transitions involving charge-transfer electrons,
iii. Transitions involving *d* and *f* electrons.

Possible *electronic* transitions of π, σ, and *n* electrons are given below:

$\sigma \rightarrow \sigma^*$ Transitions

An electron in a bonding σ orbital is excited to the corresponding antibonding σ^* orbital. The energy required is large. For example, methane (which has only C-H bonds, and can only undergo $\sigma \rightarrow \sigma^*$ transitions) shows an absorbance maximum at 125 nm. Absorption maxima due to $\sigma \rightarrow \sigma^*$ transitions are not seen in typical UV-Vis. spectra (200 - 800 nm).

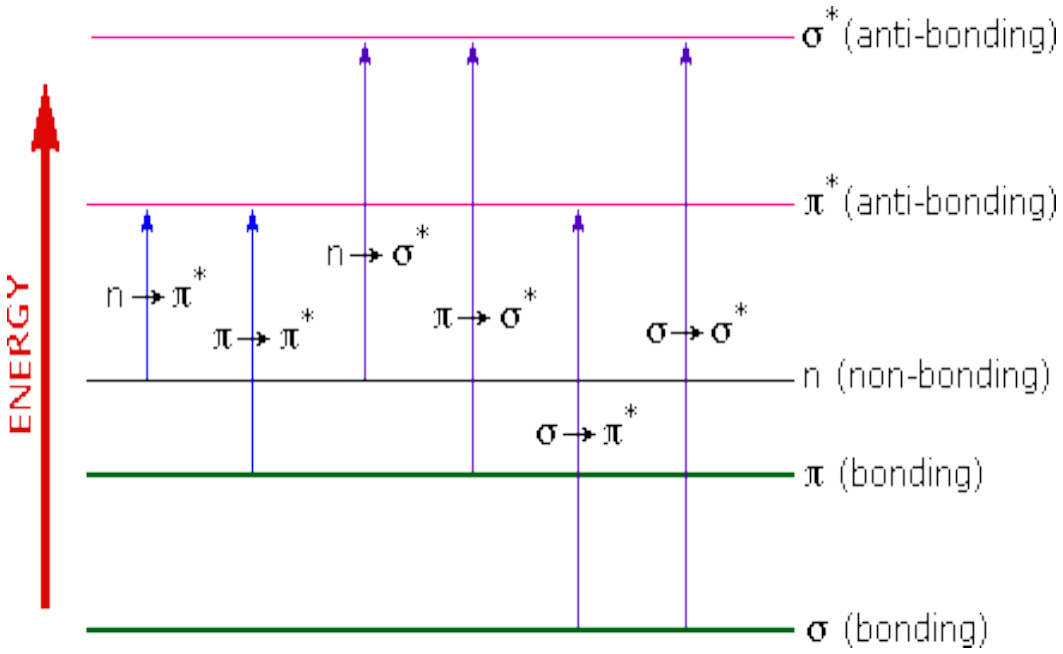

Fig. 2.13 Different electronic transitions in the UV-Visible region.

$n \rightarrow \sigma^*$ Transitions

Saturated compounds containing atoms with lone pairs (non-bonding electrons) are capable of $n \rightarrow \sigma^*$ transitions. These transitions usually need less energy than $\sigma \rightarrow \sigma^*$ transitions. They can be initiated by light whose wavelength is in the range 150 - 250 nm. The number of organic functional groups with $n \rightarrow \sigma^*$ peaks in the UV region is small.

$n \rightarrow \pi^*$ and $\pi \rightarrow \pi^*$ Transitions

Most absorption spectroscopy of organic compounds is based on transitions of n or π electrons to the π^* excited state. This is because the absorption peaks for these transitions fall in an experimentally convenient region of the spectrum (200 - 700 nm). These transitions need an unsaturated group in the molecule to provide the π electrons. Molar absorbtivities from $n \rightarrow \pi^*$ transitions are relatively low, and range from 10 to100 L mol^{-1} cm^{-1} . $\pi \rightarrow \pi^*$ transitions normally give molar absorbtivities between 1000 and 10,000 L mol^{-1} cm^{-1}. The solvent in which the absorbing species is dissolved also has an effect on the spectrum of the species. Peaks resulting from $n \rightarrow \pi^*$ transitions are shifted to shorter wavelengths (*blue shift*) with increasing solvent polarity. This arises from increased solvation of the lone pair, which lowers the energy of the *n* orbital. Often (but *not* always), the reverse (i.e. *red shift*) is seen for $\pi \rightarrow \pi^*$ transitions. This is caused by attractive polarisation forces between the solvent and the absorber, which lower the energy levels of

both the excited and unexcited states. This effect is greater for the excited state, and so the energy difference between the excited and unexcited states is slightly reduced - resulting in a small red shift. This effect also influences $n \rightarrow \pi^*$ transitions but is overshadowed by the blue shift resulting from solvation of lone pairs.

2.13.2 The Absorption Law

Two empirical laws have been formulated about the absorption intensity. Lambert's law states that the fraction of the incident light absorbed depends on the intensity of the source. Beer's law states that the absorption is proportional to the number of absorbing molecules [88]. For most spectra the solution obeys Beer's law. This is only true for dilute solutions. Combining these two laws gives the Beer-Lambert law.

$$I = I_0 e^{-\alpha d} \quad \text{..... (2.1)}$$

$$\log_e(\frac{I_0}{I}) = \alpha d \quad \text{.....(2.2)}$$

Where I_0 is the intensity of the incident radiation, I is the intensity of the transmitted radiation, d is the path length of the absorbing species i.e. thickness and • is the absorption co-efficient. The absorption spectrum can be analyzed by Beer-Lambert law, which governs the absorption of light by the molecules. It states that "When a beam of monochromatic radiation passes through a homogeneous absorbing medium then the rate of decrease in intensity of electromagnetic radiation in UV-vis region with thickness of the absorbing medium is proportional to the intensity of incident radiation". The intensity of transmittance I, is expressed as the inverse of intensity of absorbance. The values • can be calculated from the absorption data using the relation (2.3) [89, 90] as,

$$\alpha = \frac{2.303A}{d} \quad \text{..... (2.3)}$$

where $A = \log_{10}(\frac{I_0}{I})$ is the Absorbance.

The extinction co-efficient K in terms of • can be given by,

$$K = \frac{\alpha\lambda}{4\Pi} \text{ ---------- (2.4)}$$

where • is the wavelength.

2.13.3 Direct and Indirect optical transitions

In solid state physics and related applied fields, the band gap, also called an energy gap or stop band, is a region where a particle or quasi-particle is forbidden from propagating. For insulators and semiconductors, the band gap generally refers to the energy difference between the top of the valence band and the bottom of the conduction band. Fundamental absorption refers to the annihilation or absorption of photons by the excitation of an electron from the valence band up into the conduction band, leaving a hole in the valence band. Both energy and momentum must be conserved in such a transition.

In the case of an indirect-band gap semiconductor, the minimum energy in the conduction band and the maximum energy in the valence band occur at different values of crystal momentum. Photon energies much larger than the forbidden gap are required to give direct transitions of electrons from the valence to the conduction band. However, transitions can occur at lower energies by a two-step process involving not only photons and electrons but also a third particle, a phonon.

To estimate the nature of absorption a random phase model is used where the k momentum selection rate is completely relaxed. The integrated density of states *N (E)* has been used and defined by

$$N(E) = \int_{-\infty}^{+\infty} g(E)dE \quad \text{……..} \text{……(2.5)}$$

The density of states per unit energy interval may be represented by

$$g(E) = \frac{1}{V}\sum \delta(E - E_n)$$

where V is the volume, E is the energy at which $g(E)$ is to be evaluated and E_n is the energy of the n^{th} state.

If $g_v \propto E^p$ and $g_c \propto (E\text{-}E_{opt})^q$, where energies are measured from the valance band mobility edge in the conduction band (mobility gap), and substituting these values into an expression for the random phase approximation, the relationship obtained

$\bullet^2 I_2(\bullet) \propto (h\bullet - E_0)^{p+q+1}$, where $I_2(\bullet)$ is the imaginary part of the complex permittivity. If the density of states of both band edges is parabolic, then the photon energy dependence of the absorption becomes

$$\bullet h\bullet \propto \bullet^2 I_2(\bullet) \propto (h\bullet - E_{opt})^2.$$

So for higher photon energies the simplified general equation which is known as Tauc relation is,

$$\bullet h\bullet = B(h\bullet - E_{opt})^n \quad \ldots\ldots\ldots\ldots\ldots\ldots\ldots\ldots\ldots\ldots\ldots\ldots\ldots\ldots (2.6)$$

where $h\bullet$ is the energy of absorbed light, n is the parameter connected with distribution of the density of states and *B,* a constant or Tauc parameter. Here $n = 1/2$ for direct and $n = 2$ for indirect transitions [91].

Therefore, the indirect transition energy gap (E_{qi}) can be obtained by plotting $(\bullet h\nu)^{1/2}$ versus $h\nu$ curve and then extrapolating the linear portion of the curve to $(\bullet h\nu)^{1/2} = 0$. Also from the plots of $(\bullet h\nu)^2$ versus $h\nu$, direct transition energy gap (E_{qd}) can be determined from the intercept of the linear part of the curve extrapolated to zero $\bullet$ in the photon energy axis.

2.14 Differential Thermal Analysis

The technique of Differential thermal analysis (DTA) is an important tool to study the structural and phase changes occurring both in solid and liquid materials during heat treatment. DTA is a process of accurately measuring the difference in the temperature between a thermocouple embedded to a sample and a thermocouple in a standard inert material such as aluminum oxide while both are being heated at a uniform rate [92].

The principle of DTA consists of measuring heat changes associated with the physical or chemical changes occurring when any substance is gradually heated. The thermocouple for DTA is incorporated at the end of each of the balance beam ceramic tubes, and the temperature difference between the holder on the sample side and the holder on the reference side is detected. This signal is amplified and becomes the temperature difference signal used to measure the thermal change of the sample. These differences of temperatures appear because of the phase transitions or chemical reactions in the sample involving the evolution of heat and are known as exothermic reaction or absorption of heat known as endothermic reaction. The exothermic and endothermic reactions are generally shown in the DTA traces as positive and negative deviations respectively from a base line. So, DTA offer a continuous thermal record of reactions in a sample. The areas under the bands or peaks of DTA spectra are proportional to the amount of heat absorbed or evolved

from the sample under investigation, where the temperature and sample dependent thermal resistance are the proportionality factors. Thus, DTA is needed primarily for the measurement of transition temperature. A Schematic diagram of a DTA apparatus is shown in Fig. 2.14.

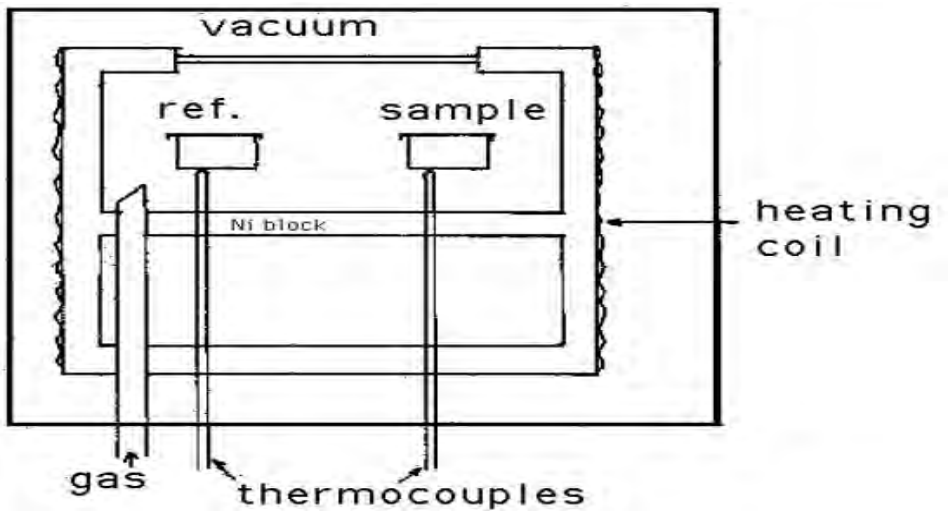

Fig.2.14 A Schematic diagram of a DTA apparatus.

2.15 Thermogravimetric Analysis

Thermogravimetric analysis (TGA) is a special branch of thermal analysis, which examines the mass change of a sample as a function of temperature in the scanning mode or as a function of time in the isothermal mode. Not all thermal events bring about a change in the mass of the sample (for example melting, crystallization or glass transition), but there are some very important exceptions which include absorption, sublimation, vaporization, oxidation, reduction and decomposition. The TGA is used to characterize the decomposition and thermal stability of materials under a variety of conditions and to examine the kinetics of the physico-chemical processes occurring in the sample [93]. Sample weight changes are measured as described below in Fig. 2.15.

Fig. 2.15 shows the sample balance beam and reference balance beam are independently supported by a driving coil/pivot. When a weight change occurs at the beam end, the movement is conveyed to the opposite end of the beam via the driving coil/pivot, when optical position sensors detect changes in the position of a slit. The signal from the optical position sensor is sent to the balance circuit. The balance circuit supplies sufficient feedback current to the driving coil so that the slit returns to the balance position. The

current running to the driving coils on the sample side and the current running to the driving coil on the reference side is detected and converted into weight signals.

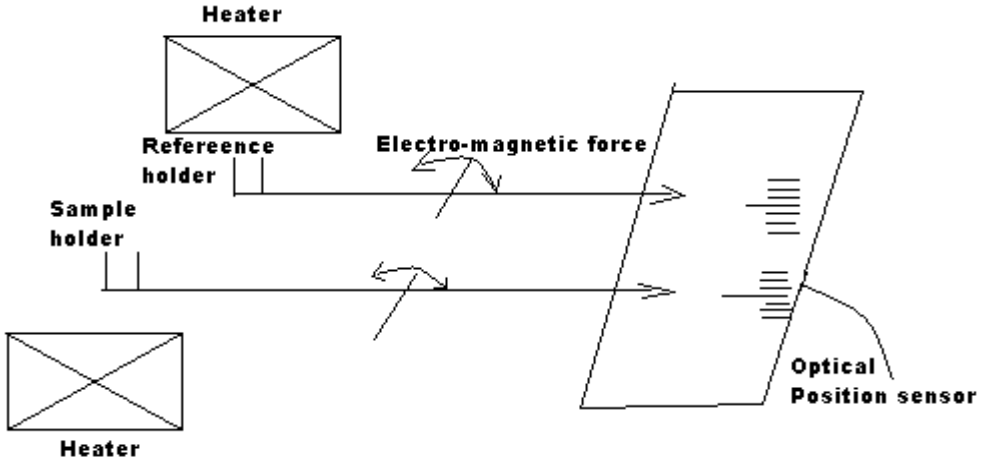

Fig. 2.15 A pictorial set-up for TGA measurements.

2.16 Theory of Direct Current Conduction Mechanism

Direct Current **(**DC) electrical conduction in plasma polymerized materials, the carriers may either be electronic or ionic in nature and conduction is considered through the film, rather than along the plane of the film. No known polymer is completely free of conduction processes, however small the quantity of charge carriers it may possess. Low level conduction in insulating polymers can take a variety of forms. Conduction may very often be contributed by impurities that provide a small concentration of charge carriers in the form of electrons or ions. At high fields, the electrodes may inject new carriers (holes and electrons) into polymers. At very high fields, these and other processes will lead to complete breakdown of polymers as insulating materials. The imposition of an electrical field upon a polymer will cause a redistribution of any charges in the polymer, provided they are mobile enough to respond in the time scale in the applied field. If some of the mobile charges are able to diffuse through out the specimen and charge migration through the electrode sample interface is possible, then the charges will support a DC conductance. The mechanisms concerned with electron transport are classified in four ways. The discussion of the four ways is given below:

a) Band conduction: Thermally activated electrons can be injected from the valence band to the conduction band of the insulator if the forbidden band gap is small enough. The

electrons may be thermally activated over the reduced potential barrier at the metal insulator interface and by thermal excitation into the conduction band from trapping levels in the dielectric.

b) Tunneling Process: The tunneling of electrons may take place from metal cathode into the conduction band, from trapping levels in the dielectric, directly between the valence band and the conduction band, from the valence band directly into the metal electrode.

c) Impurity Conduction: In this process electrons hop from one trapping (impurity level) center to another without going up into the conduction band.

d) Space Charge Effects: In some cases charge injection into the conduction band, tunneling or impurity conduction may result in a build up of space charge with in the bulk material, which sets a limit on the charge transport. When the injected carrier density is greater than the free carrier density, current becomes space-charge-limited.

Many scientists have investigated three worth-mentioning electrical conduction mechanisms which are operative in the thin films of various organic compounds [94-97]:

- The injection of carriers from the electrode by means of thermal or field assisted emission usually referred to as Schottky emission.
- The process, in which carriers are produced by the dissociation of donor-acceptor centers in the bulk of the material, is called Poole-Frenkel (PF) generation.
- If the generation process is slower than transport by the carriers through the material, the conduction is controlled by generation, specifically by either the Schottky, or PF mechanism. Conversely, when the transport is slower than generation, it constitutes the rate-determining step, and the conduction is described by the theory of Space Charge Limited Conduction (SCLC). The phenomenon is, if a charge is injected at the electrode polymer interface, a large excess carrier density at the injecting electrode will exist and a SCLC will flow [98, 99]. A brief explanation of these conduction mechanisms is stated below.

2.16.1 Schottky mechanism

Charge injected from a metal to an insulator or semiconductor at medium fields may take place by field-assisted thermionic emission, a process known as Richardson-Schottky effect or simply Schottky emission. This is a procedure of image force induced lowering potential energy for charge carrier emission when an electric field is applied. The potential step changes smoothly at the metal insulator interface as a result of the image force. This happens when the metal surface become polarized (positively charged) by an escaping

electron, which in turn exerts an attractive force $\phi_{im} = -\frac{e^2}{16\pi\varepsilon_0\varepsilon' x^2}$ on the electron. The potential energy of the electron due to the image force is thus

$$\phi_{im} = -\frac{e^2}{16\pi\varepsilon_0\varepsilon' x} \quad \text{..... (2.7)}$$

where, x is the distance of the electron from the electrode surface, e is the electronic charge, ε_0 is the permittivity of free space and ε' is the dielectric constant of the insulator. The potential step at a neutral barrier with attendant image potential as a function of the distance x from the interface is given by,

$$\varepsilon(x) = \varepsilon_0 + \varepsilon_{im} = \varepsilon_0 - \frac{e^2}{16\pi\varepsilon_0\varepsilon' x} \quad \text{..... (2.8)}$$

where ε_0 is the Coulombic barrier height of the electrode-polymer interface. The barrier potential $\phi(x)$ in the presence of image forces is illustrated by the line AB in Fig. 2.16. Schottky assumed that the image force holds only for x greater than some critical distance x_0. For $x < x_0$, he assumes a constant image force, i.e. the potential energy is a linear function of x, and such that it matches the bottom of the electrode conduction band at the surface. It is clear that eq. (2.7) is not valid at the electrode surface, since $\varepsilon = -\infty$ there.

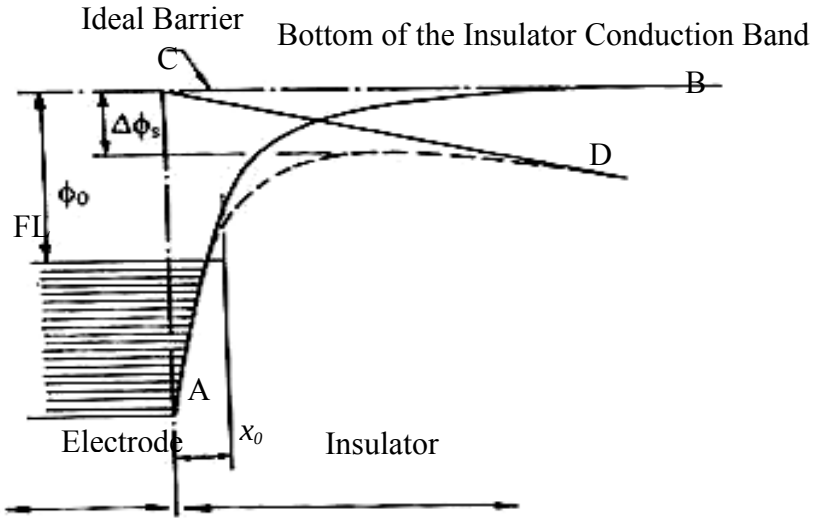

Fig. 2.16 Schottky effect at a neutral contact.

When an electric field exists at a metal-insulator interface, it interacts with the image force and lowers the potential barrier as shown in Fig. 2.16. The line CD represents the potential due to a uniform field, which when added to the barrier potential $\varepsilon(x)$ produces the

potential step shown by the dotted line which is seen to be $\bullet\bullet_s$, lower than without the electric field. The potential energy of the barrier under the influence of the field with respect to the Fermi level of the electrode is given by

$$\phi(x) = \phi_0 - \frac{e^2}{16\pi\varepsilon'\varepsilon_0 x} - eFx \quad \text{..... (2.9)}$$

This equation has a maximum at $x_m = \left(\frac{e}{16\pi\varepsilon'\varepsilon_0 F}\right)^{1/2}$

The change $\bullet\bullet_s = \bullet_0 - \bullet(x_m)$ in the barrier height due to the interaction of the applied field with the image potential is thus given by

$$\Delta\phi_s = \left(\frac{e^3}{4\pi\varepsilon'\varepsilon_0}\right)^{1/2} F^{1/2} \equiv \beta_s F^{1/2} \quad \text{..... (2.10)}$$

where, $\beta_s = \left(\frac{e^3}{4\pi\varepsilon'\varepsilon_0}\right)^{1/2}$ is the Schottky coefficient, ε' is the high frequency dielectric constant. Because of image-force lowering of the barrier, the electrode-limited current does not saturate according to the Richardson law

$$J = AT^2 \exp\left(-\frac{\phi_0}{kT}\right) \quad \text{..... ..(2.11)}$$

but rather obeys the Richardson-Schottky law

$$J = AT^2 \exp\left(-\frac{\phi_0 - \Delta\phi_s}{kT}\right) \quad \text{..... (2.12)}$$

$$J = AT^2 \exp\left(\frac{\beta_s F^{1/2} - \phi_0}{kT}\right) \quad \text{..... (2.13)}$$

$$J = AT^2 \exp\left(-\frac{\phi_0}{kT}\right) \exp\frac{\beta_s F^{1/2}}{kT} \quad \text{..... (2.14)}$$

where $A = 4\pi ek^2/h^3$ is the Richardson constant, F static electric field =V/d, V = applied voltage, d = film thickness, T = Temperature in K, k = Boltzmann constant.

The Richardson-Schottky effect in insulators appears to have been first observed by Emptage and Tantraporn [100], who reported a log I vs. $F^{1/2}$ relationship in their samples; since there have been many other reported similar observations. It was suggested that the plot should have to be linear in nature for Schottky type conduction mechanism.

2.16.2 Poole-Frenkel mechanism

Poole-Frenkel effect is also known as field-assisted thermal ionization process. This process is the bulk analog of the Schottky effect at an interfacial barrier. This effect is lowering of a Coulombic potential barrier when it interacts with an electric field as shown in Fig. 2.17.

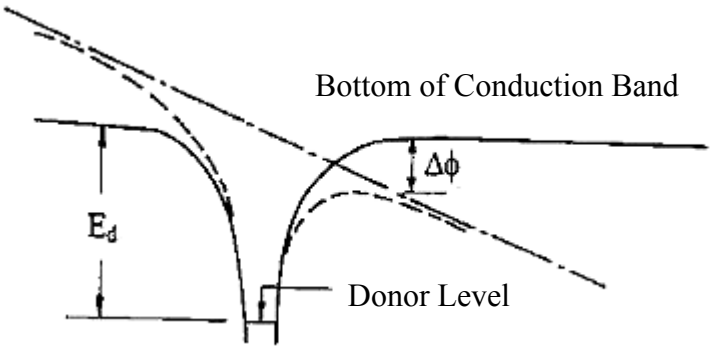

Fig. 2.17 Poole-Frenkel effect at a donor center.

Since the potential energy of an electron in a Coulombic field $-\frac{e^2}{4\pi\varepsilon_0\varepsilon' x}$ is four times that due to the image-force effects, the Poole-Frenkel reduction of a Coulombic barrier $\Delta\phi_{PF}$ in a uniform electric field is twice that due to the Schottky effect in a neutral barrier:

$$\Delta\phi_{PF} = 2\Delta\phi_s = 2\left(\frac{e^3}{4\pi\varepsilon'\varepsilon_0}\right)^{1/2} F^{1/2} \equiv \beta_{PF} F^{1/2} \quad \text{..... (2.15)}$$

Here, β_{PF} is the PF coefficient defined by

$$\beta_{PF} = 2\left(\frac{e^3}{4\pi\varepsilon'\varepsilon_0}\right)^{1/2} = 2\beta_s \quad \text{..... (2.16)}$$

This result was first applied by Frenkel to the host atoms in bulk semiconductors and insulators. He argued that the ionization potential E_g of the atoms in a solid is lowered by an amount given by eq. (2.16) in the presence of a uniform field. Thus the conductivity is obtained by substituting $E_g - \Delta\phi_{PF}$ for E_g in $I = e\mu N_c F \exp(-E_g/2kT)$ yielding a field-dependent conductivity of the form

$$\sigma = \sigma_0 \exp\left(\frac{\beta_{PF} F^{1/2}}{2kT}\right) \quad \text{..... (2.17)}$$

where $\sigma_0 = e\mu N_c F \exp(-E_g/2kT)$ is the low-field conductivity, e is the electronic charge, μ is the mobility, F is the field in the insulator, N_c is the effective density of states in the insulator, E_g is the insulator gap, k is Boltzmann's constant, and T is the absolute temperature.

Equation (2.17) may be written in the form

$$J=J_0 \exp\left(\frac{\beta_{PF}F^{1/2}}{2kT}\right) \quad \text{(2.18)}$$

where $J_0 = \bullet_0 F$ is the low-field current density.

It is to be noted that although $\Delta\phi_{PF} = 2\Delta\phi_s$, the coefficient of $F^{1/2}$ in the exponential is the same for both Richardson-Schottky and Poole-Frenkel *J-F* characteristics. Since traps abound in an insulator and that a trap having a Coulombic-type barrier would experience the PF effects at high fields, thereby increasing the probability of escape of an electron immobilized therein, the current density in thin film containing shallow traps is given by

$$J = J_0 \exp\left(\frac{\beta_{PF}F^{1/2} - \phi_c}{kT}\right) \quad \text{(2.19)}$$

where, ϕ_c is the ionization potential of the PF centers.

Therefore, the general expression for the current density, *J,* that holds equally well for both the PF and the Schottky mechanisms is of the form

$$J = J_0 \exp\left(\frac{\beta F^{1/2} - \phi}{kT}\right) \quad \text{(2.20)}$$

For a constant applied voltage at a particular temperature the current density expression (Eq. 2.20) can be written as

$$\log J \bullet d^{1/2}$$

Thus, for the PF or the Schottky mechanism the plot of log*J* against the square root of the film thickness, $d^{1/2}$, should be a straight line.

2.16.3 Space charge limited conduction mechanism

The mechanism of electrical conduction in thin insulating films has been discussed by Lamb and several important theoretical mode have been put forwarded [101]. When an Ohmic contact is made to the insulator, the space charge injected into the conduction band of the insulator is capable of carrying current and when the transport is slower than generation, it constitutes the rate-determining step, and the conduction is described by the theory of SCLC. In order to gain physical insight into this process, let us consider what happens when a bias is applied to system shown in Fig. 2.18, that is, an insulator having two ohmic contacts on its surfaces.

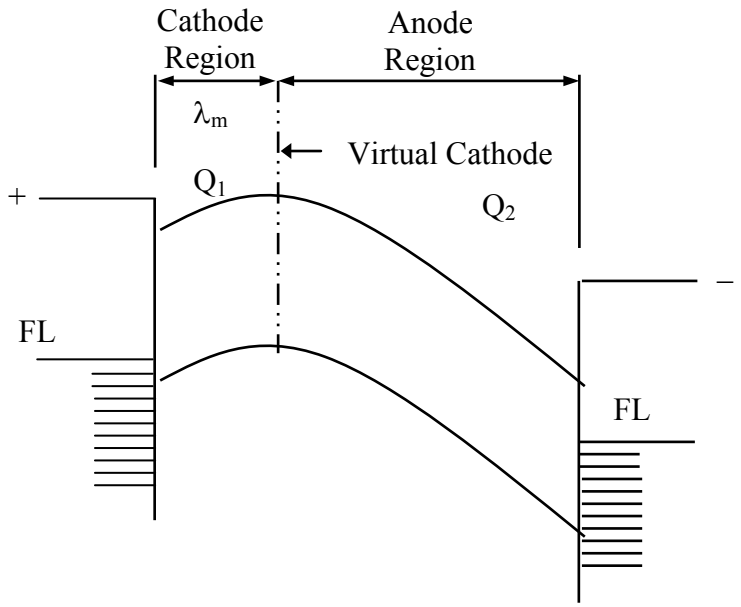

Fig. 2.18 Energy diagram for different regions under SCLC mechanism.

When a bias voltage is applied to the metal electrodes, this results an addition of positive charge to the anode and negative charge to the cathode. If now the voltage bias increases, the net positive charge on the anode increases and that on the cathode decreases. Assuming that the anode region extends throughout the insulator and neglecting the diffusion effect the current can be interpret by the Mott and Gurney relation [102].

$$J = \frac{9\mu\varepsilon'\varepsilon_0 V^2}{8d^3} \quad \text{..... (2.21)}$$

Where, μ is the mobility of charge carriers, ε the dielectric constant, ε_0 the permittivity of free space, V the applied voltage and d the thickness. Equation (2.21) predicts that SCLC is directly proportional to V^2 and inversely proportional to d^3.

If the insulator contains N_t shallow traps positioned an energy E_t below the conduction band as shown in Fig. 2.19 and N_c is the effective density of states in the conduction band, then the free component of the space charge can be given by

$$\rho_f = eN_c \exp\left(-\frac{E_F}{kT}\right) \quad \text{..... (2.22)}$$

and trapped component of space charge can be written as

$$\rho_t = eN_t \exp\left(\frac{-(E_F - E_t}{kT}\right) \quad \text{..... (2.23)}$$

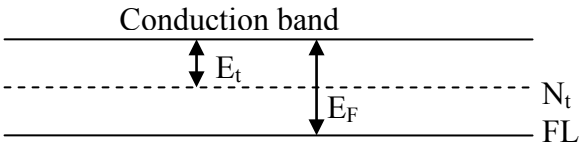

Fig. 2.19 Energy diagram showing shallow traps in an insulator.

Thus trapping factor, θ is defined as

$$\theta \equiv \frac{\rho_f}{\rho_t} = \frac{N_c}{N_t}\exp\left(-\frac{E_t}{kT}\right) \quad \text{..... (2.24)}$$

The SCLC current density with traps is defined by

$$J = \frac{9\mu\varepsilon'\varepsilon_0 V^2}{8d^3}\theta \quad \text{..... (2.25)}$$

For a shallow trap SCLC and trap-free SCLC, θ = 1. According to eq. (2.25), J varies as d^{-1} in the Ohmic region and as d^{-3} in the SCLC region for the trap-filled SCLC part. For a fixed V, the dependence of ln J on ln d should be linear with slope m ≥ -3.

Lampert calculated the voltage at which the transition from the Ohmic to shallow trap SCLC region (V_{tr}) occurs is given by

$$V_{tr} = \frac{8}{9} n_0 \frac{ed^2}{\varepsilon} \quad \text{..... (2.26)}$$

where volume generated free carrier density, n_0 is independent of both μ and J .

Lampert has pointed out that if sufficient charge is injected into the insulator, the traps will become filled (trap-filled limit, V_{TFL}). Further injected charge then exists as free charge in the conduction band and contributes in to the current. Beyond the TFL, the J-V characteristic can be given by eq. (2.21) rather than eq. (2.25).

Fig. 2.20 is a schematic current-voltage (I-V) characteristic curve for an insulator having a shallow discrete trapping level. This type of conduction process exhibits three or four distinct regions in the current-voltage characteristics curve. At the lower voltage region ($V<V_x$), the I-V characteristic is Ohmic where the variation of current with voltage is linear, because the bulk generated current exceeds the SCL current. When the applied voltage is increased the injected carriers out number the thermally generated ones and in the voltage region ($V_x<V<V_{TFL}$) the SCLC predominates and I • V^2, (Eq. 2.25).

When $V= V_{TFL}$, sufficient charge has been injected into the insulator to fill the gaps.

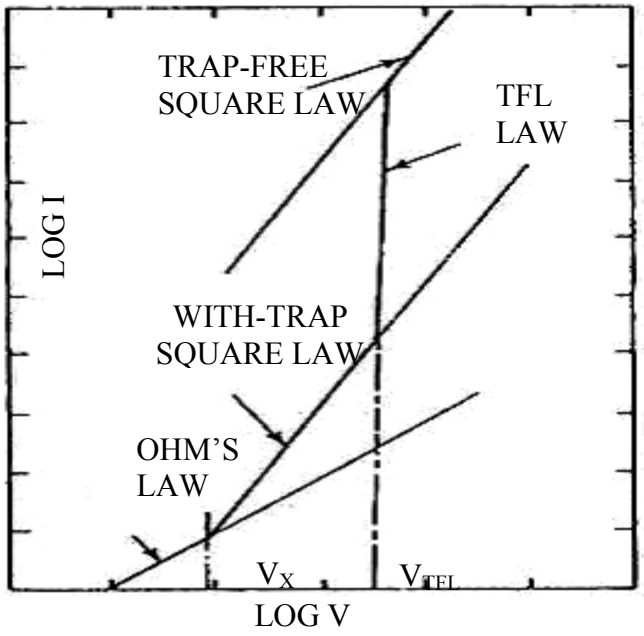

Fig. 2.20 SCLC I-V characteristic for an insulator containing shallow traps.

Hence, as V just exceeds V_{TFL} the current rises rapidly such that for $V > V_{TFL}$, the I-V characteristic obeys the trap-free law, (Eq. 2.21).

Clearly, from the structure exhibited in the characteristic, much information about the traps in insulators can be deduced from the experimental data. Thus SCLC technique provides a powerful means to interpret the number and energies of trapping sites present.

2.17 Thermally Activated Conduction Process

2.17.1 Electronic Conduction

Electronic conduction in organic, molecular compounds differs in several ways from the more familiar kind in metals and inorganic semiconductors like silicon and germanium. The well-known band theory of atomic lattices has provided the essential basis of concepts and language for the discussion of conduction in molecular solids. An important feature of the band system is that electrons are delocalized or spread over the lattice. Some delocalization is naturally expected when an atomic or bital of any atom overlaps appreciably with those of more than one of its neighbors, but delocalization reaches an extreme form in the case of a regular, 3-dimensional lattice. The band theory assumes that the electrons are delocalized and can extend over the lattice. When electronic conduction is considered in polymers, band theory is not totally suitable because the atoms are covalently bonded to one another, forming polymeric chains that experience weak

intermolecular interactions. But macroscopic conduction will require electron movement, not only along the chain but also from one chain to another.

The carrier mobility in organic molecules is usually very low. This is due to the fact that electrons, while jumping from one molecule to another, lose some energy. But the mobility's of electrons are found to increase with molecular size in such type of compounds. In polymer system, the conductivity is influenced by the factors such as dopant level, morphology of polymer, concentration of conducting species, temperature, etc. [103]. The temperature dependence of conductivity can be described by an Arrhenius type of equation.

$$\sigma = \sigma_0 \exp(\frac{-\Delta E}{kT}) \text{.....} \quad (2.27)$$

where σ_0 is a constant and ΔE is the activation energy for carrier generation. The plot of $\log \sigma$ vs $1/T$ must be linear for thermally activated conduction. Whatever the Ohmic mechanism, a $\log \sigma$ vs. $1/T$ plot (Arhennius plot) will usually exhibit increasing linear slopes (activation energies) as T is raised [104].

2.17.2 Hopping Conduction

In amorphous semiconductors hopping between localized states is well known. A group of states or levels due to impurities, physical disorder, or band tails in the band gap may exist close to the Fermi level resulting in an adequate concentration of electrons in these states and adequate concentration of empty states. Thermal excitation and de-excitation of an electron from a full state to an empty one now can occur. That is, for a random distribution of atoms the density of electronic energy states tails into what is normally the forbidden zone, and electrons in these tails are localized. There is then not so much an energy gap as a mobility gap. In other words there is an intermediate range of electronic energy states in which the mobilities are very low.When the electrons are excited to higher energy, conduction via localized electrons implies discrete jumps across an energy barrier from one site to the next as shown in Fig 2.21.

An electron may either hop over, or tunnel through, the top of the barrier, the relative importance of these two mechanisms depending on the shape of the barrier and the availability of thermal energy.

For variable range hopping the electrical conductivity is given by

$$\sigma = \sigma_o \exp\left(-\frac{T_o}{T}\right)^{\frac{1}{d+1}} \quad \text{..... (2.28)}$$

where "d" is the dimensionality of transport, σ the conductivity, σ_o the initial value of conductivity, T the absolute temperature and T_o the activation energy in terms of temperature.

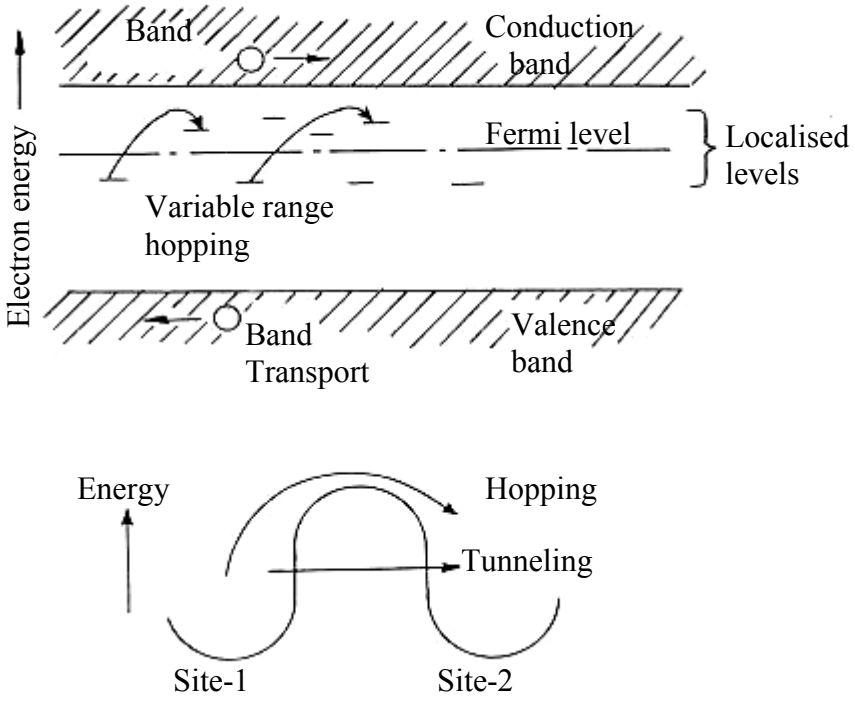

Fig. 2.21 Diagram of electron-transfer mechanisms between adjacent sites separated by a potential energy barrier.

2.17.3 Ionic Conduction

Ionic conduction consists of the transit of ions (atoms of positive or negative charge) from one site to another via point defects called vacancies in the crystal lattice. At ambient temperatures very little ion hopping takes place, since the atoms are at relatively low energy. For ionic conductivity, transport of one or more types of ions across the material is necessary. In an ideal crystal all constituent ions are arranged in regular periodic fashion and are often stacked in a close-packed form. Thus there is little space for an ion to diffuse. Often, the available space is just enough for vibration around its equilibrium position. However, at any non-zero temperature there exist defects. These could, for

example, be positional disorder due to deviation from ideal stacking. The degree of such disorder can vary from one material to another or even from one temperature or pressure to another in the same material. The current density J flowing through a specimen across which an electric field E is applied can be expressed as

$$J=\sinh(eaE/2kT) \quad \text{(2.29)}$$

where E is the electric field, a the distance between neighbouring potential wells, e the electronic charge. Although it is not possible to identify the ions experimentally, it may be assumed that they are mainly derived from fragments of polymerization catalyst, degradation and dissociation products of the polymer itself, and absorbed water.

CHAPTER 3

EXPERIMENTAL DETAILS

3.1 Introduction

This chapter describes the details of monomer and substrate and their cleaning process, capacitively coupled glow discharge plasma polymerization set up for polymer formation, generation of glow discharge plasma, deposition parameters, thickness measurement method, formation and electrode deposition.

3.2 The Monomer

2-furaldehyde (FDH) is an organic compound derived from a variety of agricultural byproducts, including corncobs, oat, wheat bran, and sawdust. The name of FDH comes from the Latin word furfur, meaning bran, referring to its usual source. The monomer FDH is manufactured by BDH Chemicals Ltd., Poole, England and is collected from local market. The chemical structure of the monomer is shown in Fig. 3.1 and its typical properties are stated in Table-3.1:

Table 3.1 General properties of 2-furaldehyde.

Parameters	Condition/Value
IUPAC name	Furan-2-carbaldehyde
Appearance	Colorless oil
Molecular formula	$C_5H_4O_2$, OC_4H_3CHO
Molecular weight	96.08 g/mol
Density	1.16 g/cm^3
Boiling point	161.7 °C
Solubility	In methanol

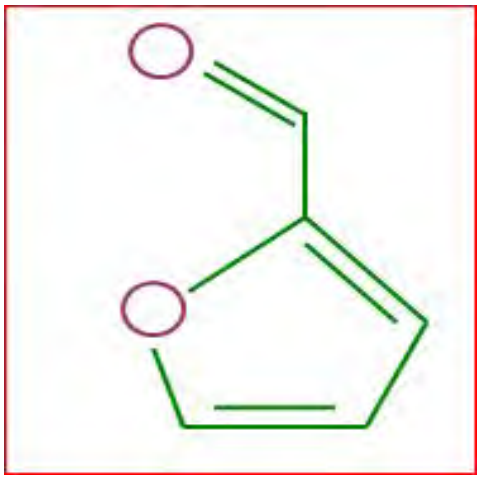

Fig. 3.1 Chemical Structure of 2-furaldehyde

3.3 Substrate Materials and its Cleaning Process

The substrates used were pre-cleaned glass slides (25.4 mm × 76.2 mm × 1.2 mm) of Sail Brand, China, purchased from local market. The samples were prepared by depositing the plasma polymerized 2-furaldehyde (PPFDH) thin films onto them.

To get homogeneous, smooth and flawless thin polymer film, which is a common property of plasma polymers, it is essential to make the substrate as clean as possible. The substrates were chemically cleaned by acetone and thoroughly rinsed with distilled water then dried in hot air.

3.4 Capacitively Coupled Plasma Polymerization Set-up

Glow discharge plasma and the plasma polymerization setup has been used enormously in recent years to form various kinds of plasma polymers. Different configuration of polymerization set up varies the properties of plasma polymers i.e., the geometry of the reaction chamber, position of the electrodes, nature of input power etc [105-108]. The glow discharge plasma polymerization setup used to deposit the PPFDH thin films consists of following components is shown in Fig. 3.2.

Plasma reaction chamber

The glow discharge reactor is made up of a cylindrical Pyrex glass bell-jar having 0.15 m in inner diameter and 0.18 m in length. The top and bottom edges of the glass bell-jar are covered with two rubber L -shaped (height and base 0.015 m, thickness 0.001 m) gaskets. The cylindrical glass bell jar was placed on the lower flange. The lower flange is well fitted with the diffusion pump by an 'I' joint. The upper flange is placed on the top edge of the bell-jar. The flange is made up of brass having 0.01 m in thickness and 0.25 m in diameter. On the upper flange a laybold pressure gauge head, Edwards high vacuum gas inlet valve and a monomer injection valve are fitted. In the lower flange two highly insulated high voltage feed-through are attached using screwed copper connectors of 0.01m high and 0.004 m in diameter via Teflon™ insulation.

Electrode system

A capacitively coupled electrode system is used in the system. Two circular stainless steel plates of diameter 0.09 m and thickness of 0.001m are connected to the

high voltage copper connectors. The inter-electrode separation can be changed by moving the electrodes through the electrode stands. After adjusting the distance between the electrodes they are fixed with the stands by means of screws. The substrates were kept on the lower electrode for plasma deposition.

Pumping unit

For creating laboratory plasma, first step is pumping out the air/gas from the plasma chamber. In this system a rotary pump of vacuubrand (Vacumbrand GMBH & Co: Germany) is used.

Vacuum pressure gauge

A vacuum pressure gauge head (Laybold AG, Germany) and a gauge meter (ThermotronTM 120) are used to measure inside pressure of the plasma deposition chamber.

Input power for plasma generation

The input power supply for plasma excitation comprises of a step-up high-tension transformer and a variac. The voltage ratio at the output of the high-tension transformer is about 16 times that of the output of the variac. The maximum output of the variac is 220V and that of the transformer is about 3.5 KV with a maximum current of 100 mA. The deposition rate increases with power at first and then becomes independent of power at high power values at constant pressure and flow rate.

Monomer injecting system

The monomer injecting system consists of a conical flask of 25 ml capacity and a Pyrex glass tube with capillarity at the end portion. The capillary portion is well fitted with metallic tube of the nozzle of the high vacuum needle valve. The conical flask with its components is fixed by stand-clamp arrangement.

Supporting frame

A metal frame of dimension 1.15 m × 0.76 m × 0.09 m is fabricated with iron angle rods, which can hold the components described above. The upper and lower bases of the frame are made with polished wooden sheets. The wooden parts of the frame are varnished and the metallic parts are painted to keep it rust free. The pumping

unit is placed on the lowed base of the frame. On the upper base a suitable hole is made in the wooden sheet so that the bottom flange can be fitted with nut and bolts.

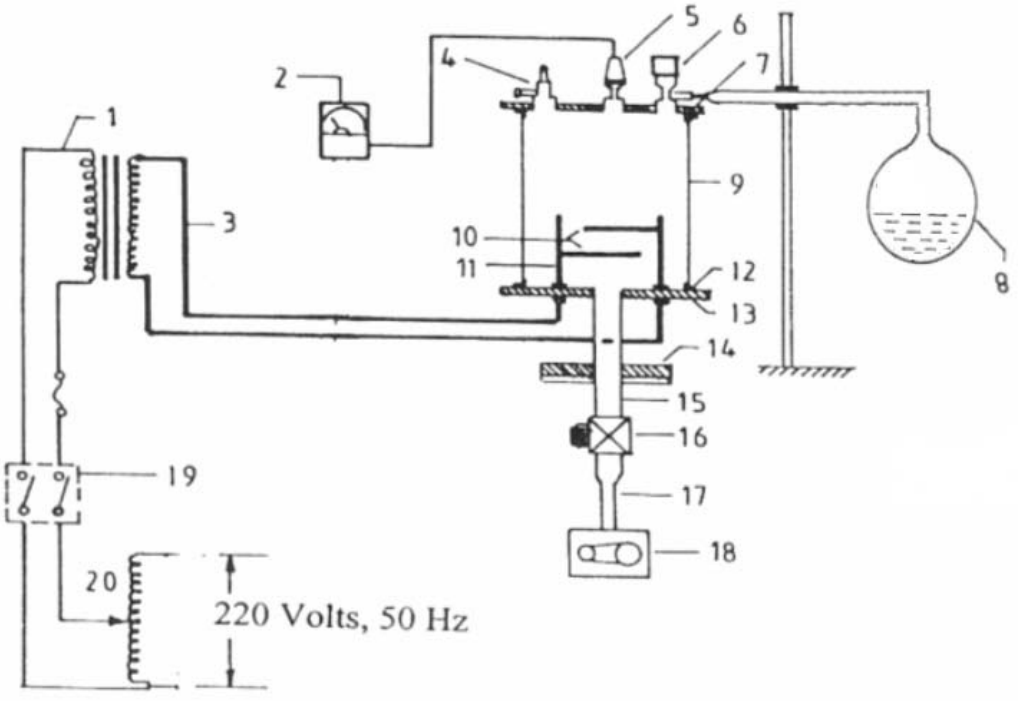

Fig. 3.2 A schematic diagram of the plasma polymerization set-up (1 high voltage power supply, 2 pirani gauge, 3 high tension leads, 4 gas inlet valve, 5 gauge head, 6 monomer injection valve, 7 flowmeter, 8 monomer container, 9 Pyrex glass dome, 10 metal electrodes, 11 electrode stands, 12 rubber gasket, 13, lower flange, 14 bottom flange, 15 brass tube, 16 valve, 17 liquid nitrogen trap, 18 rotary pump, 19 switch and 20 variac.).

Flowmeter

The system pressure of a gas flow is determined by the feed in rate of a gas and the pumping out rate of a vacuum system. The monomer flow rate is determined by a flowmeter. In the plasma polymerization set up a flowmeter (Glass Precision Engineering LTD, Meterate, England) is attached between the needle valve and the monomer bottle.

Liquid nitrogen trap

Cold trap, particularly a liquid N_2 trap, acts as a trap pump for different type gas. The liquid N_2 trap system is placed in the fore line of the reactor chamber before the pumping unit in the plasma deposition system. It consists of a cylindrical shape chamber having 6.4 cm diameter and 11.5 cm in length using brass material.

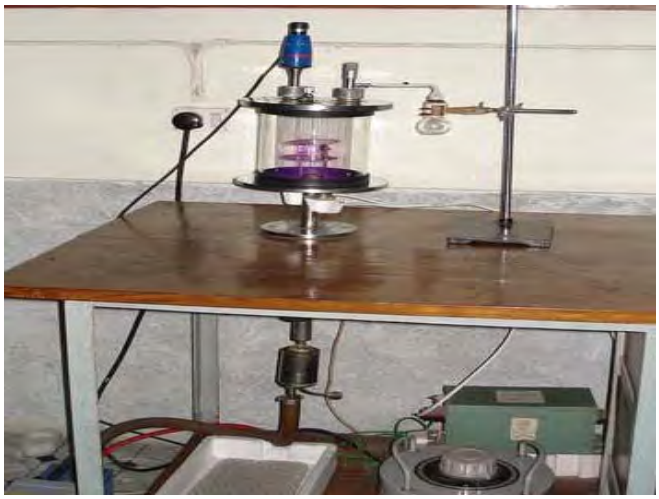

Fig. 3.3 The plasma polymerization set-up

3.5 Generation of Glow Discharge Plasma

Glow discharges are produced by an applied static or oscillating electric field where energy is transferred to free electrons in vacuum. Inelastic collisions of the energetic free electrons with the gas molecules generate free radicals, ions, and species in electronically excited states. This process also generates more free electrons, which is necessary for a self-sustaining glow [109-111]. The excited species produced are very active and can react with the surfaces of the reactors as well as themselves in the gas phase. The important feature of glow discharge plasma is the non-equilibrium state of the overall system. In the plasmas considered for the purpose of plasma polymerization, most of the negative charges are electrons and most of the positive charges are ions. Due to large mass difference between electrons and ions, the electrons are very mobile as compared to the nearly stationary positive ions and carry most of the current. Energetic electrons as well as ions, free radicals, and vacuum ultraviolet light can possess energies well in excess of the energy sufficient to break the bonds of typical organic monomer molecules which range from approximately 3 to 10 eV. Some typical energy of plasma species available in glow discharge as well as bond energies encountered at pressure of approximately 1.0 Pa. The chamber of the glow discharge reactor is evacuated to about 1.0 Pa. A high-tension transformer along with a variac is connected to the feed-through attached to the lower flange. While increasing the applied voltage, the plasma is produced across the electrodes at around 15 Pa chamber pressure. Fig. 3.3 shows the photograph of plasma deposition set-up and Fig. 3.4 shows the photograph of glow discharge plasma across the electrodes in the capacitively coupled parallel plate discharge chamber.

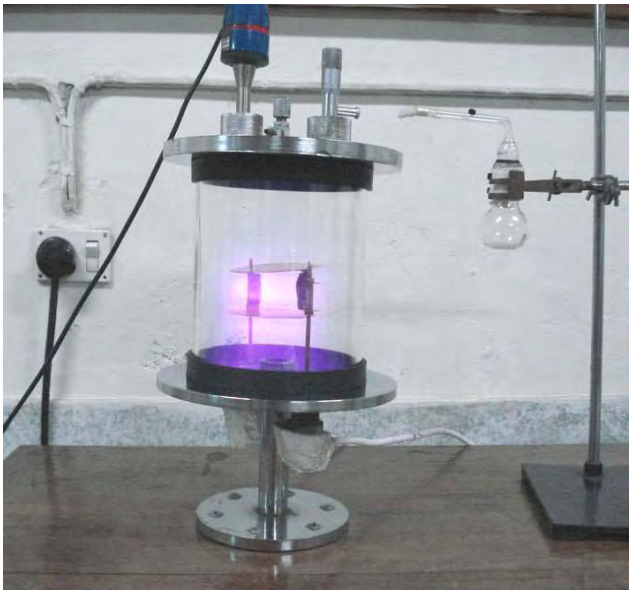

Fig. 3.4 Glow discharge plasma during deposition.

3. 6 Plasma Polymer Thin Film Deposition

The electric field, when applied to gaseous monomers at low pressures (0.01 to 1 mbar), produces active species that may react to form cross-linked polymers films. In my experiment, air was used as the primary plasma, after producing the desired plasma glow in the reactor the monomer FDH vapor was injected downstream to the primary air glow plasma. Incorporation of monomer vapor changed the usual color of plasma into a light bluish color as shown in Fig. 3.4. The deposition time was varied from 40-90 min. to get PPFDH thin films of different thicknesses. The optimized conditions for thin film deposition in the present study are shown in Table-3.2.

Table 3.2 The optimum plasma polymerization conditions for PPFDH.

Separation between two electrodes	**4 cm**
Position of the substrate	Lower electrode
Power	40W
Pressure in the reactor	1.33 Pa
Deposition time	40 min -90 min
Line frequency	50 Hz

3.7 Contact Electrodes for Electrical Measurements

Electrode material

Aluminium (Al) (purity of 4N , British chemical standard) was used as electrode material prior to deposition Al has been reported to have good adhesion to glass slide

[112]. Al film has advantages of easy self-healing burn-out of flaws in sandwich structure.

Electrode deposition

Metal electrodes of aluminium were deposited using an Edward coating unit E-306 A (Edward, UK) as shown in Fig. 3.5. The system was evacuated by an oil diffusion pump backed by an oil rotary pump. The glass substrates were masked with a 0.08m x 0.08m x 0.001m engraved brass sheet for the electrode deposition. The electrode assembly used in this study is shown in Fig. 3.7. The glass substrates with mask were supported by a metal rod 0.1 m above the tungsten filament. For the electrode deposition Al was kept on the tungsten filament. The filament was heated by low-tension power supply of the coating unit. The low-tension power supply was able to produce 100 A current at a potential drop of 10 V. During evacuation of the chamber by diffusion pump, the diffusion unit was cooled by the flow of chilled water and its outlet temperature was not allowed to rise above 305 K. When the penning gauge reads about 1.33×10^{-3} Pa, the Al on the tungsten filament was heated by low-tension power supply until it was evaporated. Fig. 3.6 shows a schematic diagram of sandwich Al/PPFDH/Al film.

Fig. 3.5 The Edward vacuum coating unit E 306A

After deposition of the 1st Al electrode on the cleaned glass substrate by conventional thermal evaporation technique under a pressure of 2.66 $x10^{-3}$ Pa, the glass substrates were taken out of the vacuum coating unit and placed on the lower electrode of the plasma polymerization chamber [113].

Fig. 3.6 Schematic diagram of sandwich Al/PPFDH/Al film

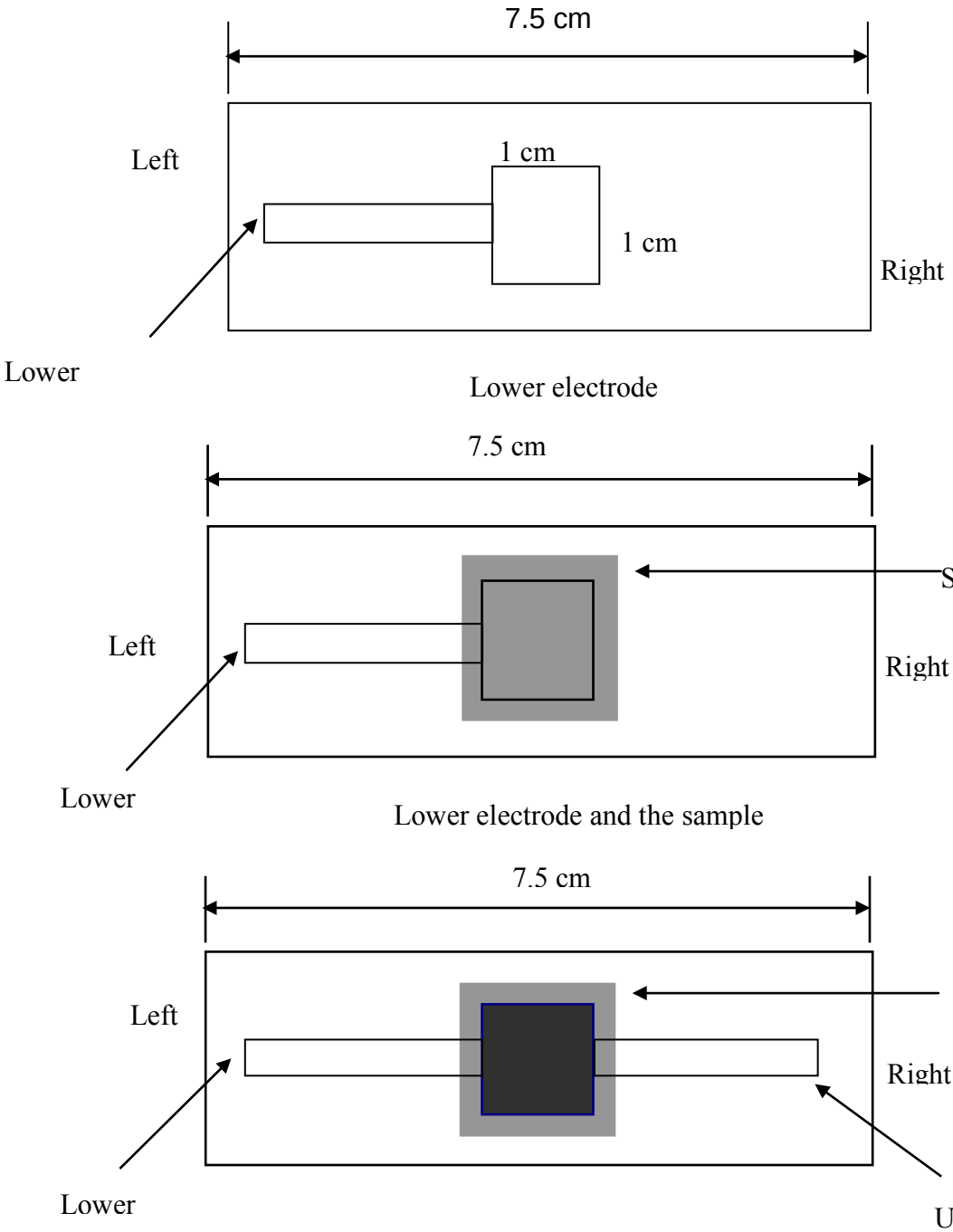

Fig. 3.7 Electrode assembly

Then the PPFDH thin films were deposited on the top of the Al electrode surface. After the deposition of the PPFDH thin films on the first electrode the samples were taken out of the polymerization chamber and brought to the vacuum coating unit. The counter electrode (2) of aluminum was deposited in the same condition as described above, by using a suitable mask such that the effective area of the M-I-M structure is 10^{-4} m^2.

3.8 Measurement of Thickness of the Thin Films

Thickness is the single most significant film parameter. It may be measured either by in-situ monitoring of the rate of deposition, or after the film is taken out of deposition chamber. Techniques of the first type often called as monitor method generally allow both monitoring and controlling of the deposition rate and film thickness. Other techniques are also used for thickness measurement. Any physical quantity related to film thickness can in principle be used to measure the film thickness. It may be measured either by several methods with varying degrees of accuracy. The methods are chosen on the basis of their convenience, simplicity and reliability. Since the film thicknesses are generally of the order of a wavelength of light, various types of optical interference phenomena have been found to be most useful for measurement of film thicknesses. Several of the common methods are i) During Evaporation, ii) Multiple-Beam Interferometry, iii) Michelson interferometer iv) using a Hysteresis graph. Here, Multiple-Beam Interferometry method is employed for the measurement of thickness of the thin films. The technique is described below.

This method utilizes the resulting interference effects when two silvered surfaces are brought close together and are subjected to optical radiation. This interference technique, which is of great value in studying surface topology in general, may be applied simply and directly to film-thickness determination. When a wedge of small angle is formed between unsilvered glass plates, which are illuminated by monochromatic light, broad fringes are seen arising from interference between the light beams reflected from the glass on the two sides of the air wedge. At points along the wedge where the path difference is an integral and odd number of wavelengths, bright and dark fringes occur respectively. If the glass surfaces of the plates are coated

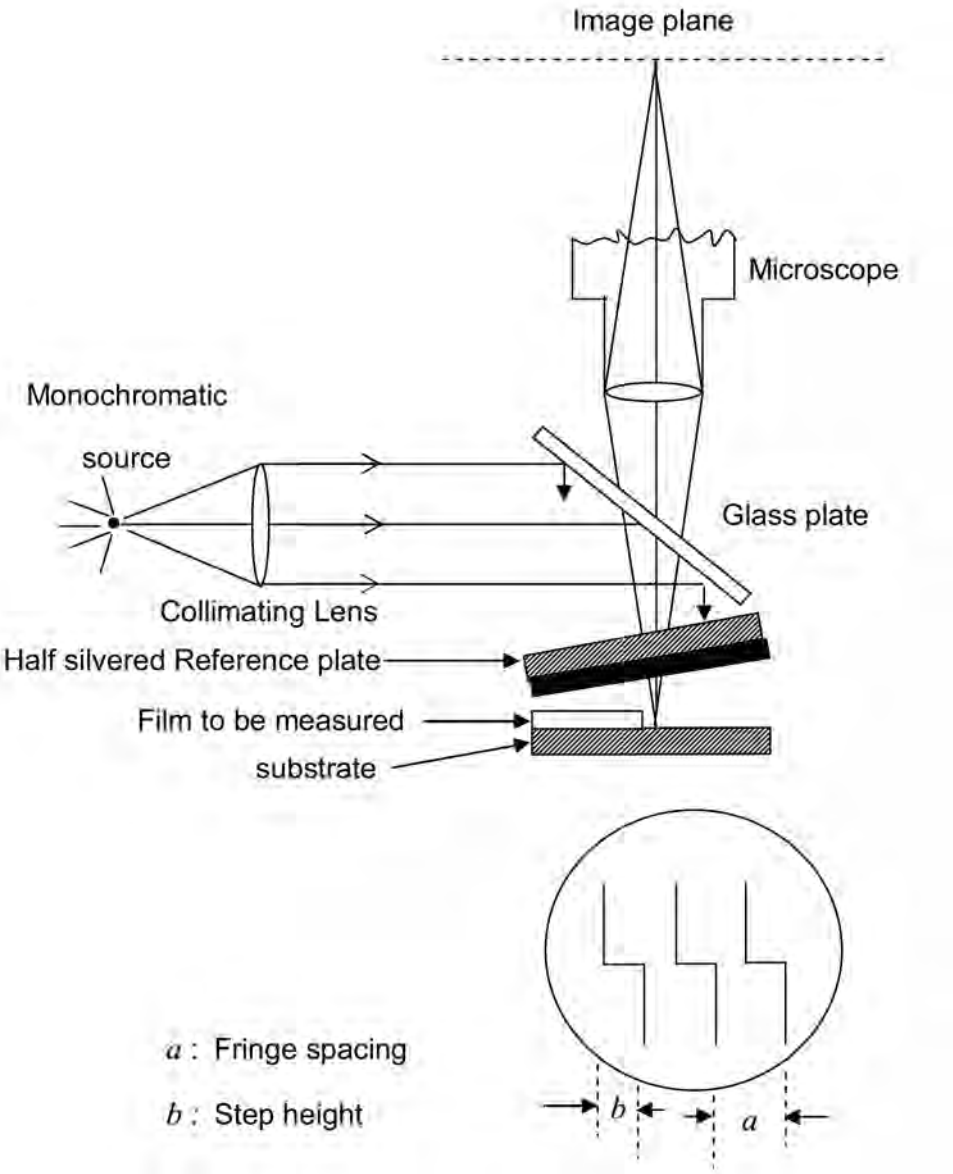

Fig. 3.8 Interferometer arrangement for producing reflection Fizeau fringes of equal thickness.

with highly reflecting layers, one of which is partially transparent, then the reflected fringe system consists of very fine dark lines against a bright background. A schematic diagram of the multiple-beam interferometer along with a typical pattern of Fizeau fringes from a film step is shown in Fig.3.8. As shown in this figure, the film whose thickness is to be measured is over coated with a silver layer to give a good reflecting surface and a half-silvered microscope slide is laid on top of the film whose thickness is to be determined. A wedge is formed by the two microscope slides, and light multiply reflected between the two silvered surfaces forms an interference pattern with a

discontinuity at the film edge as shown in Fig.3.5. The thickness of the film *d* can then be determined by the relation,

$$d = \frac{\lambda}{2}\frac{b}{a}$$

where, λ is the wavelength and *b/a* is the fractional discontinuity identified in the figure.

In general, the sodium light is used, for which λ = 589.3 nm. In conclusion, it might be mentioned that the Tolansky method of film-thickness measurement is the most widely used and in many respects also the most accurate and satisfactory one [114].

3.9 Samples for Different Measurements

PPFDH thin films were deposited on to chemically cleaned microscope glass substrates for optical and electrical properties. For Energy dispersive analysis of X-ray (EDAX), Differential thermal analysis (DTA), Thermogravimetric analysis (TGA) study and Fourier transform infrared (FTIR) spectroscopy, the films were scraped off from the substrate and kept into the glass bottle.

3.10 Scanning Electron Microscopy

The surface of PPFDH thin films deposited onto chemically cleaned glass substrates by plasma polymerization technique were coated with a thin layer of gold by gold sputtering. Scanning electron micrographs of the PPFDH thin film surface was taken using an SEM (Inspect F 50, EFI Company, Netherlands) with a maximum operating voltage of 20 kV and with two magnifications (× 5,000 and ×10,000). EDAX which is connected to the Microscope also performed for the elemental analysis of the samples.

3.11 Fourier Transform Infrared Spectroscopy

FTIR spectrum of PPFDH was recorded at room temperature by a double beam FTIR spectrophotometer (SHIMADZU, FTIR-8900 spectrophotometer, JAPAN) in the wavenumber range of 400-4000 cm^{-1}. The FTIR spectrum of the monomer FDH was obtained by putting the liquid monomer in a potassium bromide (KBr) measuring cell. PPFDH powder was collected from the PPFDH deposited substrates and then pellets of PPFDH powder mixed with KBr were prepared for recording the FTIR spectra of

PPFDH sample. FTIR spectra of the FDH and the PPFDH were recorded in transmittance (%) mode.

3.12 Thermal Analyses

The PPFDH films were scrapped off from the substrate to use as the sample for the DTA/TGA investigation. Melting and degradation temperatures of the neat PPFDH samples were monitored by a DTA and TGA (Seiko-Ex-STAR-6300, Japan). The measurements using DTA and TGA were carried out from room temperature 300 K to 873 K at a heating rate of 10 K/min under nitrogen gas flow. While the DTA traces give the melting and degradation temperatures as determined from the exothermic versus temperature curves, the TGA runs exhibit the weight-loss of the sample with temperature.

3.13 Ultraviolet-Visible Spectroscopy

The PPFDH thin films were deposited on to glass substrates (Sail brand, China) having a dimension of 18mm×18mm×1mm. The UV-Vis spectrum of the monomer FDH and the as-deposited PPFDH thin films were recorded in absorption mode using a dual beam UV-Vis spectrophotometer (SHIMADZU UV-1601, JAPAN) in the wavelength range of 200-800 nm at room temperature. For measuring the optical absorption of the monomer, it was kept in a quart cell and for the PPFDH films a similar glass slide was used as the reference.

3.14 DC Electrical Measurements

Suitable electrical contacts were made with the Al electrode by fine conducting wire of Cu using silver paste. Now the samples are ready for DC measurements. The electrical measurements were carried out in the PPFDH films by loading the samples in a cylindrical metal holder. The measurements were carried out under dynamic vacuum of about 1.33 Pa. The current flowing through the films was measured by using a high impedance Keithley 614 electrometer. DC bias voltage was applied by an Agilent 6545A stabilized DC power supply. The DC measurements were carried out at different constant temperatures (298, 348, 398 and 423 K). The sample chamber as well as the samples was heated by a heating coil wrapped around the specimen chamber. A Chromel-Alumel thermocouple mounted on the sample holder, with the fused end in contact with the PPFDH thin film, permitted temperature measurements using a 197A

digital mic rovoltmeter (DMV).The bl ock diagram f or DC measurements and DC measurement set up are shown in Fig. 3.9 and Fig. 3.10 respectively.

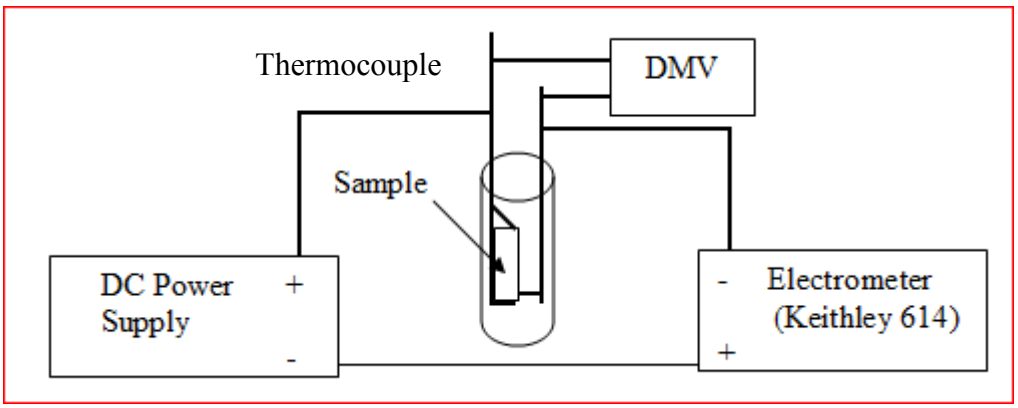

Fig. 3.9 A schematic circuit diagram of DC measurements.

Fig. 3.10 DC measurement set up.

CHAPTER 4

RESULTS AND DISCUSSION

4.1 Introduction

Structural characterization of plasma polymerized thin films may be possible by several methods, such as scanning electron microscopy (SEM), energy dispersive analysis of X-rays (EDAX), Fourier transform infrared (FTIR) spectroscopy, Ultraviolet visible (UV-Vis) spectroscopy, differential thermal analysis (DTA) and thermogravimetric analysis (TGA). For inspection of surface morphology of specimens at very high magnifications SEM is employed. The composition of PPFDH thin films have been studied by EDAX. The FTIR analysis is a digital technique that may be used for the investigation of molecular structure, bonding and identification of chemical functional groups in organic compounds. The DTA is applied to study structural and phase change that occurs during heating a polymeric sample. The TGA is to measure the weight loss of the sample as a function of temperature.

The wavelength of light that a compound will absorb is the characteristic of its chemical structure. Specific regions of the electromagnetic spectrum are absorbed by exciting specific types of molecular and atomic motion to higher energy levels. Absorption of UV-Vis radiation is associated with excitation of electrons, in both atoms and molecules, to higher energy states. Light in the UV-Vis region is adequate for molecules containing conjugated electron systems.

4.2 Surface Morphology

The SEM of PPFDH thin films were recorded at different magnifications (5k×, 10k×) at accelerating voltage of 25 kV are shown in Fig. 4.1. From the micrographs it can easily be visualized that the surface of the plasma polymerized thin films is uniform, flawless, pinhole free and fracture free.

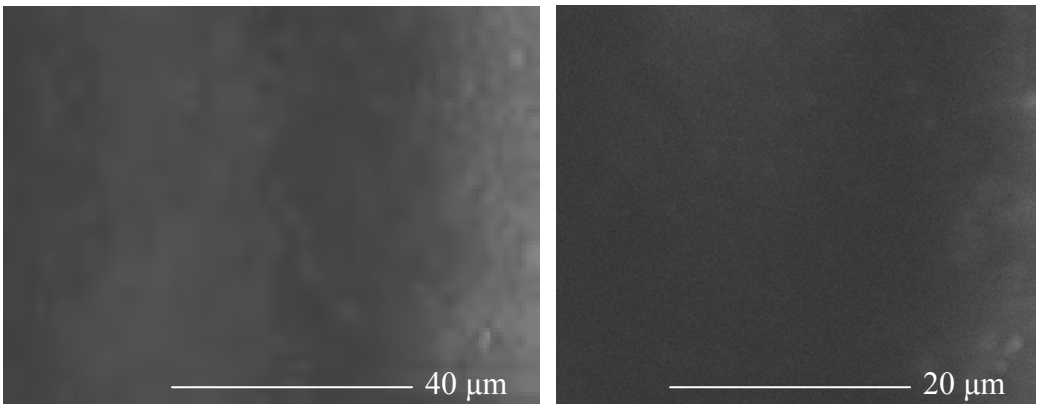

(a) (b)

Fig. 4.1 SEM micrographs of as-deposited PPFDH thin film (a) 5k× and (b) 10k×.

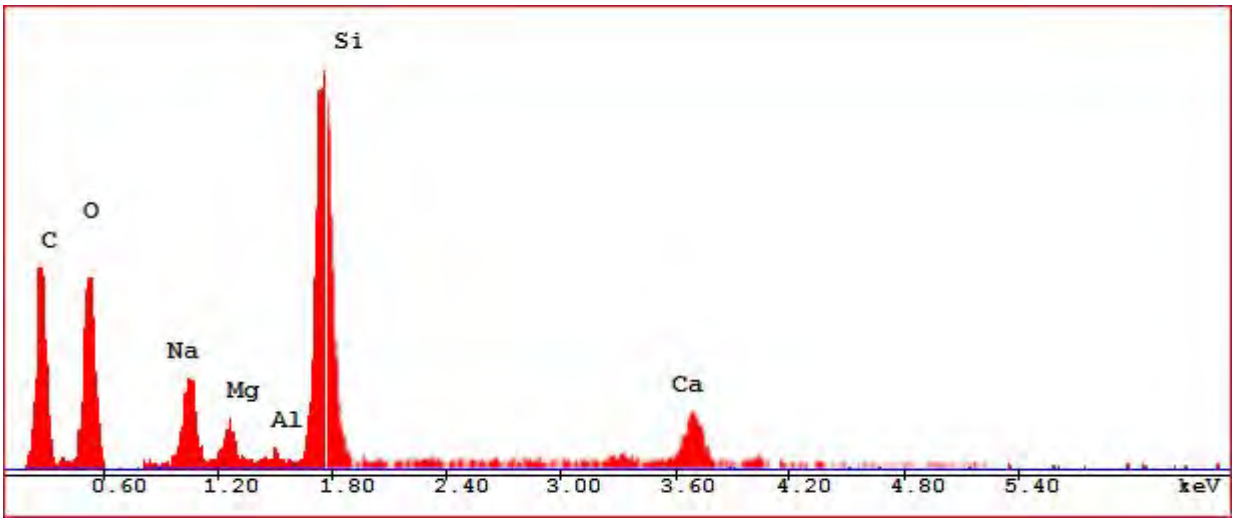

Fig. 4.2 EDAX spectra of PPFDH thin film.

Table 4.1 Composition of elements in PPFDH thin films

Element	At%
C	60.60
O	22.50
Na	2.9
Si	10.5
Ca	2.3
Mg	1.1

From the results it is clear that carbon (C) has the highest percentage and the presence of oxygen (O) follows a very good ratio as we can predict from the monomer. The higher percentage of O in the polymer is due to the incorporation of ambient oxygen when samples were taken out side from the reactor chamber. The presence of sodium (Na) and silicon (Si) in EDAX though it was not present in the monomer FDH is because the films were deposited onto glass substrate. In addition, from the EDAX result it is observed that it cannot identify the hydrogen present in the PPFDH thin films.

4.3 Infrared Spectroscopy

Fig. 4.3 shows the FTIR spectra of the FDH and PPFDH. These spectra reveal the structural changes due to plasma polymerization of the FDH. In the spectrum of FDH and of PPFDH a broad band at about 3133 and 3407 cm^{-1} (A), respectively are due to the presence of O-H stretching vibration for absorbed water. The characteristic

absorption band in PPFDH at 2926 cm^{-1} (B) may be assigned to aromatic C-H stretching vibration. The wider bands observed at 2850, 2811 (C) in FDH spectrum may be O=C-H stretching vibration attached to FDH. The band at 2214 cm^{-1} (D) in PPFDH may be arisen due to C≡C stretching vibration during plasma polymer. The aliphatic conjugation C=C stretching vibration band at 1689 and 1674 cm^{-1} (E) is observed in FDH. The band at 1603 cm^{-1} (E) in PPFDH is observed due to conjugation during polymerization. The band at 1569 cm^{-1} (F) in FDH is due to C=O bending vibration. The absorption bands at 1472 and 1464 cm^{-1} (G) correspond to the asymmetric C-H bending vibration and 1393 and 1367 cm^{-1} (H) correspond to the symmetric C-H bending vibrations. A band at around 1278 cm^{-1} (I) in FDH and at 1262 cm^{-1} (I) in PPFDH is due to C-H twisting. The band at 1157 cm^{-1} (J) in only FDH represents a C-C skeletal vibration. In spectrum of FDH, the bands at 1082 and 1020 cm^{-1} (K) correspond to the C-H in plane bending. The absorption bands at 930 and 883 cm^{-1} (L) in FDH and at 877 and 806 cm^{-1} in PPFDH may be arisen due to C-H rocking vibrations. The sharp absorption peaks at 755 cm^{-1} (M) is due to =C-H out-of-plane bending vibrations and the absorptions at 594 cm^{-1} indicate C=C out of plane bending.

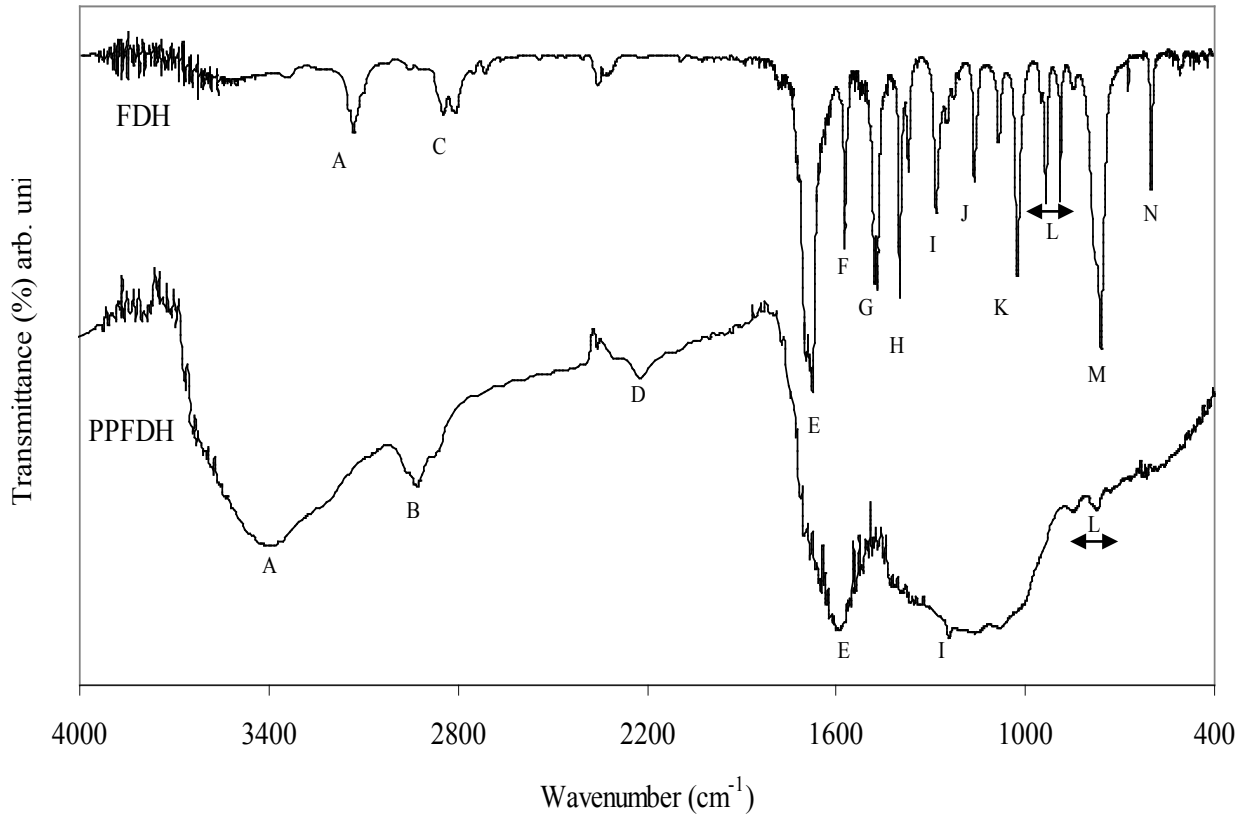

Fig. 4.3 FTIR spectra of FDH and PPFDH.

For comparison, the assignments to the different FTIR absorption bands of these two samples are presented in Table 4.2. From Table 4.2, it is seen that the chemical structure of PPFDH thin films contains C=C and C≡C conjugation instead of C-C skeletal structure.

Table 4.2 Assignments of FTIR absorption bands for FDH and PPFDH.

Assignments	**Wavenumber (cm^{-1})**	
	FDH	**PPFDH**
O-H stretching (A)	3133	3407
Asym. C-H stretching (B)	-------	2926
O=C-H stretching (C)	2850, 2811	-------
C≡C stretching (D)	-------	2214
C=C stretching (E)	1689, 1674	1603
C=O bending (F)	1569	-------
Asym.C-H bending (G)	1472, 1464	-------
Sym. C-H bending (H)	1394, 1368	-------
C-H twisting (I)	1278	1262
C-C skeletal (J)	1157	-------
C-H in plane bending (K)	1082,1020	-------
C-H rocking (L)	930, 883	877-806
=C-H out of plane bending (M)	755	-------
C=C out-of-plane bending (N)	594	-------

4.4 Thermal analyses

DTA and TGA traces of the as deposited PPFDH thin films taken in the temperature range 300-873 K at a scan rate of 10 K/min in nitrogen atmosphere are shown in Fig. 4.4 and Fig. 4.5 respectively.

It is seen that the TGA trace of PPFDH has showed different stages of mass loss due to heating. In the low temperature region, i.e. up to about 360 K, the weight loss may be due the removal of absorbed surface water/ non-constitutional, which is not associate with any change in the PPFDH structure. After that there is a small plateau region up to 450 K, i.e. the PPFDH is stable upto 520 K. After that the mass decreases gradually. This decrease in mass of PPFDH above 520 K may be due to evolution of hydrogen and/or low molecular mass hydrocarbon gases like CO and CO_2 etc.

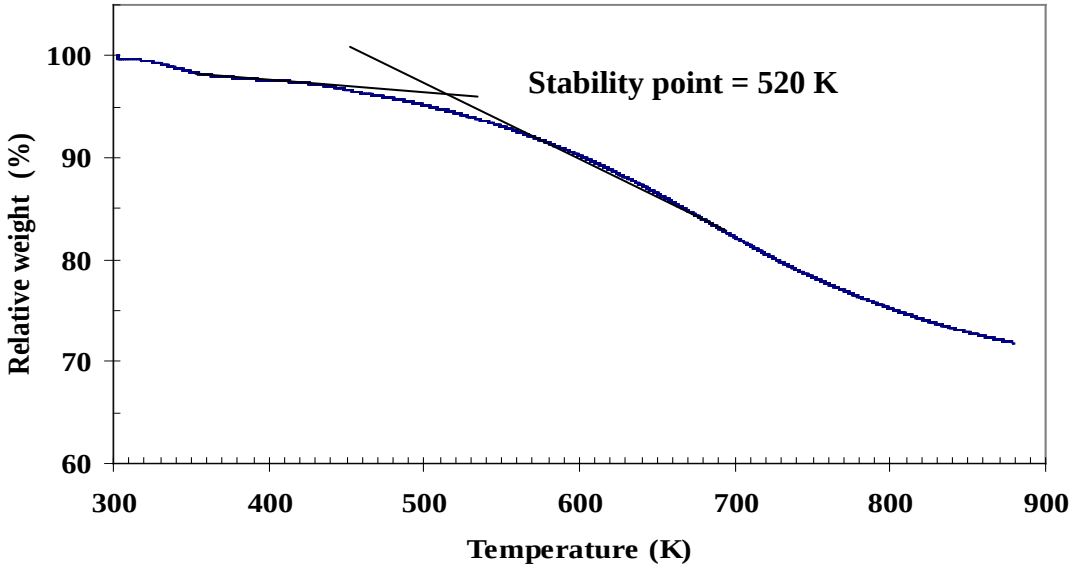

Fig. 4.4 TGA thermogram of as deposited PPFDH.

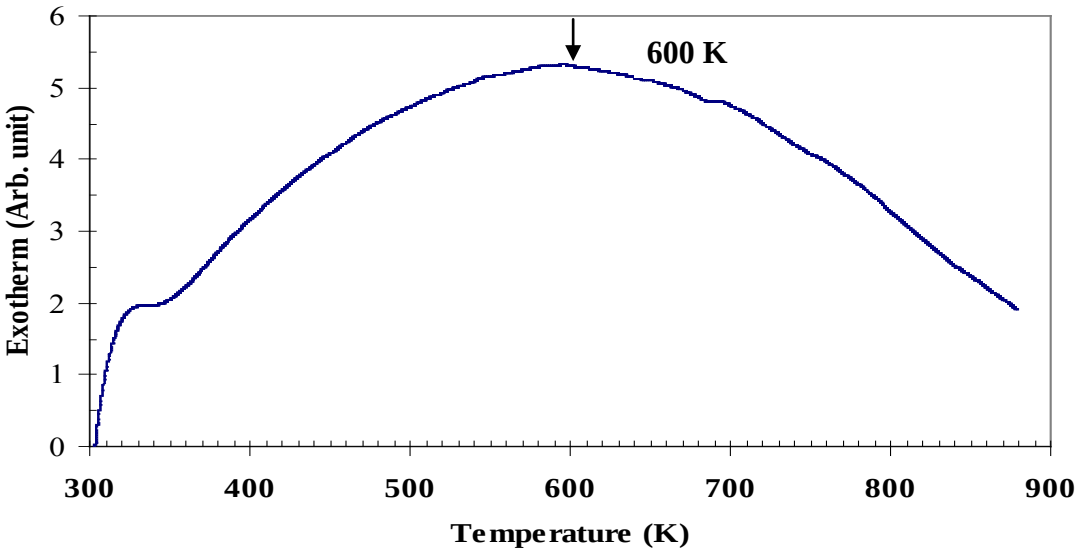

Fig. 4.5 DTA thermogram of as deposited PPFDH.

It is observed in the DTA trace around a temperature 335 K a transition occurs that may be due to the removal of water content. The DTA thermogram shows an exothermic broad band which has a maximum centered around 600 K indicating a gradual change of its original properties. The corresponding TGA trace shows a uniform weight loss up to 760 K.

4.5 Ultraviolet-visible spectroscopic analyses

The wavelength of light that a compound will absorb is the characteristic of its chemical structure. Specific regions of the electromagnetic spectrum are absorbed by exciting specific types of molecular and atomic motion to higher energy levels. Absorption of ultraviolet and visible (UV-Vis) radiation is associated with excitation of electrons, in both atoms and molecules, to higher energy states. Most molecules require very high energy radiation. Light in the UV-Vis region is adequate for molecules containing conjugated electron systems and as the degree of conjugation increases, the spectrum shifts to lower energy.

Amorphous films have a random network in contrast to the crystalline structure. In these materials no long range order is present. The disorderness associated with the deficiency of long range order in these materials introduces a low density of localized electronic states in the band gap which influence the electronic properties of the material.

Fig. 4.6 shows the UV-Vis spectral behavior of as deposited PPFDH thin films for various thicknesses at room temperature (300 K). From Fig. 4.6 it is seen that the absorbance increases with the increase of thickness of the PPFDH thin films and the absorption peak broadens with increasing thickness. It is also observed that the absorbance rises very rapidly before 300 nm, attains its maximum value and then decreases rapidly up to 700 nm.

The absorption coefficient (α) is calculated from the measured absorbance data for different wavelengths corresponding to different photon energies at room temperature by using equation,

$$\alpha = 2.303\frac{A}{d} \quad \text{..... (4.1)}$$

where, $A = \log_{10}(\frac{I_0}{I})$ is the absorbance and d is the thickness of the film. The spectral dependence of α on hν for all the as-deposited samples is presented in Fig. 4.7.

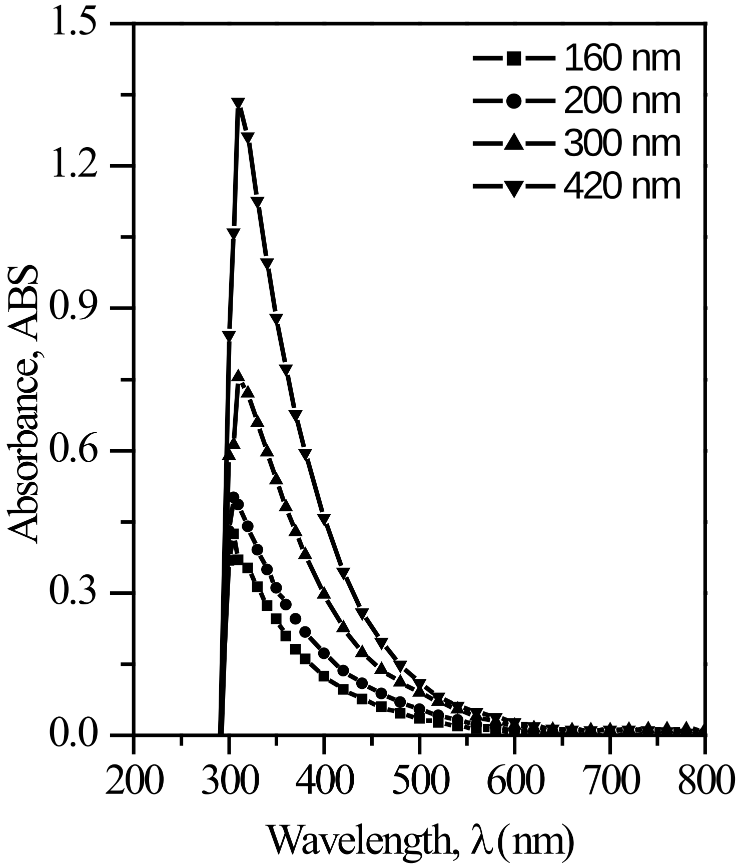

Fig. 4.6 Wavelength versus absorbance plot for different PPFDH thin films.

The dependence of optical absorption coefficient on the photon energy helps to study the band structure and the type of electron transition involved in absorption process.The absorption edge starts increasing around 1.9 eV and there is a rapid rise in absorption coefficient from 2.8 eV. It is observed that in the low energy region the curves are non-linear and the edges have an exponential fall for values of • below about 2×10^4 cm^{-1} for all the samples. It can be noticed that the curves have two different slopes in the experimental photon energy range. This may indicate the presence of direct and indirect optical transitions in the PPFDH thin films. These exponential falling edges may either be due to lack of long-range order or due to the presence of defects in the films.

In crystalline and amorphous materials the photon absorption is observed to obey the Tauc relation equation [115],

$$\bullet h\nu=B\,(h\nu-E_{opt})^{n} \quad \ldots\ldots(4.2)$$

where, hν is the incident photon energy, h Planck constant, ν the frequency of

incident radiation, B an energy independent constant, E_{opt} the optical band gap and n is an index depending on the type of optical transition caused by photon absorption. The index n equals ½ and 2 for allowed direct and indirect transitions respectively. Therefore, the indirect transition energy gap (E_{qi}) can be obtained by plotting $(\alpha h\nu)^{1/2}$ versus hν curve and then extrapolating the linear portion of the curve to $(\alpha h\nu)^{1/2} = 0$.

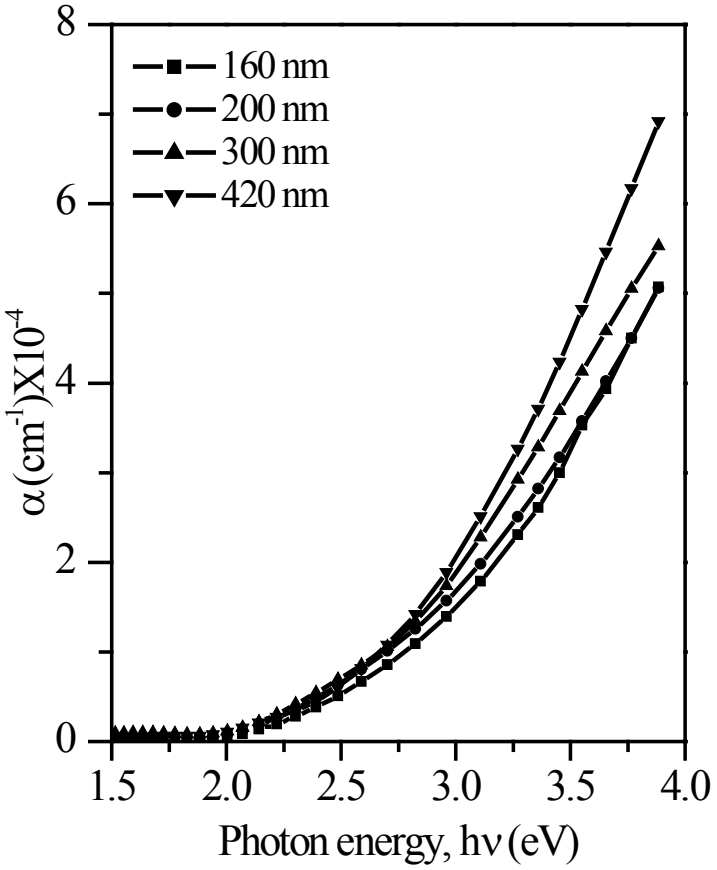

Fig. 4.7 Plot of α with hα, for as-deposited PPFDH thin films of different thicknesses.

In Fig. 4.8 $(\alpha h\nu)^2$ as a function of hν is plotted to obtain the E_{qd} of the as deposited PPFDH thin films. The E_{qd} is determined from the intercept of the linear part of the curves extrapolated to zero α in the energy axis. $(\alpha h\nu)^{1/2}$ as a function of hν is plotted in Fig. 4.9 to obtain the E_{qi} of the as deposited PPFDH thin films. The E_{qi} is determined from the intercept of the linear part of the curves extrapolated to zero α in the energy axis. The values of the E_{qi} and E_{qd} for as deposited PPFDH thin films are recorded in Table 4.3.

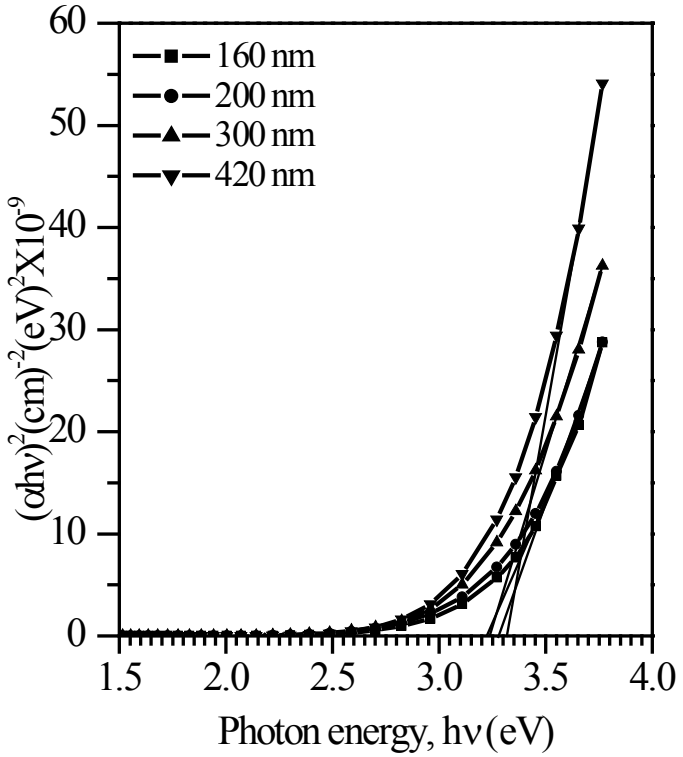

Fig. 4.8 $(\alpha h\nu)^2$ vs. $h\nu$ curves for as deposited PPFDH thin films of different thicknesses.

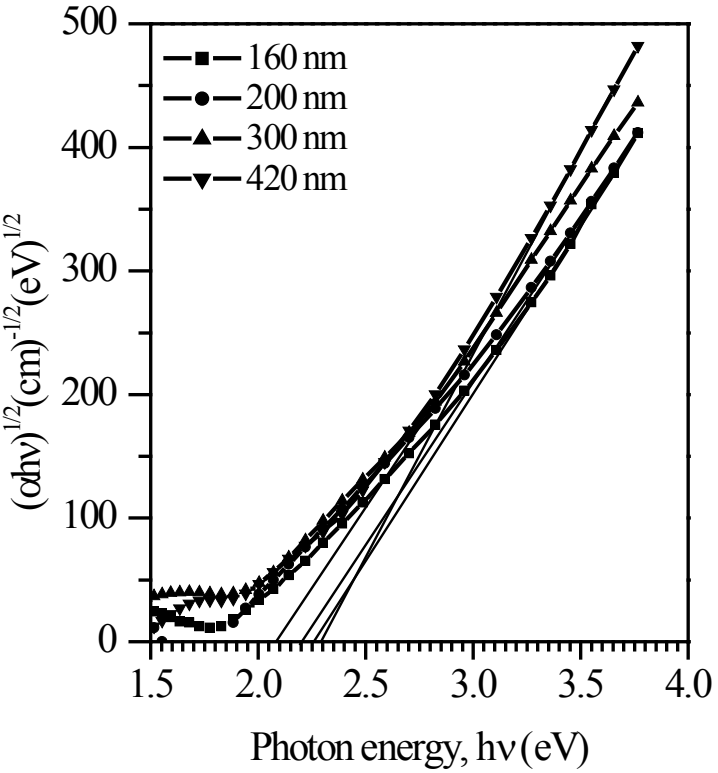

Fig. 4.9 $(\alpha h\nu)^{1/2}$ versus $h\nu$ curves for as deposited PPFDH thin films of different thicknesses.

The spectral dependence of • was studied at photon energies less than the energy gap of t he films, i.e. in the region of the so called Urbach spectral tail, which characterizes the slope of the exponential edge and is expressed as [116],

$$\bullet = \bullet_0 \exp (E/E_U) \quad \text{.....(4.3)}$$

where $\bullet_0$ is a constant and E_U the Urbach energy. Thus, the plots of ln• vs h• should be linear whose slope gives Urbach energy (E_U), interpreted as the width of the tails of localized states in the band gap. An increase in the optical band gap of the amorphous thin films can be explained due to the decrease of the band tails in the gap. The ln• vs h• plots for the thin films of different thicknesses are shown in Fig.4.10 and the corresponding values of E_U are also listed in Table 4.3. It can be noticed that the values of E_U, which is the band width of the localized states, decreases as the thickness increases, except the film having thickness of 200 nm. This behavior may be due to the decrease in the degree of disorder [117] and decrease in density of defect states.

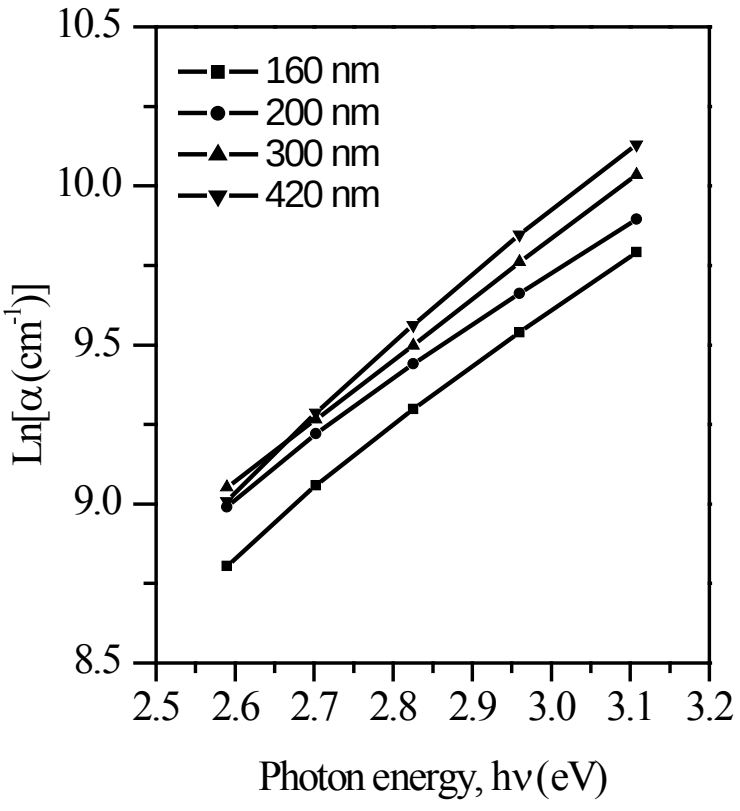

Fig. 4.10 The Urbach plots for PPFDH thin films of different thicknesses.

The steepness p arameter •, which characterizes the b roadening of t he opt ical absorption edge due to electron phonon or exciton-phonon interactions [118], can be calculated by the equation,

• = kT / E_U……(4.4)

where k is the Boltzmann constant and T is the absolute temperature. The values of • were calculated by taking T= 298 K and are noted in Table 4.3.

The extinction coefficient, K, can be calculated from • using the relation,

• = 4• K/• ……(4.5)

where • is the wavelength. The variation of K for PPFDH thin films with h• is shown in Fig.4.11. It is seen from the plot that the increase of K with the increase in h• indicating the probabilities of electron transfer across the mobility gap raises with h•.

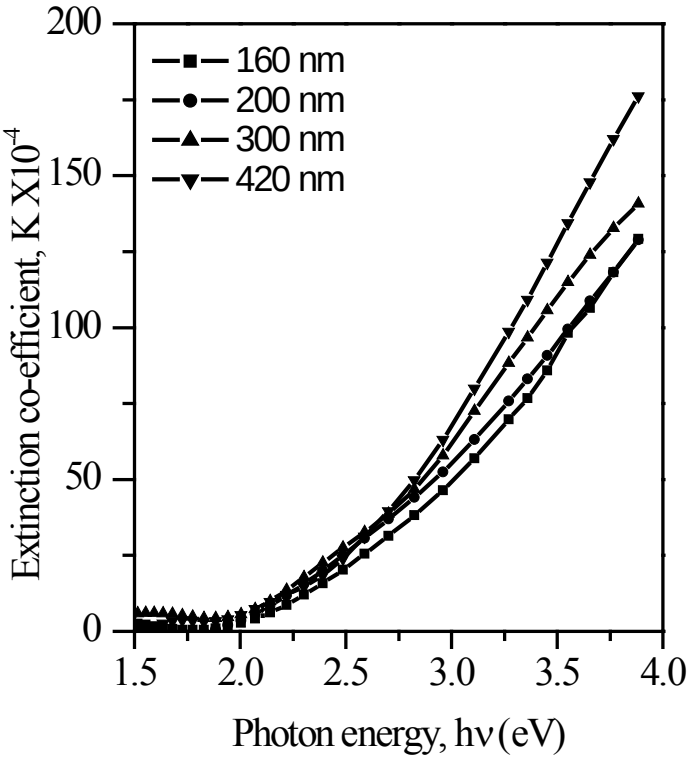

Fig. 4.11 Plot of K with h• for PPFDH thin films of different thicknesses.

Table 4.3 The optical parameters of PPFDH thin films of different thicknesses.

Film thickness, d (nm)	**Direct transition energy gap, E_{qd}** (eV)	**Indirect transition energy gap, E_{qi}** (eV)	**Urbach energy, E_U** (eV)	**Steepness parameter, •**
160	3.23	2.26	0.56	0.046
200	3.28	2.21	0.61	0.042
300	3.24	2.09	0.55	0.047
420	3.31	2.30	0.51	0.050

4.6 Electrical Properties

4.6.1 J-V characteristics

The J-V characteristics curves of PPFDH thin films of 160, 220, 280 and 330 nm thicknesses at the temperatures of 298, 348, 398 and 423 K in the voltage range 0.5 to 49 V are represented in Fig. 4.12, 4.13, 4.14 and 4.15 respectively. The variation of J with V seems to be linear in the low voltage region, but at higher voltages, the rate of increase of current density is faster. The J-V characteristics follow a power law of the form $J \bullet V^n$ with different values of 'n' (slopes), where n is a power factor. In the low voltage region the values of slope are $0.79 \bullet n \bullet 1.12$ and slope in the high voltage region lie between $1.81 \bullet n \bullet 2.58$ as shown in Table-4.4. These observations indicate that the current conduction is Ohmic in the low voltage region and non-Ohmic in the high voltage region. In addition, at the higher temperatures the current density increases significantly, revealing a strong temperature dependence of the current density.

4.6.2 Conduction mechanism in PPFDH thin films

One of the three different conduction mechanisms will be dominant for a specific polymeric material. The probable conduction mechanisms are space charge limited conduction, electrode limited Schottky type conduction and bulk limited Poole-Frenkel conduction.

(a) **Space Charge Limited Conduction (SCLC)**: The steady-state SCLC current density (J) in a plane-parallel dielectric sample with an electrode separation d is proportional to the square of the applied voltage (V). That is, the current density obeys an equation of the form [119]

$$J = \frac{9\mu\varepsilon'\varepsilon_0 V^2}{8d^3} \quad \text{..... (4.6)}$$

where ε' is the dielectric constant of the material, $\bullet_o$ the permittivity of the free space and μ the mobility of charge carriers. Therefore, for SCLC mechanism the slope of the J-V characteristics should be greater than or equal to 2.

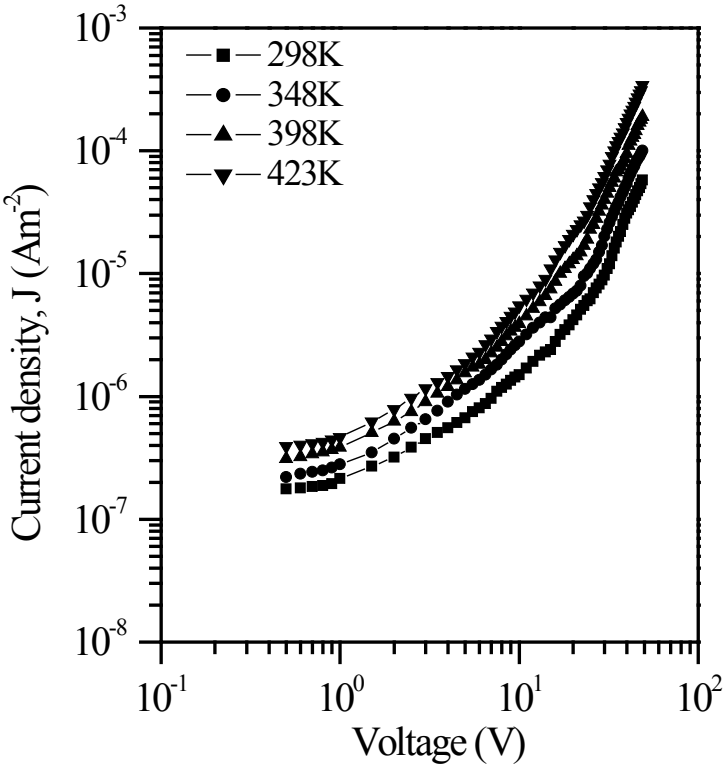

Fig. 4.12 Variation of J with V at different temperatures for PPFDH thin film (d=160 nm).

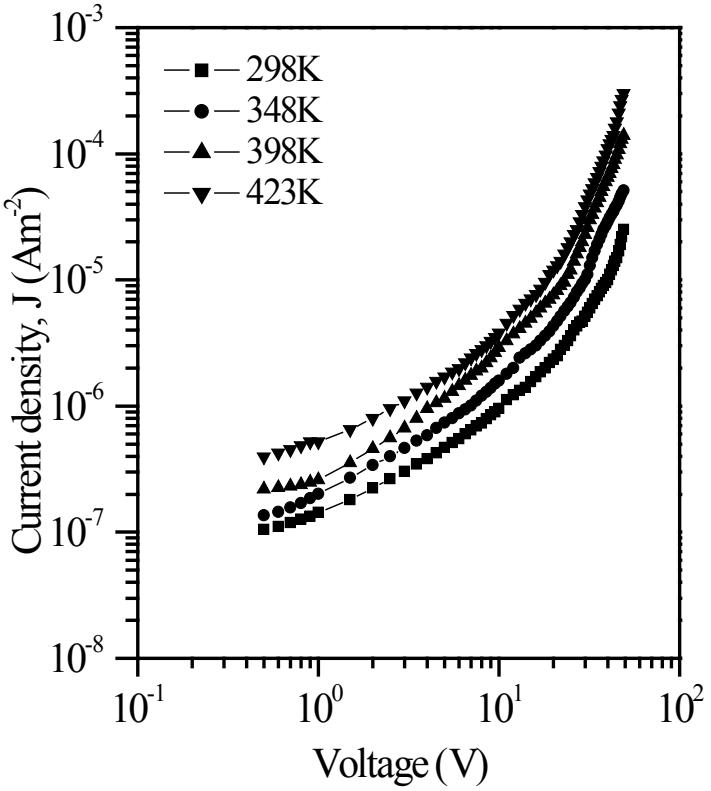

Fig. 4.13 Variation of J with V at different temperatures for PPFDH thin film (d=220 nm).

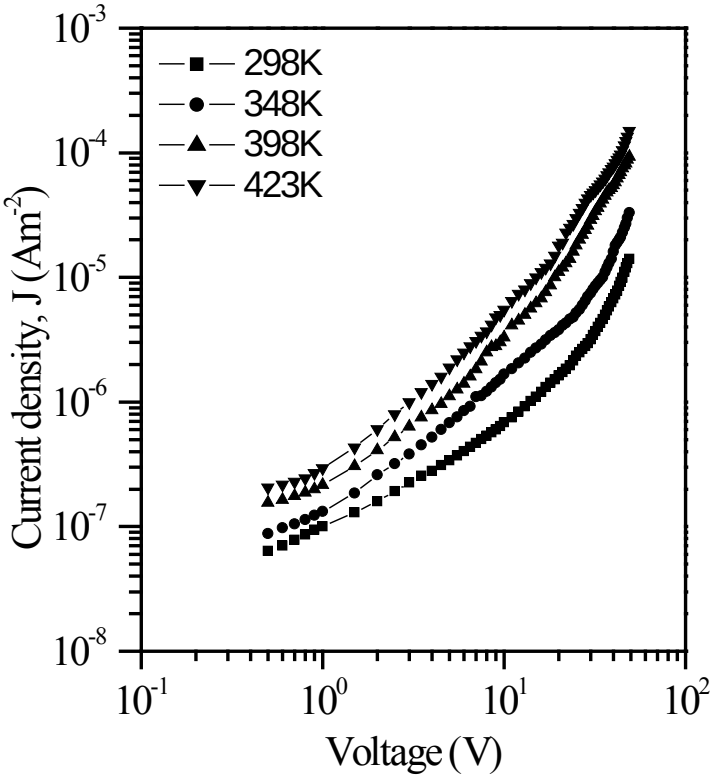

Fig. 4.14 Variation of J with V at different temperatures for PPFDH thin film (d=280 nm).

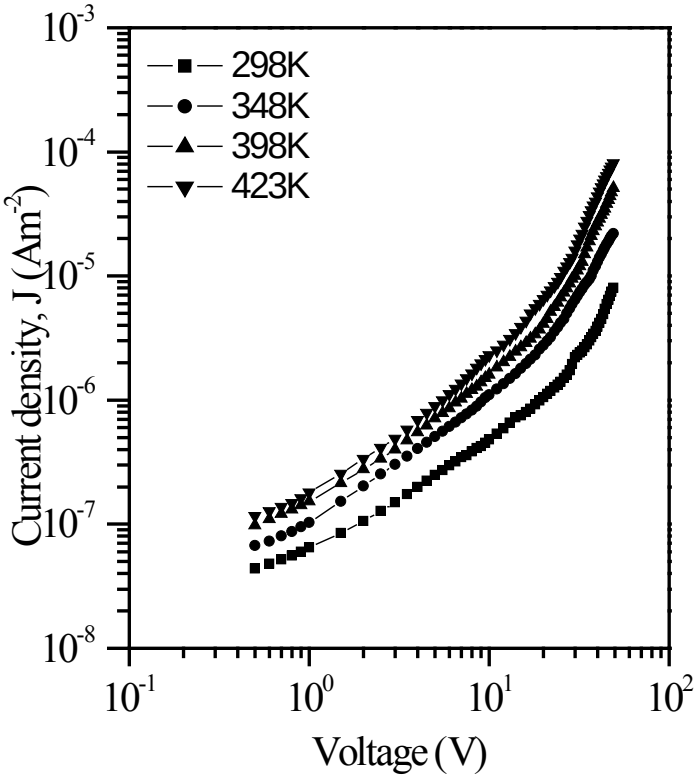

Fig. 4.15 Variation of J with V at different temperatures for PPFDH thin film (d=330 nm).

Table-4.4 Values of 'n' at different temperatures for PPFDH sample

Thickness (nm)	**Temperature** T (K)	**Values of the slope, n**	
		Low voltage region	**High voltage region**
160	298	0.79	1.98
	348	1.00	2.28
	398	0.94	2.29
	423	0.94	2.58
220	298	0.88	2.56
	348	1.10	2.13
	398	1.10	2.51
	423	0.99	2.58
280	298	0.80	1.96
	348	0.99	1.81
	398	1.00	2.23
	423	1.12	2.24
330	298	0.98	1.89
	348	0.99	2.02
	398	1.00	2.14
	423	1.02	2.24

From the J-V plots in Fig. 4.12, 4.13, 4.14 and 4.15, it is observed that in the higher voltage region the calculated values of n (Table-4.4) are $1.81 \bullet n \bullet 2.58$, which suggest the possibility of SCLC or PF or Schottky type mechanisms in the PPFDH thin films. According to SCLC theory, the thickness dependence of the space charge limited current follows the relation $J \bullet d^{-m}$, where m is a parameter which depends on the trap distribution and is equal to or greater than three in the presence of traps. The thickness dependence of the current density for PPFDH thin films is shown in Fig. 4.16. From Fig. 4.16 it is seen that the J varies as $d^{-2.7}$. The value 2.7 is much less than the required exponent value for SCLC. So, SCLC conduction mechanism is ruled out.

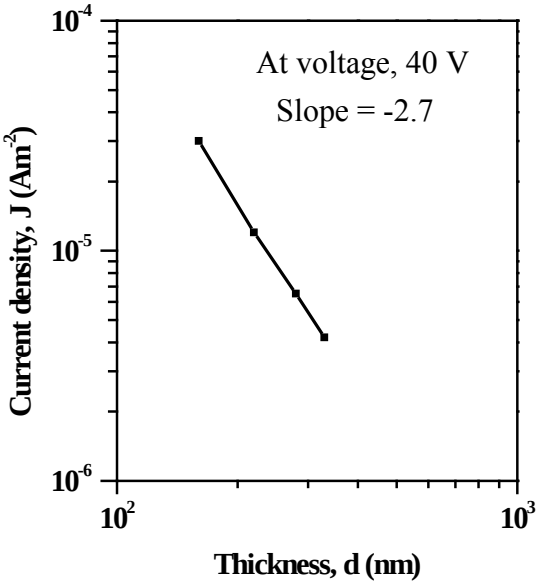

Fig. 4.16 Variation of J with d for PPFDH thin films.

(b) **Poole-Frenkel mechanism/Schottky mechanism**

The general expression for both Schottky and PF type conductions is expressed by the equation of the form [120],

$$J = J_0 \exp\left(\frac{\beta F^{1/2} - \phi}{kT}\right) \text{.....} \quad (4.7)$$

where J_0 is the low-field current density, F the applied electric field, k the Boltzmann constant, T the absolute temperature and ϕ the ionization energy of localized centers in PF conduction and Coulomb barrier height of the electrode polymer interface in Schottky type conduction and β the coefficient of the static electric field. The coefficient β for the Schottky type conduction is known as Schottky coefficient (β_s) and defined as

$$\beta_s = \left(\frac{e^3}{4\pi\varepsilon'\varepsilon_0}\right)^{1/2} \text{.....} \quad (4.8)$$

For the PF mechanism, it is called the PF coefficient (β_{PF}) and is defined as

$$\beta_{PF} = 2\left(\frac{e^3}{4\pi\varepsilon'\varepsilon_0}\right)^{1/2} = 2\beta_s \text{.....} \quad (4.9)$$

where, e is the electronic charge. Therefore according to equation (4.7) a plot of LnJ versus $V^{1/2}$ (Schottky plots) should be a straight line in the higher voltage region with a positive slope. Fig. 4.17, 4.18, 4.19 and 4.20 show the plots between LnJ versus $V^{1/2}$ for PPFDH thin film of different thicknesses (160, 220, 280 and 330 nm).

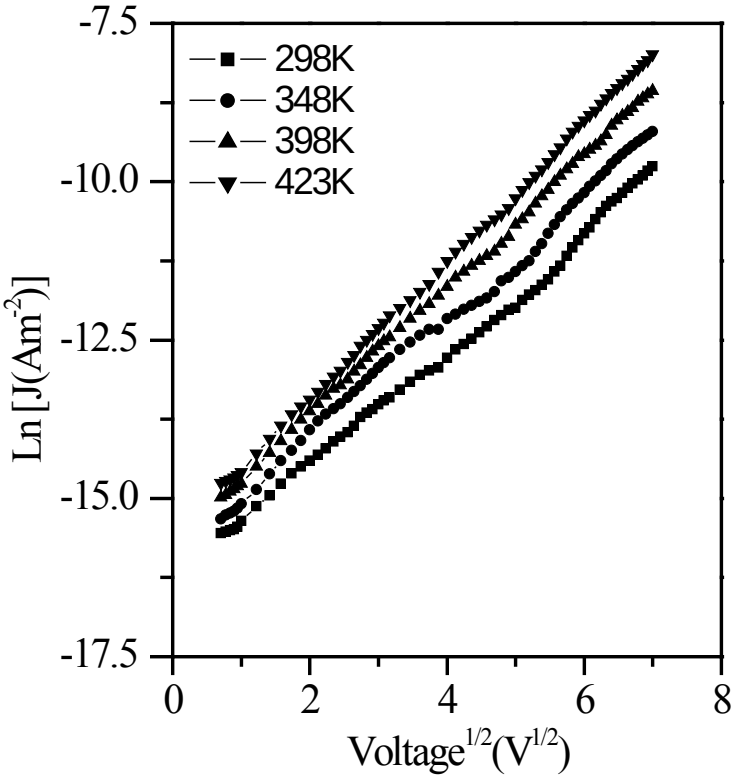

Fig. 4.17 Variation of Ln J with $V^{1/2}$ for PPFDH thin film (d=160 nm).

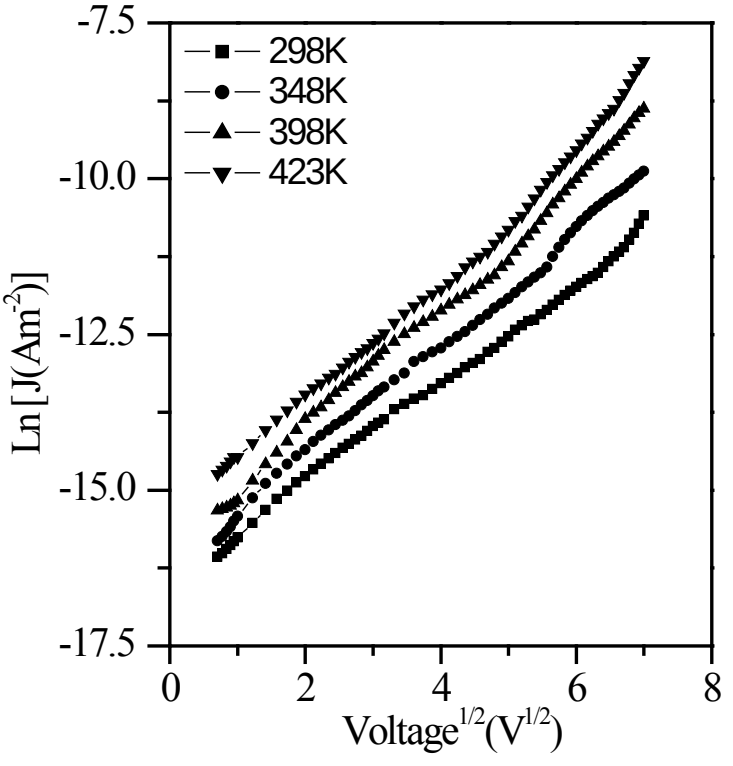

Fig. 4.18 Variation of Ln J with $V^{1/2}$ for PPFDH thin film (d=220 nm).

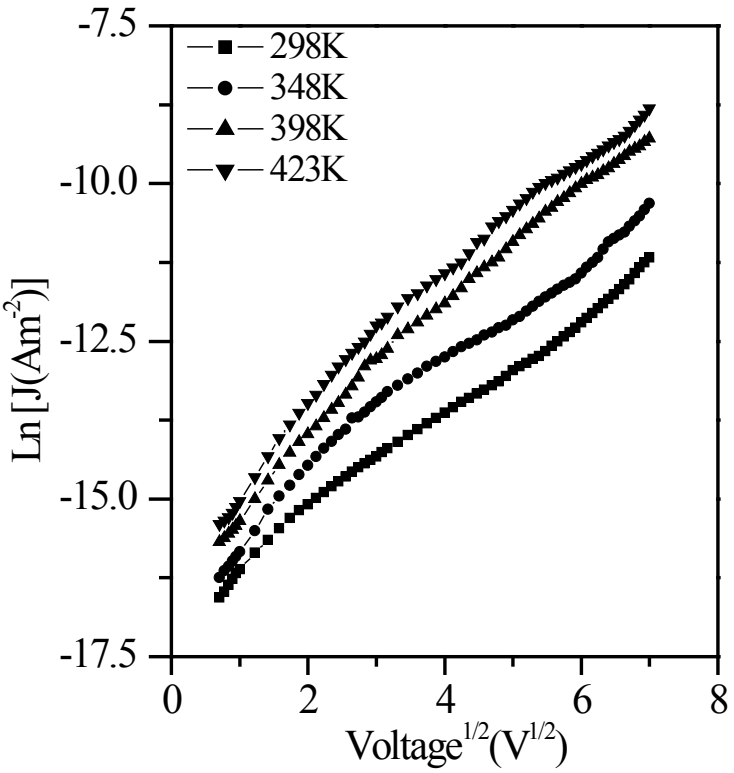

Fig. 4.19 Variation of Ln J with $V^{1/2}$ for PPFDH thin film (d=280 nm).

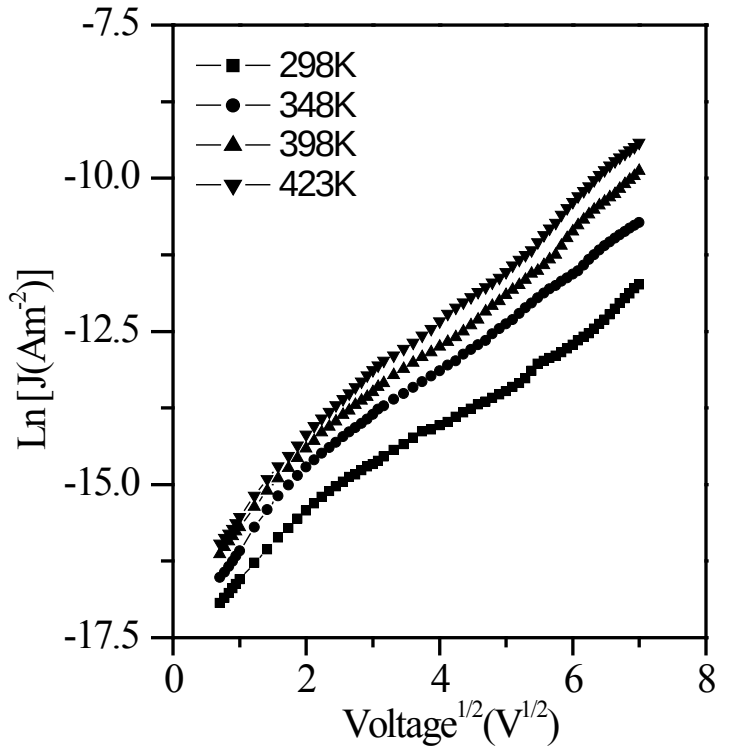

Fig. 4.20 Variation of Ln J with $V^{1/2}$ for PPFDH thin film (d=330 nm).

It is observed from Fig. 4.17, 4.18, 4.19 and 4.20 that Schottky plots are approximately straight line with positive slopes indicating the probable conduction mechanism to be of Schottky or PF type. Therefore, from the voltage dependence of current density data at different elevated temperatures it is found that the mechanism of charge transport in PPFDH thin films may be due to Schottky or PF type.

To differentiate between these two conduction mechanisms, β_s and β_{PF} have been calculated theoretically and then compared them with the β calculated from experimental results. The relation $\beta_{expt} = skTd^{1/2}$ were used to calculate experimental values of the β, where, s is the slope ($s = \Delta Ln\ J/\Delta V^{1/2}$) of the graph plotted between Ln J and $V^{1/2}$. The theoretical values of the β were calculated from the equations (4.8) and (4.9) and tabulated in table-4.5.

Table-4.5 Comparison between the theoretical (β_{th}) and experimental (β_{exp}) coefficients (β).

Thickness (nm)	**Dielectric constant** f =1000 Hz	**Theoretical, β_{th}**		**Experimental, β_{exp}** ($eV\text{-}m^{1/2}V^{-1/2}$)
		β_S ($eV\text{-}m^{1/2}V^{-1/2}$)	**β_{PF}** ($eV\text{-}m^{1/2}V^{-1/2}$)	
160	6.7	1.47×10^{-5}	2.92×10^{-5}	1.25×10^{-5}
220	6.2	1.52×10^{-5}	3.04×10^{-5}	1.34×10^{-5}
280	5.7	1.59×10^{-5}	3.18×10^{-5}	1.40×10^{-5}
330	4.5	1.79×10^{-5}	3.58×10^{-5}	1.49×10^{-5}

From the values of data in Table- 4.5, it is clearly seen that the values of β_{exp} are close to the values of β_{th} which indicate that the probable mechanism of charge transport in the PPFDH thin film is Schottky type. Furthermore in Schottky-Richardson mechanism the current density (J) shows strong temperature (T) dependence but not in the case of PF mechanism. Therefore an alternative way to identify whether the conduction mechanism is PF or Schottky, it is appropriate to investigate the T dependence of J.

4.6.3 Temperature dependence of current density

The temperature dependence of the current density, *J*, can be expressed by the well-known Arrhenius law

$$J = J_0 \exp(-\frac{\Delta E}{kT}) \quad \text{..... (4.10)}$$

where J_0 is a constant, • E the thermal activation energy of electrical conduction and k the Boltzmann constant. Fig. 4.21, 4.22, 4.23 and 4.24 show the dependence of J on inverse absolute temperature, 1/ T, for various PPFDH thin films of different thicknesses (160, 220, 280 and 330 nm). In these figures there are two curves, corresponding to the temperature dependence in the low voltage region (V= 5V) and in the high voltage regions (V= 35V) respectively. It is observed that the J increases slowly for T <340 K and above this J increases rapidly with T. This increase in J with T may be due to the increased movement of the ions and/or electrons.

It is seen that both the curves can be characterized by two different slopes in the low and high temperature regions. The curves have varying slope at low temperatures but become almost linear in the high temperature region, corresponding to well-defined activation energy (E). The activation energies associated with two temperature regions were calculated from the slopes of $J - \frac{1}{T}$ plot for samples of different thicknesses and are depicted in Table-4.6. From Table-4.6, for applied voltage of 5V, at low temperature region the activation energies are found to be around 0.13 ± 0.02 eV and at higher temperature region it is 0.50 ± 0.05 eV. Where as, the low and high temperature region activation energies are found to be 0.11 ± 0.01 eV and 0.55 ± 0.02 eV, respectively for an applied voltage of 35 V.

These small values of the activation energies in the low and high temperature regions suggest the existence of the shallow traps levels in PPFDH thin films. The low activation energies in the low temperature region indicate that the thermally activated hopping conduction is operative in this material. This change in • E from lower to higher values may be attributed to a transition from a hopping regime to a regime dominated by distinct energy levels [121].

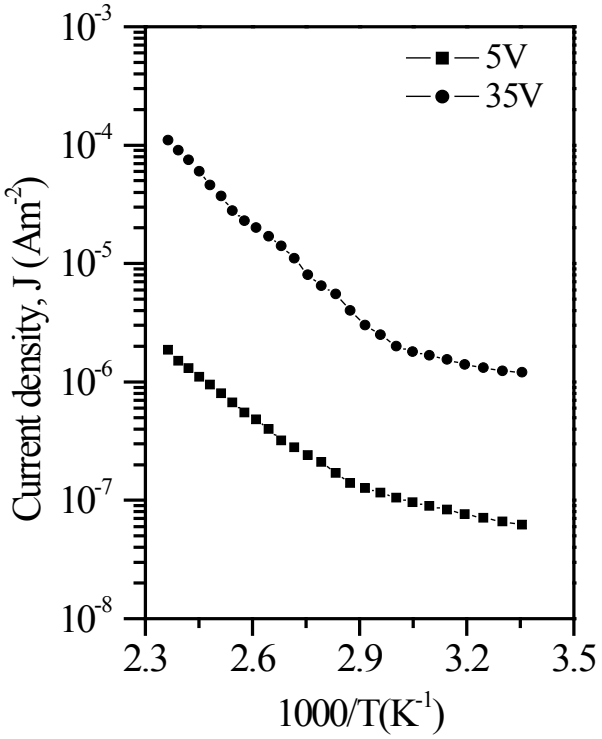

Fig. 4.21 Variation of J with 1/T for PPFDH thin film in ohmic and non-ohmic regions (d=160 nm).

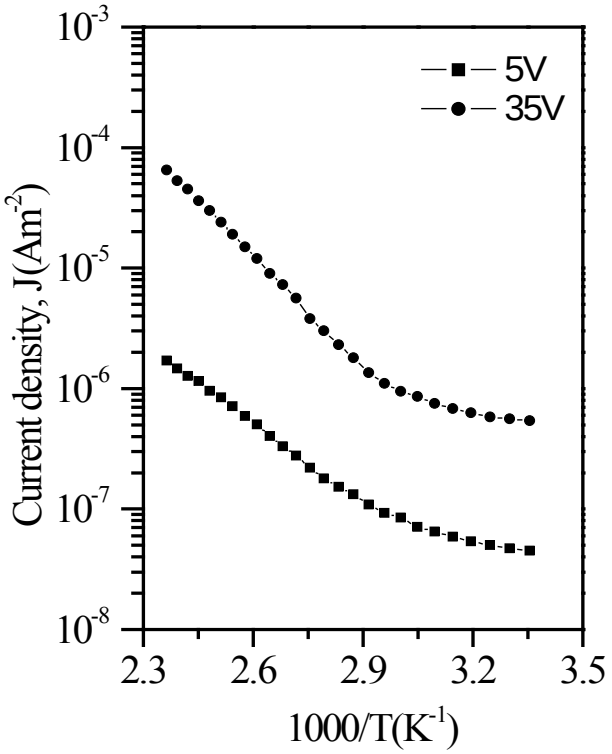

Fig. 4.22 Variation of J with 1/T for PPFDH thin film in ohmic and non-ohmic regions (d=220 nm).

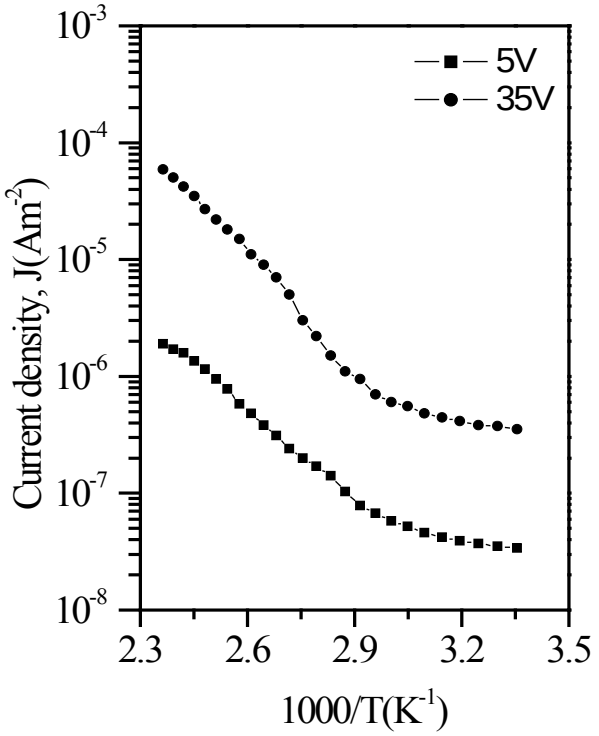

Fig. 4.23 Variation of J with 1/T for PPFDH thin film in ohmic and non-ohmic regions (d=280 nm).

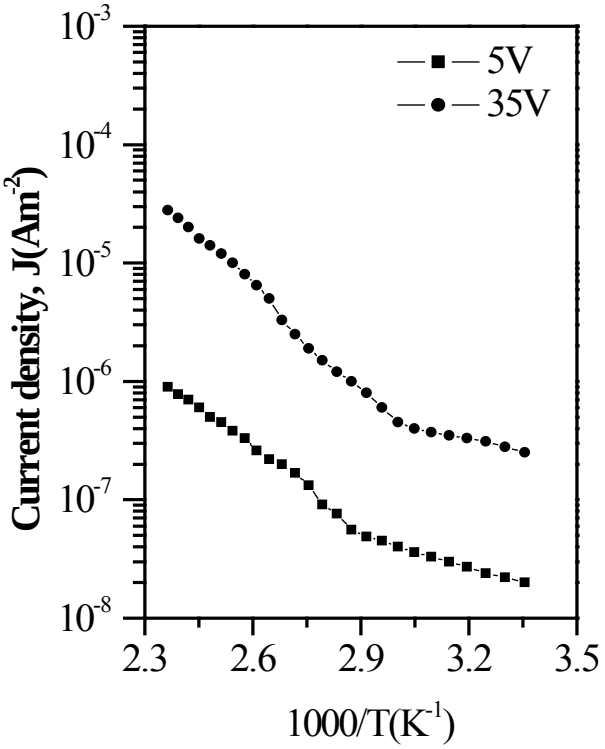

Fig. 4.24 Variation of J with 1/T for PPFDH thin film in ohmic and non-ohmic regions (d=330 nm).

Table 4.6 The values of activation energy • E for PPFDH thin films of different thicknesses.

Thickness d (nm)	**Activation energy, • E (eV)**			
	5 V		35V	
	Temperature		**Temperature**	
	Low	**High**	**Low**	**High**
160	0.11	0.47	0.11	0.57
220	0.12	0.46	0.10	0.57
280	0.15	0.55	0.12	0.53
330	0.12	0.45	0.11	0.56

CHAPTER 5

CONCLUSION

5.1 Conclusion

Based on the results and discussion, the following conclusions can be drawn:

It is observed that the surface of the PPFDH thin films is uniform, flawless, pinhole free and fracture free. The FTIR analyses show that the PPFDH is structurally different from the monomer and contains C=C and C≡C conjugation instead of C-C skeletal structure. The TGA trace of PPFDH shows that up to about 360 K, the weight loss may be due to the removal of absorbed surface water. The PPFDH is stable up to temperature 520 K. After that the mass decreases gradually which may be due to evolution of hydrogen and/or low molecular mass hydrocarbon gases. The DTA thermogram shows an exothermic broad band which has a maximum centered around 600 K indicating a gradual change of its original properties. The corresponding TGA trace shows a uniform weight loss up to 760 K. UV-vis spectra show that the absorbance increases with the increase of thickness of the PPFDH thin films. The values of E_{qd} and E_{qi} were found to be about 3.23 -3.31 eV and 2.09-2.30 eV respectively for as deposited PPFDH thin flims. The values of E_U and • were 0.51-0.61 eV and 0.042 -0.050 respectively for different thicknesses of PPFDH thin films. Theoretically calculated values β_s and β_{PF} and the values of these coefficients calculated from the experimental J-V characteristics have lead to comment on the conduction mechanism as Schottky type. The temperature dependence of current density also suggests Schottky type mechanism. So it may be concluded that the most probable conduction mechanism in the PPFDH thin films is of Schottky type.

5.2 Suggestion for Future Research

For quantitative information of the element present in the thin films of different thickness, XPS investigation could be carried on to study the bonding of different functionalities and chemical states. For more accuracy about the surface morphology XPS is most essential. The electron spin resonance (ESR) study may be carried out to go insight the nature and source of radicals in this material.

For precise information about the chemical structure of the materials, the XRD analysis might be performed.

In order to know more precisely the probable structural change due to the change of the thickness, the FTIR spectra could be taken for the films of different thickness separately and analyzed to study the thickness dependence.

The optical study revealed that band gap is independent of thickness but depends on temperature. It was observed that the electrical properties are thickness and temperature dependent. A very few literature was found that emphasizes on the properties with thickness variation.

Asymmetric configuration of M/I/M sandwich structure is essential to comment on the conduction mechanism in thin films. So we tried to use Ag as one of the electrode in metal/Polymer/metal sandwich structure for electrical measurement but we failed for several times to deposit Ag as it flashes and evaporation is not so easy. Next time Au may be used as an electrode for electrical measurements. In electrical measurement heat treated sample may be taken into consideration. The aging effect of a large number of samples may be studied. All the results of the above analyses might then be correlated with the thickness dependent optical and electrical properties of the thin films.

References

[1] Wrobel, A. M., Wertheimer, M. R., Dib, J., Schreiber, H. P., "Polymerization of organo-silicones in microwave discharges", J. Macromol. Sci.-Chem., Part A, **14**(3), 321-325, (1980).

[2] Inagaki, N., Kondo, S., Hirata, M., Urushibata, H., "Plasma polymerization of organo-silicon compounds", J. Appl. Polym. Sci., **30**(8), 3385-3388, (1985).

[3] Inoue, Y., Sugimura, H., Takai, O., "In situ observation of behavior of organo-silicon molecules in low-temperature plasma enhanced CVD", Thin Solid Films, **345**(1), 90-93, (1999).

[4] Chermisinoff, N. P., "Handbook of Polymer Science and Technology", Vol. **4** Marcel Dekker Inc, New York (1989).

[5] Biederman, H. and Osada, Y., "Plasma Chemistry of Polymers", Vol. **95** Advance in Polym Sci., Berlin (1990).

[6] Polonskyi, O., Matousek, J., Drabik, M., Kousal, J., Choukourov, A., Slavinska, D.,Biederman, H., Pleticha, D. and Hanley, L., "Deposition and Basic Properties of Thiophene Plasma Polymer Films", WDS'08 Proceedings of Contributed Papers, **Part III,** 159-165, (2008).

[7] Yasuda, H., "Plasma polymerization", Academic Press, Orlando, (1985).

[8] Morita, S. and Hattori, S., "Applications of Plasma Polymers in Plasma Deposition, Treatment, and Etching of Polymers," R d' Agostino, (Ed.), Academic Press, San Diego, CA, (1990).

[9] Zhao, X. Y., Wang, M. Z. and Xiao J., "Deposition of plasma conjugated polynitrile thin films and their optical properties", Euro. Polym J., **42**(9), 2161-2167, (2006).

[10] Lakshmi, G.B.V.S., Dhillon, A., Siddiqui, A.M., Zulfequar, M., Avasthi, D.K, "RF-plasma polymerization and characterization of polyaniline", Euro. Polym J., **45**(10), 2873-2877, (2009).

[11] Mathai, C. J., Saravanan, S., Anantharaman, M. R., Venkitachalam, Jayalekshmi, S., "Characterization of low dielectric constant polyaniline thin films synthesized by ac plasma polymerization technique", J. Phys. D Appl. Phys.**, 35**(3), 240-245, (2002).

[12] Bae, I.-S., Cho, S.-H., Lee, S.-B., Kim Y. and Boo, J.-H., "Growth of plasma-

polymerized t hin f ilms by P ECVD m ethod a nd s tudy on t heir s urface and optical characteristics", Surf. Coat. Technol., **193**, 142-146, (2005).

[13] Karim, R., "Preparation and investigation of the optical and DC electrical properties of plasma polymerized thin films of 1,1,3,3-tetramethoxypropane", M.Phil. Thesis, BUET, Dhaka (2005).

[14] Majumder, S., "Investigation of the optical and electrical properties of plasma polymerized vi nylene c arbonate t hin films", Ph.D. T hesis, BUET, D haka (2011).

[15] Sarker R.B., "Preparation and investigation of the different properties of plasma polymerized thin films of organic materials" , Ph.D. Thesis, BUET, Dhaka (2011).

[16] Chowdhury, F-U-Z., "Preparation and characterization of plasma polymerized diphenyl thin films", Ph.D. Thesis, BUET, Dhaka (2000).

[17] Zaman, M., "Preparation and study of DC electrical mechanism in plasma polymerized thin films of tetraethylorthosilicate", M.Phil. Thesis, BUET, Dhaka (2005).

[18] Akther, H., "Preparation and study of the electrical properties of plasma polymerized thin films of N,N,3,5–tetrametlylaniline", M.Phil. Thesis, BUET, Dhaka (2005).

[19] Jalal, A.B.M.S., "Characterization of plasma polymerized m-xylene thin films for its application in electrical devices", Ph.D. Thesis, BUET, Dhaka (2011).

[20] Rahman, M.J., "Optical and AC electrical properties of plasma polymerized o-methoxyaniline thin films", M.Phil. Thesis, BUET, Dhaka (2011).

[21] Matin, R.," Preparation and study of DC electrical conduction mechanism in plasma polymerized 2,6, diethylaniline thin film ", M.Phil. Thesis, BUET, Dhaka (2007).

[22] Afroze T.," Investigation of the optical and AC electrical properties of plasma polymerized 1, 1, 3, 3 tetramethoxypropane thin films", M.Phil. Thesis, BUET, Dhaka (2007).

[23] Dey, H., "Study of the optical and electrical properties of plasma polymerized cedar wood oil thin films", M.Phil. Thesis, BUET, Dhaka (2012).

[24] Goodman, J., "The formation of thin polymer films in the gas discharge", J. Polym. Sci., **44,** 551-552, (1960).

[25] Cho, S.-J., Bae, I.-S., Boo, J.-H., Park, Y. S. and Hong, B., "Study on the Plasma-Polymer Thin Films Deposited by Using PECVD and Application Tests for Low-k Insulator", J. Korean Phys. Soc., **53(3),** 1634-1637, (2008).

[26] Matin, R., Bhuiyan A.H., " Electrical transport mechanism in plasma polymerized 2,6, diethylaniline thin film " , Thin Solid Films **519** (11), 3462-3467, (2011).

[27] Afroze T., Bhuiyan A.H., " Infrared and ultraviolet-visible spectroscopic studies of plasma polymerized 1, 1, 3, 3 tetramethoxypropane thin films" , Thin Solid Films **519** (6), 1825-1830, (2011).

[28] Yague J. L., and Borro S., "Conducting Plasma Polymerized Polypyrrole Thin Films as Carbon Dioxide Gas Sensors", Plasma Process. Polym. **9**, 485–490, (2012).

[29] Blaszczyk-Lezak, I., Aparicio, F. J., Borra´s, A., Barranco, A., Alvarez-Herrero, A., Ferna´ndez-Rodrı´guez, M. and Gonza´lez-Elipe, A. R., "Optically Active Luminescent Perylene Thin Films Deposited by Plasma Polymerization", J. Phys. Chem. C, **113,** 431–438, (2009).

[30] Sarker R.B., Bhuiyan A.H., " Electrical conduction mechanism in plasma polymerized 1- Benzyl-2 methylimidazale thin films under static electric field" , Thin Solid Films **519** (18), 5912-5916 (2011).

[31] Matin, R., Bhuiyan A.H., "Heat treatment and aging effect on the structural and optical properties of plasma polymerized 2,6-diethylaniline thin films" , Thin Solid Films **520** (21), 6463–6470, (2012).

[32] Cho, S.-J., Bae, I.-S., Boo, J.-H., Park, Y. S. and Hong, B., "Study on the Plasma-Polymer Thin Films Deposited by Using PECVD and Application Tests for Low-k Insulator", J. Korean Phys. Soc., **53(3),** 1634-1637, (2008).

[33] Zhao, X.Y., Wang, M.Z., Zhang, B.Z. and Mao, L., "Synthesis, characterization and nonlinear optical properties of plasma-prepared poly(4-biphenylcarbonitrile) thin films", Polym. Int. **56,** 630-631 (2007).

[34] Majumder, S. and Bhuiyan, A. H., "DC Conduction Mechanism in Plasma Polymerized Vinylene Carbonate Thin Films Prepared by Glow Discharge Technique", Polymer Science, Ser. A, **53**(1), 85-91, (2011).

[35] Zaman, M. a nd B huiyan, A. H., "Direct current el ectrical cond uction mechanism in plasma p olymerized thin films of te traethylorthosilicate", Thin Solid Films, **517**(18)**,** 5431-5434, (2009).

[36] Nespurek, S., Zmeskal, O. and Sworakowski, J. 'Space-charge-limited currents in or ganic f ilms: S ome ope n pr oblems', Thin Solid Films **516,** 8949-8955, (2008).

[37] Chowdhury, F-U-Z and Bhuiyan, A. H., "An investigation of the optical properties of the plasma polymerized diphenyl thin films", This Solid Films, **360**(1-2), 69-74, (2000).

[38] Chowdhury, F-U-Z and Bhuiyan, A. H., "Dielectric properties of plasma polymerized diphenyl thin films", Thin Solid Films, **370,** 78-84, (2000).

[39] Guermat, N., Bellel, A. and Raynaud, P. 'Thin plasma-polymerized layers of hexamethyldisiloxane for humidity sensor development', Thin Solid Films **517,** 4455-4460, (2009).

[40] Akther, H. and Bhuiyan, A. H., "Infrared and ultraviolet-visible spectroscopic investigation of pl asma pol ymerized N ,N,3,5–tetrametlylaniline thi n films", Thin Solid Films, **474,** 14 -18, (2005).

[41] Akther, H. and Bhuiyan, A. H., "Electrical and Optical properties of plasma polymerized N, N , 3, 5 tetramethylamiline thi n films", New J . P hys. **7,** 173-176, (2005).

[42] Sakthi, K. D. and Yasuhika, Y., "Dielectric properties of plasma polymerized pyrrole thin film capacitors", Surf. Coat. Technol, **169-170,** 600-603, (2003).

[43] Vikram Kumar, S. C. Jain, A. K. Kapoor, J. Poortmans, R. Mertens, 'Trap density in conducting organic semiconductors determined from temperature dependence *J-V* characteristics', J. Appl. Phys. **94,** 1283-1285, (2003).

[44] Sajeev, S. and Anantharaman, M. R., "Determination of charge carrier transport in radio frequency plasma polymerized aniline thin films", J. Phys. D: Appl. Phys. **43,** 055403, (2010).

[45] Akhmedov, M., Kerimov, M.K. and Suleimanov, B.A., 'Space charge limited current in films obtained in Glow discharge plasma', Tr. J. of Phys., **22,** 253 -261, (1997).

[46] Olayo, M. G., Cruz, G. J., López, S., Morales, J. and Olayo, R., "Conductivity

and Activation Energy in Polymers Synthesized by Plasmas of Thiophene", J. Mex. Chem. Soc., **54**(1), 18-23, (2010).

[47] Cherpak, V., Stakhira, P., Hotra, Z., Aksimentyeva, O., Tsizh, B., Volynyuk, D. and Bordun, I., "Vacuum-deposited poly(o-methoxyaniline) thin films: Structure and electronic properties", J. of Non-Cryst. Solids, **354**(35-39), 4282-4286, (2008).

[48] Fischer, A. E., McEvoy, T. M. and Long, J. W., "Characterization of ultrathin electroactive films synthesized via the self-limiting electropolymerization of o-methoxyaniline", Electrochimica Acta, **54** (11), 2962-2970, (2009).

[49] Raj, J. A., Mathiyarasu, J., Vedhi, C. and Manisankar, P., "Electrochemical synthesis of nanosize polyaniline from aqueous surfactant solutions", Materials Letters, **64**(8), 895-897, (2010).

[50] Cowie, J. M. G., "Polymers: Chemistry and Physics of Modern Materials", Blackie Academic and Professionals, U K, 2nd Ed. (1991).

[51] Ghosh, P., "Polymer Science and Technology of Plastics and Rubbers" Tata McGraw-Hill Pub. Co. Ltd., New Delhi, 4th Ed., (1996).

[52] Bhuiyan. A.H., " The Phys. Bulletin", Bangladesh Phys. Soc., **16**(1), 26-36, (1996).

[53] Bogaerts, A. and Neyts, E., "Gas discharge plasma and their applications", Spectrochimica Acta Part B, **57,** 609-658, (2002).

[54] Biederman, H. and Osada Y., " Plasma Chemistry of Polymers", Advance in Polymer Sci., Berlin (1990).

[55] Lieberman, M. A. and Lichtenberg A. J., "Principles of Plasma Discharges and Materials Processing", John Wiley and Sons, New York, (1994).

[56] Grill, A., "Cold Plasma in Materials Fabrication: From Fundamentals to Applications", IEEE Press, New York, (1994).

[57] Chu, P. K., Chen, J. Y., Wang, L. P. and Huang, N., "Plasma surface modification of biomaterials", Materials Science & Engineering, R: Reports, R36 (5-6), 143-206, (2002).

[58] Yasuda, H., "Plasma Polymerisation", Academic Press, INC: NY, (1985).

[59] Denes, F., "Synthesis and surface modification by macromolecular plasma chemistry", Trends in Polymer Science (Cambridge, United Kingdom)**, 5** (1)**,** 23-31, (1997).

[60] Stark, R.H., and Schoenbach, K. H., " Direct current high pressure glow discharges", J. of Appl. Phys. **85,** 2075-2080, (1999).

[61] Stark, R.H., and Schoenbach, K. H., " Direct current glow discharges in atmospheric Air", J. of Appl. Phys. Lett. **74,** 3770-3772, (1999).

[62] Chan, C. M., "Polymer Surface Modification and Characterization", Hanser/Gardner Publications, Inc.: Cincinnatti, OH, (1994).

[63] Chan, C. M., Ko, T. M. and Hiraoka, H., "Polymer surface modification by plasmas and photons", Surface Science Reports, **24** (1/2), 1-54, (1996).

[64] Biederman, H. and Stavinska, D., "Plasma polymer films and their future prospects", Surf. Coat. Technol., **125** (1-3), 371-376, (2000).

[65] Shah Jalal, A. B. M., Ahmed, S., Bhuiyan, A. H. and Ibrahim, M., "On the conduction mechanism in plasma polymerized m-xylene thin films", Thin Solid Films, **295**, 125-130, (1997).

[66] Wang, X., Zheng, W.T., Tian, H.W., Yu, S.S., Xu, W., Meng, S.H., He, X.D., Han, J.C., Sun, C.Q. and Tay, B.K. "Growth, structural, and magnetic properties of iron nitride thin films deposited by dc magnetron sputtering", Appl. Surf. Sci., **220**, 30- 39, (2003).

[67] Leonhardt, D., Muratore, C., Walton, S.G., Blackwell, D.D., Fernsler, R.F. and Meger, R.A., "Generation of electron-beam produced plasmas and applications to surface modification", Surf. Coat. Technol., **177-178**, 682-687, (2004).

[68] Schlemm, H., Mai, A., Roth, S., Roth, D., Baumgärtner, K.-M. and Muegge, H., "Industrial large scale silicon nitride deposition on photovoltaic cells with linear microwave plasma sources", Surf. Coat.Techno., **174-175**, 208-211, (2003).

[69] Yasuda, H., Vossen, J. L., and Kern, W., "Thin Film Processes", Academic Press, New York, (1978).

[70] Hopwood, J., "Review of Inductively Coupled Plasmas for Plasma Processing", Plasma Source Sci. Technol. **1,** 109-116, (1992).

[71] Yasuda, H. and Hirotsu, T., "Critical evaluation of conditions of plasma polymerization", J. Polym. Sci., Polym. Chem. Ed., **16,** 313-317, (1978).

[72] Yasuda, H. and Lamaze C. E., "Polymerization in an electrode less glow discharge-III. Organic compounds without olefinic double bond", J. Appl. Polym. Sci., **17,** 1533-1544, (1973).

[73] Sioshansi, P. and Tobin, E. J., "Surface treatment of biomaterials by ion beam processes", Surf. Coat. Techno., **83,** 175-182, (1996).

[74] Szycher, M., Sioshansi, P. and Frisch, E. E., Biomaterials for the 1990s: Corporation, Polyurethanes. Silicones and Ion Beam Modification Techniques (Part II), Spire Patriots Park, Bedford, (1990).

[75] Ohl, A. and Schroder, K., "Plasma-induced chemical micropatterning for cell 830,culturing applications: a brief review", Surf. Coatings Technol., **116-119**, 820-825, (1999).

[76] Vargo, T. G., Bekos, E. J., Kim, Y. S., Ranieri, J. P., Bellamkonda, R., Aebischer, P., Margevich, D. E., Thompson, P. M. and Gardella J. A. Jr., "Synthesis and characterization of fluoropolymeric substrate with immobilized minimal peptide sequences for cell adhesion studies. I", J. Biomed. Mater. Res., **29,** 767-778, (1995).

[77] Vurzel, F.B., Acad. Sci., Moscow, USSR, "Plasma Chemistry, Technology, Application", Inst. Plasma Chem. And Technol. Carlsbad, CA (1983).

[78] Mathai, C. J., Saravanan, S., Jayalekshmi, S., Venkitachalam, S., Anantharaman, M. R., "Conduction mechanism in plasma polymerized aniline thin films", Mater. Lett. **57**, 2253-2257, (2003).

[79] Lindford, R.G., "In Applications of Electroactive Polymers; Scrosati, B.", Ed; Chapman and Hall; London, 1-28 (1993).

[80] Segui, Y. and Bui, A., " Microelectronic applications of plasma- polymerized films", Thin Solid Films **50**, 321-324, (1978).

[81] Hammer, T., "Applications of plasma technology in environmental techniques, contrib.", Plasma Phys. **3**, 441-462, (1999).

[82] Chowdhury, F.-U.-Z., Islam, A. B. M. O. and Bhuiyan, A. H., "Chemical anlysis of plasma-polymerized diphenyl thin films", Vacuum **57**, 43-50, (2000).

[83] Morosoff, N., "Surface Modification by Plasma Polymerization in Innovations in Materials Processing", Plenum, New York (1985).

[84] Conley, R. T., "Infrared Spectroscopy", 2nd Ed., Allyn and Bacon, Inc., Boston, (1975).

[85] Silverstein, R. M., Bassler, G. C., Morrill, T. C., "Spectrometric Identifacation of Organic Compounds", John Willey & Sons, New York (1981).

[86] Williams, D. H. and Fleming, I., "Spectroscopic Methods in Organic Chemistry", 4th Ed., Tata McGraw-Hill. Pub. Com. Ltd., New Delhi (1986).

[87] Kalsi, P. S., "Spectroscopy of Organic Compounds", 2nd Ed., New Age Inter. Pub. Ltd., New Delhi (1995).

[88] Williams, D. H. and Fleming, I., Ed."Spectroscopic Methods in Organic Chemistry", Tata McGraw-Hill, New Delhi (1990).

[89] Tauc, J., " Optical Properties of Solids", F. Abbeles Ed., North-Holand, Amsterdam (1972).

[90] Kumar, D. S., Nakamura, K, Nishiyama, S., Ishil, S., Noguchi, H., Kashiwagi, K., and Yoshida, Y., "Optical and electrical characterization of plasma polymerized pyrrole films",J. Appl. Phys. **93**(5), 2705-2711, (2003).

[91] Davis, E. A. and Mott, N. F., "Conduction in non-crystalline system, Optical absorption and photoconductivity in amorphous semiconductors", Philos. Mag. **22,** 903-922, (1970).

[92] www.msm.cam.ac.uk/phase-trans/2002/Thermal1.pdf.

[93] http://www.cea.com/techniques/analytical_techniques/tga_dta.php

[94] Mathai ,C. J., Saravanan, S., Jayalekshmi, S., Venkatachalam, S., Anantharaman, M. R., "Conduction mechanism in plasma polymerized aniline thin films" Mater. Lett, **57**, 2253-2257, (2003).

[95] Shah, J. A.B.M., Ahmed, S., Bhuiyan, A.H., and Ibrahim, M. "On the conduction mechanism in plasma-polymerized m-Xylene thin films", Thin Solid Films, **288**, 108-111, (1996).

[96] Kumar, S., Nakamura, K., Nishiyama, S., Ishii, S., Noguchi, H., Kashiwagi, K., Yoshida, Y., " Optical and electrical characterization of plasma polymerized pyrrole films", J. of App. Phys. **93**, 205-217, (2003).

[97] John, R. K., Kumar, D. K., " Structural, Electrical and Optical studies of plasma

polymerized and iodine doped poly pyrrole", J. of App. Polymer Science, **83**, 1856-1859, (2002).

[98] Valaski, R., Ayoub, S., Micaroni, L., Hummelgen, I.A., " Influence of thin thickness on charge transport of electrodeposited polypyrrole thin films", Thin Solid Films **415,** 206-210, (2002).

[99] Chen, C. Ku and Raimond, L., "Electrical properties of polymers"; Hanser publishers, Munich - Vienna – New York (1987).

[100] Yasuda, H., "Plasma Polymerization"; Academic Press, Inc, New York (1985).

[101] Emtage, P. R., Tantraporn, W., "Schottky emission through thin insulating films", Phys. Rev. Lett. **8**, 267-273, (1962).

[102] Lamb, D.R., "Electrical conduction Mechanisms in Thin Insulating Films", Methuen and Co. Ltd., London, (1967).

[103] Mott, N. F., Gurney, R. W., "Electronic Processes in Ionic Crystals", Clarendon Press, Oxford, 168-170, (1940).

[104] Lampert, M. A.,"Simplified theory of space-charge-limited currents in an insulator with traps", Phys. Rev. **103**, 1648, (1956).

[105] Chowdhury, F .-U.-Z., Islam, A . B . M . O . a nd B huiyan, A . H ., " Chemical anlysis of plasma-polymerized diphenyl thin films", Vacuum **57**, 43-50, (2000).

[106] Yasuda, H., "Plasma Polymerization" Academic Press, Inc., Tokyo (1985).

[107] Akther, H . a nd B huiyan, A . H ., " Space c harge limited c onduction i n pl asma polymerized N, N, 3, 5 tetramethylaniline thin film ", Thin Solid Film **488**, 93-97, (2005).

[108] Anghel, S . D ., F rentiu, T ., C ordos, E . A ., Simon, A a nd P opescu, A ., "Atmospheric pr essure capa citively coupl ed plasma s ource f or t he di rect analysis of non-conducting solid samples", J. Anal. At. Spectrom. **14**, 541-545, (1999).

[109] Chen, F. F., 'Introduction to Plasma Physics', Plenum Press, New York (1974).

[110] Inagaki, N., "Plasma S urface M odification and Plasma P olymerization", Technomic Publishing Co. Inc., New York (1996).

[111] Bogaerts, A .A. a nd N eyts, E ., " Gas di scharge pl asma a nd t heir a pplications", Spectrochimica Acta Part B **57**, 609-615, (2002).

[112] Lamb, D. R., "Electrical Conduction Mechanisms in Thin Insulating Films", Methuen and Co. Ltd., London, (1967).

[113] Phadke, S. D., Sathianandan, K. and Karekar, R. N., "Electrical conduction in polyferrocene thin films", Thin Solid Films, **51,** 9-11, (1978).

[114] Tolansky, S., "Multiple Beam Interferometry of Surfaces and Films", Clarendon Press, Oxford (1948).

[115] Tauc, J., Menth, A. and Wood, D., "Optical and Magnetic Investigations of the Localized States in Semiconducting Glasses", Phys. Rev. Lett., **25**, 749-752, (1970).

[116] Urbach, F., "The long-wavelength edge of photographic sensitivity and electronic absorption of solids", Rev. **92**, 1324-1330, (1953).

[117] Fayek, S. A., Balboul, M. R., Marzouk, K. H., Thin Solid Films **515**, 7281-7286, (2007).

[118] Mahr, H., Phys. Rev. **125,** 1510-1515, (1962).

[119] Wang, Y. and Balbuena, P. B., "Theoretical insights into the reductive decompositions of propylene carbonate and vinylene carbonate: density functional theory studies", J. Phys. Chem. B, **106**, 4486-4495, (2002).

[120] Deshmukh, S, H., Burghate, D. K., Akhare, V. P., Deogaonkar, V. S., Deshmukh, P. T., Deshmukh, M. S.,"Electrical conductivity of polyaniline doped PVC- PMMA polymer blends", Bull. Mater .Sci., **30**(1), 51-56, (2007).

[121] Gould, R.D., 'The interpretation of space-charge-limited currents in semiconductors and insulators', J. Appl. Phys. **53,** 3353-3355, (1982).